NASA CR-1087

PILOT DYNAMIC RESPONSE TO SUDDEN FLIGHT CONTROL SYSTEM FAILURES AND IMPLICATIONS FOR DESIGN

by David H. Weir and Walter A. Johnson

Prepared by
SYSTEMS TECHNOLOGY, INC.
Hawthorne, Calif.
for Ames Research Center

NATIONAL AERONAUTICS AND SPACE ADMINISTRATION   •   WASHINGTON, D. C.   •   JUNE 1968

PILOT DYNAMIC RESPONSE TO SUDDEN FLIGHT CONTROL

SYSTEM FAILURES AND IMPLICATIONS FOR DESIGN

By David H. Weir and Walter A. Johnson

NATIONAL AERONAUTICS AND SPACE ADMINISTRATION

FOREWORD

This report documents a study to determine the effect of the difference in controlled element dynamics at transition on the pilot's performance and behavior, and its implications for flight control design. The research was accomplished under Contract NAS2-3607 between Systems Technology, Inc., and the Ames Research Center of the National Aeronautics and Space Administration. The NASA project monitors were M. K. Sadoff and W. E. Larsen. The STI technical director was D. T. McRuer and the project engineer was D. H. Weir.

The assistance of C. P. Shortwell in performing the single-axis experiments, and the help of A. V. Phatak in analyzing their results is gratefully acknowledged. The authors are indebted to the fine and patient work of the STI Publications Department in the preparation of this report.

ABSTRACT

The dynamic response of the human pilot is studied during sudden changes in the effective controlled element dynamics caused by flight control system failure. Experimental results from single-loop and multiple-loop fixed-base studies are presented. A hypothesis of graceful degradation is shown to be valid which states that the pilot's transition response and performance are improved if the difference in controlled element dynamics at failure is reduced. The design implications of this principle are detailed. A model for the pilot's dynamic response is presented which accounts for his behavior during the several phases of transition.

CONTENTS

FIGURES

TABLES

SYMBOLS

a	Inverse time constant
A	Constant
c	Pilot output
dB	Decibels
e	System error
e	Base of the Napierian logarithm
g	Acceleration due to gravity
i	Input forcing function
j	$\sqrt{-1}$
$j\omega$	Imaginary part of Laplace operator, $s = \sigma \pm j\omega$
K	Gain constant
K_c	Controlled element gain
K_{CF}	Pilot gain for crossfeed
K_M	Gain margin
K_p	Pilot gain
K_r	Pilot gain for yaw rate control
K_{r_1}	Pilot gain for yaw rate control prior to failure
K_{r_2}	Pilot gain for yaw rate control after failure
$K_{r\delta_r}$	Stability augmenter gain
K_φ	Pilot gain for bank angle control
L'_p	Rolling moment due to roll rate
L'_r	Rolling moment due to yaw rate
L'_β	Rolling moment due to sideslip
L'_{δ_a}	Rolling moment due to aileron deflection

m	System output
N_p'	Yawing moment due to roll rate
N_P	Number of significant yaw rate error overshoots during transition
N_r'	Yawing moment due to yaw rate
N_β'	Yawing moment due to sideslip
N_{δ_a}'	Yawing moment due to aileron deflection
N_{δ_r}'	Yawing moment due to rudder deflection
r	System yaw rate
r_{max}	Maximum yaw rate error peak during transition for soft-failures
r_1	Magnitude of first yaw rate error peak for hard-failures
r_ϵ	Yaw rate error
R	Autocorrelation function
s	Laplace transform variable, $s = \sigma \pm j\omega$
t	Time
t_o	Time of failure
t_1	Time of start of nonlinear response phase
t_2	Time of end of nonlinear response phase
T	Duration of first rudder pulse for hard-failures
T_R	Roll subsidence time constant
T_R'	Closed-loop roll subsidence time constant
T_s	Spiral mode time constant
T_{WO}	Washout time constant
u	Generalized variable for spectral analysis
U_o	Steady-state velocity along the x-axis
Y_c	Controlled element transfer function
Y_{CF}	Pilot crossfeed

Y_{c_1}	Prefailure controlled element
Y_{c_2}	Postfailure controlled element
Y_{p_1}	Prefailure pilot model
Y_{p_2}	Postfailure pilot model
Y_r	Pilot model for control of yaw rate
Y_v	Side force due to lateral velocity
Y_φ	Pilot model for control of bank angle
α	Phase angle
β	Sideslip angle
β_g	Gust disturbance input
δ	Control or surface deflection
δ_a	Pilot aileron deflection
δ_r	Rudder deflection
$\delta_{r_{CF}}$	Pilot rudder output due to crossfeed
δ_{r_0}	Magnitude of first rudder pulse for hard-failures
δ_{r_p}	Pilot rudder pedal deflection
δ_{r_r}	Pilot rudder output due to yaw rate
$\delta_{r_{r_1}}$	Pilot's rudder output due to yaw rate prior to failure
$\delta_{r_{r_2}}$	Pilot's rudder output due to yaw rate, after failure
$\delta_{r_{SAS}}$	Rudder deflection from stability augmenter
Δ	Incremental change
ζ	Damping ratio
ζ'	Closed-loop damping ratio
ζ_d	Damping ratio of the Dutch roll mode
ζ_φ	Damping ratio of the roll numerator
σ	Standard deviation (square root of the variance)

σ_r	Yaw rate standard deviation
τ	Pure time delay
τ_F	Pilot's retention duration
τ_r	Pilot time delay for yaw rate control
τ_T	Transition duration (or total settling time)
τ_φ	Pilot time delay for bank angle control
φ	Roll or bank angle
φ_M	Phase margin
Φ	Power spectrum
Φ_{β_g}	Power spectrum of gust input
$\Phi_{\beta_g r}$	Cross spectra between gust input and yaw rate
$\Phi_{\beta_g \delta_a}$	Cross spectra between gust input and aileron deflection
$\Phi_{\beta_g \delta_{r_p}}$	Cross spectra between gust input and rudder pedal deflection
ω	Undamped natural frequency
ω'	Closed-loop undamped natural frequency
ω_c	System crossover frequency, i.e., frequency at which $\lvert Y_p Y_c \rvert = 1$
ω_d	Undamped natural frequency of Dutch roll mode
ω_r	Undamped natural frequency for yaw rate numerator
ω_φ	Undamped natural frequency of roll numerator
$\doteq$	Approximately equal to
$\lvert\ \rvert$	Magnitude
$\lvert\ \rvert_{dB}$	Magnitude in dB
$\angle$	Angle of
$(\dot{\ })$	$d(\ )/dt$
$(\ddot{\ })$	$d^2(\ )/dt^2$

SECTION I

INTRODUCTION

Failure of the flight control system[*] can cause a sudden change in the dynamics of a vehicle or the effective controlled element. The resultant controlled element transition requires that the pilot retain control of the vehicle while adapting to the new dynamics and/or taking corrective measures. The pilot can be relieved of the problem by employing fail operational control systems. An attractive alternative for some applications is to use the pilot's manual control capability plus reduced control system redundancy to achieve a design compromise with its attendant savings in weight, cost, etc. To take advantage of such a mix of manual and automatic functions, it is necessary to have a better understanding of what the pilot can be expected to do, and how best to tailor the pre- and postfailure vehicle dynamics to make the system degradation at failure as "graceful" as possible.

A. BACKGROUND

Prior research into operator response in the presence of changing controlled element dynamics relates directly to this problem. The earliest work was accomplished by Sheridan (Ref. 1) who studied gradual changes (over an interval of about 6 sec) and found that adaptation took about 15 sec on the average. The first investigation of the more pertinent "sudden change" was done by Sadoff (Ref. 2) who compared the response of skilled pilots in fixed-base and moving-cab simulators. His results show that cab motion has a significant adverse effect as evidenced by larger errors and longer transition times.

A series of experimental investigations was performed by Young, Elkind, et al (e.g., Refs. 3—5), involving sudden transitions in single-axis compensatory tracking tasks. A fixed-base facility with

---

[*]The concern here is with systems (e.g., stability augmenters) which modify the dynamics of the effective controlled element which are in series with the pilot in his control task.

a side stick manipulator was used. These experiments resulted in data for a variety of transitions, a few of which correspond to flight control system failures. Their analysis and modelling efforts have centered on detection of the transition and identification of the posttransition controlled element dynamics among the known alternatives.

The study reported herein is an outgrowth of past STI work (Ref. 6) which concentrated on deriving a model for the human operator's dynamic response before, during, and after a controlled element transition which could be useful in control system preliminary design. The resultant "mode-switching" model contained the following phases:

- Pretransition steady-state
- Retention of pretransition conditions
- Optimal control
- Posttransition steady-state

It defined the operator's response in terms of a duration (for the retention phase), a solution to an optimal control problem, and quasi-linear models for the stationary compensatory control initial and terminal condition (Ref. 7). The investigations showed transition performance could vary depending on the change in controlled element dynamics. From this came the notion that a flight control system could be designed to be more "forgiving" at failure by making the transition in the controlled element dynamics easier to control.

B. GRACEFUL DEGRADATION

The central concern in this study relates to the pilot's ability to exercise adequate control in the presence of a flight control system (e.g., stability augmenter) failure. The degree to which he can successfully and reliably do so can influence the philosophy and detailed design of the flight control system. For example, if the augmented airplane is so good that the pilot has little to do, then when the system fails not only is the increment in his readaptation large, but his ability to cope with demanding tasks may be reduced because of the poor pilot/vehicle performance. If, instead, the level of prefailure augmentation is reduced so that there are modest demands on the pilot's capabilities at all times,

2

the increment of readaptation will be smaller and the pilot will be more alert and more capable if and when transition occurs. The latter philosophy is of course directly counter to the popular notion of always putting the controller/vehicle characteristics in the center of a desirable region or "bulls-eye."

These notions can be summarized in terms of a "Graceful Degradation Hypothesis" which states that the operator's transition response and performance are a function of the difference in controlled element dynamics at transition, as well as their respective dynamics; the larger the difference the greater the control difficulty and the poorer the performance.

The question at the core of this concept is the effect of the augmentation level on the difficulty of transition following failure. Answers were sought in this program by conducting experiments to:

- Demonstrate the improvement in pilot control following failure obtainable by reducing the augmentation level.

- Provide new direction to pilot-modelling activities pertinent to time-varying situations, and to refine the current model.

In connection with the modelling aspect, it is pertinent to note that the only time-varying situations of importance seem to be those associated with sudden or step changes in the controlled element; and that past applications of pilot models have always improved our appreciation for their utility or shortcomings.

C. EXPERIMENTAL TASKS

Two experimental series were conducted as part of this program. The first involved a single-axis roll tracking task. The second involved multiple axis control of roll angle with aileron and yaw rate with rudder. Both were run in a fixed-base cockpit using dynamics simulated on an analog computer.

The single-axis task involved roll control of a VTOL in hover with series stability augmentation provided by a roll rate gyro and a roll

attitude gyro. The resultant effective controlled element dynamics were a pure gain, K, a single integration, K/s, or a double integration, K/s^2; depending on which augmentation loops were functioning. At the time of failure the (reaction nozzle) control could center to neutral, ramp to a hardover position, or step to a hardover.

The primary task in the multiloop experiments was roll control of a conventional airframe. The dynamics in roll (roll subsidence and spiral modes) were adjusted for good handling. The Dutch roll was added as a nuisance mode and its dynamics were varied from good to bad by making minor changes (e.g., the ω_ϕ/ω_d ratio) in the basic airframe and large changes in the level of stability augmentation. As a result, no rudder control (damping) was required from the pilot in the good configuration, while various amounts of pilot damping were needed in the poorer ones. At failure the effective airframe went from good to bad, or poor to bad, in order to test the graceful degradation hypothesis. Hardover and soft failure modes were also utilized.

D. REPORT ORGANIZATION AND PREVIEW

The single-loop experiments are reported in Section II, supported by Appendix A. The multiloop-loop procedures and results are given in Section III, with details in Appendix B. Digital techniques used to analyze the multiple-loop data are given in Appendix C, together with ensemble-average time-varying power spectra for selected sets of runs.

The graceful degradation hypothesis is shown to be valid, and the resultant implications for design are summarized in Section IV.

The transition model of the operator's response (existing at the outset of the study) is further confirmed by these experimental results. It is extended in the case of hardovers to account for a deterministic nonlinear pilot output which compensates for the failure transient. The revised model is given in Section V.

Overall conclusions of the study and recommendations for appropriate additional research are given in Section VI.

SECTION II

SINGLE-AXIS DATA AND ANALYSIS

The purpose of the single-axis experiments was twofold; to assess the dynamic response of the pilot under fairly realistic transition situations, and to investigate the concept of graceful degradation.

A. DESCRIPTION OF THE EXPERIMENTS

The single-axis experiments involved simulated roll control of an augmented VTOL in hover. Three levels of augmentation were used:

- None, $Y_c \doteq K/s^2$
- Roll rate feedback, $Y_c \doteq K/s$
- Roll rate and attitude feedback, $Y_c \doteq K$

The system block diagram is given in Fig. 1. The forcing function, i, was a low frequency random-appearing command with a cutoff at 1.5 rad/sec. The mechanization is given in Fig. 2, and the analog diagram in Fig. 3. Details are presented in Appendix A.

Transitions in the effective controlled element dynamics were achieved by failing either or both of the feedback loops in accordance with estimated (relative) failure rates and failure modes as discussed in Appendix A. The resultant transitions are summarized in Table I.

A typical experimental run lasted 3 to 4 minutes with the failure occurring at random, 1 to 3 minutes after the start. The subject was a well-trained pilot who had about 10 hr of practice (180 trials) in the failure tasks prior to the actual experimental runs. The task was to minimize the displayed roll angle error prior to, during, and after the failure. Failure transients in the augmentation system (ramp, hardover) occurred simultaneously with the opening of the loop(s). Amplifying details relating to the subject and the experimental procedure are given in Appendix A. In all, about 159 actual experimental runs were made with the distribution shown in Table A-VII. The data consist of pen-recorder time histories of the forcing function, roll error, sensor outputs, pilot output, and system output.

5

TABLE I

SINGLE-AXIS FAILURE SITUATIONS

PREFAILURE AUGMENTATION	POSTFAILURE AUGMENTATION	POSSIBLE MODES OF FAILURE	EFFECTIVE TRANSITION
Rate	None	Soft, hardover	$\dfrac{K}{s} \rightarrow \dfrac{K}{s^2}$
Rate plus attitude	Rate	Soft, ramp, hardover	$K \rightarrow \dfrac{K}{s}$
	Attitude	Soft, hardover	$K \rightarrow \dfrac{K}{s^2 + 2\zeta\omega s + \omega^2}$, ζ neg
	None	Soft	$K \rightarrow \dfrac{K}{s^2}$

B. ANTICIPATED TRANSITION CHARACTERISTICS

Prior studies (summarized in Ref. 6) had resulted in a model which divided the transition into phases with respect to time, each of which had certain distinguishing characteristics. The phases were

- Prefailure steady state; stationary compensatory tracking
- Retention; prefailure pilot describing function plus the postfailure controlled element dynamics operating closed-loop
- Nonlinear control*; large control actions (sometimes time-optimal) which stabilize the system and reduce the error to some acceptable level
- Postfailure steady state; stationary compensatory tracking

These phases are illustrated in Fig. 4, which is a sample of data from this experimental series. The units are also shown in Fig. 4. Note that the units for rate and attitude feedback are inches of equivalent pilot output (lateral stick movement at the grip).

---

*This is called the "optimal control phase" in Ref. 6, but "nonlinear control" is more descriptive because many of the responses are suboptimal.

The retention phase starts at the failure. It consists of the pre-failure pilot adaptation and the postfailure controlled element operating in a closed-loop fashion on the system error. This frequently results in an unstable condition because the typical failure results in a substantial increase in the controlled element lag. The end of the retention phase is defined as the point in time where an abrupt change in manipulator motion begins. It is most evident in transitions where the nonlinear control phase can be clearly seen.

The nonlinear control phase starts at the end of retention and continues until the system error has been reduced (approximately) to within the post-failure steady-state envelope. This envelope may exhibit a further, more gradual decay during the first seconds of this steady-state period, corre-sponding to an additional "adjustment phase" (Ref. 6) wherein the pilot's final adaptation is being achieved by an optimizing process. Identifying the nonlinear control phase duration is a subjective process and it is sometimes difficult.

Other measures of the transition response are shown in Fig. 4. The "total settling time" is the sum of the retention and nonlinear control phases. The "divergence rate" is the magnitude of the slope of the error curve at the end of the retention phase. The "number of significant error peaks" is the number of peaks of all sizes (changes of sign of the error rate) which occur before the end of the nonlinear control phase. It is two in Fig. 4 and four in Fig. 14, for example.

The prior studies have shown that differences in performance occur, depending on the change in controlled element dynamics at transition; and that these performance differences arise largely in the retention phase and the early part of the nonlinear control phase. Hence, the major differences between various types of failures in the sense of graceful degradation was expected to lie in the retention phase and early portions of the nonlinear control phase. In the case where the nonlinear control was time-optimal (with a given stick amplitude limit), the retention phase would be the only place where differences would arise, by definition.

7

The steady-state characteristics of the pilot (in control of the various effective controlled element dynamics) were estimated using the quasi-linear describing function model of Ref. 7. The closure criteria were about 15 — 25 deg phase margin and less than 5 dB gain margin. The resultant describing functions and closed-loop roots are given in Table A-V of Appendix A. Combining the prefailure pilot describing function and postfailure controlled element dynamics gives the open- and closed-loop characteristics during the retention phase, and these are shown in Table A-VI of Appendix A. Although predictions for the nonlinear control phase were not made, representative time-optimal ones are included in Ref. 6. Specific applicable suboptimal forms among the competing alternatives were not defined at the outset (unfortunately, they are still undefined for the most part).

The effect of different prefailure controlled element dynamics on the retention phase and difficulty of control can be illustrated with an example based on the predictions discussed above. Consider the two transitions $K \rightarrow K/s^2$ and $K/s \rightarrow K/s^2$, and assume that the modes of failure and initial conditions are the same in each case.

The first transition, $K \rightarrow K/s^2$, is shown in Fig. 5a. It gives the location of the closed-loop roots in the s-plane for the sequence of approximate closed-loop transfer functions which occur during transition for the pilot-plus-airframe system. These root locations are taken from Tables A-V and A-VI. For prefailure there is a real pole at 1.87 rad/sec, a quadratic pair at about 3.6 rad/sec, and a pilot-induced zero at 3 rad/sec. This becomes the highly unstable pole location during retention shown by the subscript "2". Then, after the pilot goes from a lag to a lead equalization, the postfailure system results.

The second transition, $K/s \rightarrow K/s^2$, is given in Fig. 5b, taken from Tables A-V and A-VI. The pilot needs no equalization before the failure, and the response is characterized by the second-order pair at 3.4 rad/sec denoted by the subscript "1". During retention these poles move to —.35 damping ratio, and then move back to .11 damping in postfailure steady state (with pilot lead at about 0.2 rad/sec).

The reduced movement of the quadratic poles and the lack of a first-order lag during retention is evident in Fig. 5b, although the divergence

rate of the quadratic pair during retention is larger than in Fig. 5a. Note
that each transition could be improved if the pilot used a lower prefailure
gain, thereby reducing the retention phase instability. The results suggest
that the $K/s \rightarrow K/s^2$ transition should give the pilot less difficulty.

C. EXPERIMENTAL RESULTS

The single-axis data consist of time histories for 159 experimental runs
containing eight types of failures allocated as shown in Table A-VII in
Appendix A. They have all been analyzed in detail with the objectives of
substantiating the graceful degradation concept and extending and refining
the transition model of the human operator. Examples of the data are presented
below, together with comparative observations and discussion relevant to both
objectives. The transition response measures have also been made, and these
are presented in histogram form in connection with the discussion on graceful
degradation in subsection D.

An example of the $K \rightarrow K/s$ (soft) failure in which the attitude loop
steps to zero feedback is given in Fig. 6. In general, the time of failure
cannot be detected by examining the error trace alone even when the "step
shutoff" is fairly large. Examination of the envelope of the postfailure
steady-state error shows it to be slightly higher than before the failure,
suggesting that the pilot's postfailure adaptation may be less than optimum
with respect to mean square error. The nonlinear control phase is absent
in these data, as is the retention time in its usual sense. Hence the transi-
tion response measures (divergence rate, etc.) are inappropriate and have not
been made. The adaptation to the postfailure steady state is immediate for
all practical purposes.

The $K \rightarrow K/s$ (ramp) data, in which the attitude feedback loop ramps to
its full authority following failure, are typified by Fig. 7. Sometimes
the error peaks a little following failure, but generally it does not and
the transition response measures are again inappropriate. The postfailure
error envelope is slightly larger than that for soft failure. The big
difference relative to the soft failure is the presence of the ramp and
steady-state bias superimposed on the pilot's output, c. The ramp and bias
from the failure are drawn on c for comparison. This suggests the existence

9

of a pilot feedforward (possibly open-loop) of a ramp and bias which cancels that from the augmentation loops. Such a feedforward could be triggered after an appropriate identification process among the alternative failures on those runs.

The $K \rightarrow K/s$ (hard) failure involves the attitude feedback loop going to its full authority in a steplike manner. A typical set of results is shown in Fig. 8. There is usually one error peak (sometimes two) which is induced by the hardover. The postfailure steady-state error level is noticeably larger than that before failure. The pilot's output shows a rapid correction for the error followed by a steady-state bias due to the step. The hardover is shown on the pilot's output trace in Fig. 8 for comparison. Figure 9 shows another example where a rapid steplike correction on the part of the pilot is very evident, suggesting a feedforward (open-loop) step response superimposed on his quasi-linear output. Note that the rise time in Fig. 9 is that appropriate to step responses, i.e., it is much shorter than that which results from the step response of the describing function plus controlled element closed-loop. Comparing Figs. 7 and 9 shows that in each case the deterministic signal (ramp or step) at failure comes through in the pilot's output following a short time delay.

The $K \rightarrow K/s^2$ (soft) failure results when both the attitude and rate feedbacks step to zero. Typical response is poor, and this is illustrated by Fig. 10, which shows several significant error peaks and a lack of time-optimal control in the nonlinear phase. An alternative view is to assume that the nonlinear control phase is absent, as it was in the $K \rightarrow K/s$ (soft) data. Then the first 5 or 6 sec following failure might be a combination retention and adjustment phase where the pilot gradually introduces the appropriate lead equalization. An example of good response is shown in Fig. 11, which shows one error peak and nearly time-optimal control during the nonlinear phase. About 20 percent of this type of failure showed nearly time-optimal characteristics akin to Fig. 11. Note that the "clipping" evident in Figs. 10 and 11 during the large motions occurred in the recorder. This was the only type of $K \rightarrow K/s^2$ transition in these experiments, and ramps and hardovers were not studied.

Failures of the rate feedback loop alone (attitude loop still operating) resulted in controlled element transitions of the form

$$K \longrightarrow \frac{K}{s^2 + 2\zeta\omega s + \omega^2} \; , \; \zeta \text{ negative}$$

Considerable training and practice were required before the pilot could consistently retain control in the presence of this failure. Even then, in one of the three runs made with a soft-failure mode the pilot lost control immediately after the failure, probably because the initial conditions around the loop were relatively large. Interestingly enough, the postfailure controlled element is near the limits of controllability reported in Ref. 8 for the human operator under stationary conditions, and the transition is more difficult. A typical example of a soft-failure where control was retained is shown in Fig. 12. The limiting in the error and system output occurred in the recorder. The pilot achieves a limit cycle type of control, although he occasionally reduces the error for a short time. This type of failure was also done with a hardover mode, and the pilot lost control within 1 to 2 sec in five of the ten runs. It was subjectively more difficult than the soft mode and very tiring even for short periods of time. An example of the hardover failure is given in Fig. 13. Note the lack of bias (due to the step) in the pilot's output, and the similarity with Fig. 10. Apparently the pilot adjusts the timing of his (bang-bang) stick pulses to provide the required bias. The mode of failure seems to make little difference in this case where the dynamics are so difficult, while in the simpler transitions (e.g., $K \longrightarrow K/s$) the failure mode dominated the pilot's response.

The $K/s \longrightarrow K/s^2$ (soft) failure occurs when the rate feedback steps to zero. The majority of these runs have well-defined retention and nonlinear control phases. Typical runs, an example of which is given in Fig. 14, had two or three significant error peaks (Fig. 14 has four) followed by a decay in the error to a postfailure steady-state level which was somewhat larger than that before failure. About 15 percent of the runs were approximately time-optimal with one error peak and bang-bang-like control as shown in Fig. 15. The error peak is large in Fig. 15 because of the large initial

11

conditions at the time of failure. About 10 percent of the runs show no significant error peak following failure, and the level of the postfailure steady-state envelope is not exceeded.

The $K/s \rightarrow K/s^2$ (hard) failure results when the rate feedback loop steps hardover. Performance is much poorer than in the soft mode of the same transitions, and the error is large following the failure and stays large. This is typified by the data of Fig. 16 (note that the limiting is in the recorder). In three of the 17 experimental runs the pilot lost control within 1 or 2 sec after failure. The size of the step change to the hardover position seemed to be directly related to loss of control. In cases where the step to hardover was small, performance was much better, and this is illustrated by Fig. 17. The bias in the pilot's output following failure can be seen in both Figs. 16 and 17. Both the mode of failure and the change in dynamics make a large contribution to the control difficulty in these transitions, and it appears to be a middle ground between $K \rightarrow K/s$ where the mode of failure dominates and $K \rightarrow K/[\zeta,\omega]$, $\zeta_{negative}$, where the change in dynamics is the major factor.

D. GRACEFUL DEGRADATION CONSIDERATIONS

System degradation at failure is determined by the change in dynamics and the failure mode. To assess the degree of degradation, sensitive measures of the quality and difficulty of control are needed. In early work, Elkind (Ref. 9) used several deterministic performance criteria to study differences among transitions. In view of his results, plus detailed examination of more recent data, the measures previously mentioned were chosen; i.e.,

- Magnitude of first major error peak
- Magnitude of divergence rate (to first error peak)
- Time from end of retention phase to first error peak
- Retention phase duration
- Total settling time

These terms are defined on Fig. 4.

An attempt was made to apply these measures to each of the experimental runs. In cases where there was no identifiable nonlinear control phase (i.e., no observable transition or change in form of the operator's response)

12

the measures were of course inappropriate. This was true for the $K \rightarrow K/s$ (soft) results, most of the $K \rightarrow K/s$ (ramp) data, and some of the $K \rightarrow K/s^2$ (hard) data. About 10 percent of the $K/s \rightarrow K/s^2$ (soft) failures showed apparent nonlinear control phase, also. These measures were not obtained for the $K \rightarrow K/[\zeta, \omega]$, $\zeta_{negative}$, transitions because the performance was so poor that the nonlinear phase essentially continued indefinitely or until loss of control.

There remained three transitions where the performance measures could be obtained and the validity of the graceful degradation idea investigated:

$$K \rightarrow K/s^2 \text{ (soft)}$$
$$K/s \rightarrow K/s^2 \text{ (soft)}$$
$$K/s \rightarrow K/s^2 \text{ (hard)}$$

The individual measures have been summarized in histograms for ease of comparison. The same engineer/analyst made all the measures using a consistent set of criteria in order to reduce the subjective variability. A few of the soft-failures were excluded because they did not show a non-linear control phase, as noted before. This in effect means that there are some points at zero or infinity (depending on the measure) which have not been plotted.

Histograms for the magnitude of the first error peak are shown in Fig. 18. They show that $K/s \rightarrow K/s^2$ (soft) gives a substantially smaller peak error than $K \rightarrow K/s^2$ (soft). This supports the graceful degradation hypothesis. The $K/s \rightarrow K/s^2$ (hard) failure gives much larger peak errors than the soft case, supporting the widely held contention that hardovers are bad.

The divergence rate results are given in Fig. 19. The $K/s \rightarrow K/s^2$ (soft) and $K/s \rightarrow K/s^2$ (hard) results are about the same. The $K \rightarrow K/s^2$ (soft) gives much higher divergence rates than either. This supports the graceful degradation hypothesis. The divergence rate is a strong function of the signal levels at the time of failure, and hence the magnitude of the step to hardover from the augmenter feedback loops. The effect averages out in these comparisons, of course.

The times from retention to peak are shown in Fig. 20. These times are roughly equal to the peak amplitude divided by the divergence rate. The data

13

show this measure to be invariant among the transitions. Apparently the constant time resulted in the larger rates being accompanied by higher peaks.

The retention phase durations are shown in Fig. 21. The $K \rightarrow K/s^2$ (soft) and $K/s \rightarrow K/s^2$ (soft) cases are about the same. The relatively large variability in these data is probably due to the variability in the magnitude of the step to zero in the failures. The $K/s \rightarrow K/s^2$ (hard) results show a shorter duration and less variability, undoubtedly due to the alerting effect of the hardover.

The total settling times are shown in Fig. 22. All three cases show about the same mean. The $K/s \rightarrow K/s^2$ (hard) case shows greater variability. Most of the points in each case fall between 2 and 6 sec, although there are a few very long times. This measure is particularly sensitive to the subjective assessment of the engineer/analyst, but this was minimized by having the same person do all the analyses.

The results of this investigation of the single-loop data can be summarized as follows:

- The magnitude of the error peak and the divergence rate show substantial differences between $K \rightarrow K/s^2$ (soft) and $K/s \rightarrow K/s^2$ (soft), and the differences are such that the latter is better. This supports the graceful degradation hypothesis.

- There are no data which counter the graceful degradation hypothesis.

- The only other substantial differences which occurred were between hard and soft-failures. The hardovers had larger error peaks and shorter retention times (probably due to alerting). This supports the self-evident fact that hardovers are bad because they are in effect a large disturbance input.

These results are combined with the multiple-loop results in Section IV in order to derive implications for flight control system design.

E. TRANSITION RESPONSE MODEL

Further insight into the pilot transition response model for single-axis tasks derives from an examination of the data in Subsection C above. The transition model at the start of this experimental program had the following main phases:

- Prefailure steady state
- Retention of pretransition conditions
- Nonlinear control
- Postfailure steady state

In addition, the early part of postfailure steady state could contain an adjustment phase where the pilot optimized his adaptation.

Remarks concerning the data (from Subsection C above) are summarized in Table II according to transition phase. On the basis of Table II it is apparent that the general form of model given in Ref. 6 is still valid with the following extensions and modifications:

- Numerical estimates are now available for the retention duration when this phase exists.

- Hardover failures have shorter retention durations than soft failures except for the most difficult postfailure controlled elements where there is no difference.

- The pilot compensates for failure transients (hardovers, etc.) during the nonlinear control and postfailure steady-state phases. In some cases this appears to be a feedforward signal which cancels the failure transients, although this was not apparent for the most difficult postfailure controlled elements. An alternative is to treat the transient as an initial condition to nonlinear control, and then produce a trim bias in postfailure steady state.

- Time-optimal control during the nonlinear phase is still a valid idealization for the soft-failures, as an attainable limiting case. Some suboptimal control mode is more typical.

- Postfailure steady-state error characteristics were generally larger than that predicted by an optimized quasi-linear model. This suggests that any adjustment (optimization) phase is relatively long-term and does not happen immediately following the nonlinear phase.

These results are integrated in Section V with those of the multiple-loop experiments to provide the basis for evolving an updated transition model.

15

TABLE II

CHARACTERISTICS OF THE TRANSITION PHASES (SINGLE-AXIS)

FAILURE	Prefailure Steady State	TRANSITION PHASE		
		Retention	Nonlinear Control	Postfailure Steady State
$K \rightarrow \dfrac{K}{s}$ (soft)	Normal quasi-linear control to minimize error	Not present	Not present	Quasi-linear control with error larger than prefailure.
$K \rightarrow \dfrac{K}{s}$ (ramp)		Not present	Ramp feedforward superimposed on postfailure quasi-linear control.	Quasi-linear control with prefailure error level. Pilot output bias due to limited ramp.
$K \rightarrow \dfrac{K}{s}$ (hard)		Time delay prior to step response; average duration about 0.5 sec	Step feedforward superimposed on postfailure quasi-linear control.	Quasi-linear control with error larger than prefailure. Pilot output bias due to step.
$K \rightarrow \dfrac{K}{s^2}$ (soft)		Average duration about 1 sec	20% time-optimal, balance suboptimal. Alternative explanation might be an adjustment phase where lag is replaced by lead.	Normal quasi-linear control to minimize error.
$K \rightarrow [\zeta,\omega]$, ζ_{neg} (soft)		Average duration about 0.6 sec	Approximately time-optimal control giving stable limit cycle. Lost control at failure in 1 out of 3 cases.	Nonlinear control phase continues indefinitely.
$K \rightarrow [\zeta,\omega]$, ζ_{neg} (hard)		Average duration about 0.5 sec	Approximately time-optimal control giving stable limit cycle. Lost control in 5 out of 10 cases. Hardover not evident in pilot's output.	Nonlinear control phase continues indefinitely. Amplitude bias due to hardover not present; accounted for by timing of stick reversals.
$\dfrac{K}{s} \rightarrow \dfrac{K}{s^2}$ (soft)		Average duration about 1 sec	15% time-optimal, balance suboptimal. Not present in 10% of the runs.	Quasi-linear control with error larger than prefailure.
$\dfrac{K}{s} \rightarrow \dfrac{K}{s^2}$ (hard)		Average duration about 0.6 sec	Suboptimal control, with an average total settling time of about 6 sec. Lost control in 3 of 17 cases. Superposition of step not obvious.	Quasi-linear control with error larger than soft-failure. Pilot output bias due to step.

SECTION III

MULTIPLE-LOOP DATA AND ANALYSIS

The primary purpose of the multiloop experiments was to investigate the graceful degradation hypothesis, and the dynamic configurations were tailored accordingly. Modifications to the transition response model to account for the multiple loop situation were also sought.

A. DESCRIPTION OF THE EXPERIMENTS

The multiple-axis experiments involved compensatory control of bank angle and yaw rate of a simulated fixed-wing aircraft subjected to a sideslip gust disturbance. A fixed-base cockpit was used with conventional center stick and rudder pedals. A yaw rate augmenter (SAS) was included so that the prefailure Dutch roll dynamics of the effective airframe could be varied over a region from poor to good. The post-failure dynamics were generally unacceptable for normal operation, involving an unstable airframe alone, but one that could be controlled by suitable pilot rudder activity. During the experimental runs the SAS was failed and a rudder transient introduced. Pilot response to this step change in controlled element dynamics was recorded for analysis. The system block diagram is shown in Fig. 23, and the mechanization for failure analysis is given in Fig. 24. Details of the dynamics, mode of failure analyses, and the analog mechanization are given in Appendix B. The analog diagram and switching logic are given in Figs. 25 and 26.

The lateral directional dynamics of the effective airframe are summarized in Table III for the prefailure and postfailure configurations. The approximate locations in the s-plane of the transfer function poles and zeros are given in Fig. 27. The main effect of the augmentation is seen to be in the Dutch roll mode. The desire was to have a situation that the pilot had to fly with a manual rudder-plus-aileron in the event of a yaw rate augmenter failure.

Two kinds of rudder transients were used in order to simulate hard and soft failure modes. These were applied to the rudder at the instant

TABLE III

DYNAMIC PROPERTIES OF ROLL CONTROL OF THE PREFAILURE AND POSTFAILURE CONFIGURATIONS

CONFIG.	PREFAILURE AUGMENTATION	FAILURE	ΔY_c AT FAILURE
A	$\omega'_\varphi \doteq \omega'_d \doteq 2$ $\zeta'_\varphi \doteq \zeta'_d \doteq 0.7$ $K_{r\delta_r}$ optimum	$K_{r\delta_r} \rightarrow 0$	$\dfrac{K}{s\left(s + \frac{1}{T'_R}\right)} \longrightarrow \dfrac{K\left(s^2 + 2\zeta_\varphi \omega_\varphi s + \omega_\varphi^2\right)}{s\left(s + \frac{1}{T_R}\right)\left(s^2 + 2\zeta_d \omega_d s + \omega_d^2\right)}$ $\zeta_\varphi \doteq \zeta_d < 0, \quad \dfrac{\omega_\varphi}{\omega_d} > 1$
B	$\omega'_\varphi \doteq \omega'_d \doteq 2$ $\zeta'_\varphi \doteq \zeta'_d \doteq 0.2$ $K_{r\delta_r} <$ optimum	$K_{r\delta_r} \rightarrow 0$	$\dfrac{K\left(s^2 + 2\zeta'_\varphi \omega_\varphi s + \omega_\varphi'^2\right)}{s\left(s + \frac{1}{T'_R}\right)\left(s^2 + 2\zeta'_d \omega_d s + \omega_d'^2\right)} \longrightarrow \dfrac{K\left(s^2 + 2\zeta_\varphi \omega_\varphi s + \omega_\varphi^2\right)}{s\left(s + \frac{1}{T_R}\right)\left(s^2 + 2\zeta_d \omega_d s + \omega_d^2\right)}$ $\zeta_\varphi \doteq \zeta_d < 0, \quad \dfrac{\omega_\varphi}{\omega_d} > 1$
C	$\omega'_\varphi > \omega'_d \doteq 2$ $\zeta'_\varphi \doteq \zeta'_d \doteq 0.2$ $K_{r\delta_r} <$ optimum	$K_{r\delta_r} \rightarrow 0$	

of failure (when the vehicle dynamics changed). The hard-failure transient
consisted of a washed-out rudder step, as shown in Fig. 28. The soft-
failure was simulated by a "hold" of the rudder signal from the augmenter.
As a result of freezing the rudder command from the augmenter, there was
no disturbance imposed on the airplane by the failure. Therefore, there
was no immediate cue available to the pilot in the soft case to indicate
that the augmenter had failed.

With three prefailure configurations (A, B, and C) and two modes of
failure, there were six possible types of experimental runs. The post-
failure configuration, called E, was the same in each case.

Two subjects were used in the experiments, one a high time military
pilot and the other a private pilot. They practiced the failure tasks
two hours a day for several days, until each had accomplished about 200
trials over all configurations. Subsequent to the learning period, their
performance and response were substantially the same in a given task. The
experimental runs lasted about 2 minutes each, with the SAS failure
occurring after about 1 minute. The runs were grouped in consecutive
sets of 5 (with the same prefailure dynamics), followed by a rest period
between sets. Additional details regarding training and the experimental
procedure are given in Appendix B.

B. EXPERIMENTAL RESULTS

The transition model resulting from prior research has been summarized
in Section II-B. The results for the multiple-loop case were expected to
be substantially the same with regard to the nature of the successive
phases of transition, i.e.:

- Prefailure steady state
- Retention of prefailure conditions
- Nonlinear control
- Postfailure steady state

Preliminary experiments showed that the several phases could be distinguished
by features of the error signal in the axis of control which experienced the
failure, i.e., yaw rate.

The multiple-loop data consist of 90 experimental runs recorded on magnetic tape and as pen recordings. They have all been analyzed in detail in order to investigate graceful degradation and extend and refine the transition response model. Primary emphasis in analysis and interpretation was placed on the pen recording, because the nonlinear aspects and "quality" of the transition are more readily apparent. Some digital data reduction was accomplished (see subsection C), but it was necessarily limited in scope. Examples of the data are presented and discussed below.

Typical examples of failures from Configuration A are shown in Figs. 29 and 30. This prefailure configuration was designed to give enough Dutch roll damping that the effective airframe would be subjectively good and no pilot rudder control would be needed. Despite this, the pilot used the rudder intermittently before the failure[*] as shown in Figs. 29 and 30, presumably because of the high level of gust disturbance (which excited the aircraft) and the fact that the pilot knew a failure was coming. Interestingly enough, the approximate level of rudder gain which this represents is enough to make the postfailure configuration marginally stable. Hence, the pilot appears to close a low gain rudder loop with Configuration A in anticipation of the failure. With the soft-failures involving Configuration A, a retention phase and a transition phase are both evident. The transition phase is defined as the interval following failure during which the pilot has not yet reduced the yaw rate amplitude envelope to the steady-state level (see Fig. 29). It shows up just after a failure as a period during which the yaw rate amplitude envelope builds up and then decreases. The retention phase is obvious in that during the first few seconds following failure the pilot continues to respond as he did with the prefailure configuration. It is interesting to note the relatively long duration of the retention phase (several seconds) for this situation, as shown in Fig. 29.

---

[*]He could have been instructed not to use rudders with "A", but instead was allowed to evolve his own tactics (consistent with minimizing mean square error in bank angle).

Typical failures from Configuration B are shown in Figs. 31 and 32. This prefailure configuration was designed to give a lightly damped Dutch roll nuisance mode, but one that was not destabilized by aileron control of bank angle. The figures show that the pilot used larger rudder amplitudes with "B" than with "A". A rapid recovery following failure can be seen in the yaw rate trace of Fig. 32.

Configuration C failures are typified by Figs. 33 and 34. This configuration was similar to "B" except that bank angle control with aileron tended to destabilize the Dutch roll mode because of the adverse ω_φ/ω_d ratio. These figures show that the pilot's rudder activity before and after the failure is about the same. The rapid recovery following a hardover failure is shown in Fig. 34. On some of the runs involving soft-failures with Configuration C it was not possible to detect the failure from the time traces of yaw rate, bank angle, aileron, and rudder because they all look essentially the same (in magnitude and frequency content) before and after failure. This suggests a rapid adaptation for such cases. An example is given in Fig. 33. The hardover failures for Configuration C show a retention time of about 0.5 sec. After retention a large rudder pulse (also lasting about 0.5 sec) was applied in the direction to oppose the input, followed by a crude rudder step of opposite polarity lasting for several seconds. This opposite step was needed to cancel the yawing moment due to the aileron which the pilot was using to remove the bank angle induced by the failure transient. This is shown in Fig. 34.

The data for Configurations B, C, and E typically show a crossfeed by the pilot of aileron to rudder control. An example of the crossfeed is shown in the data of Fig. 35 taken from a run with Configuration B. The effect of the crossfeed is to augment N'_{δ_a} thereby reducing or cancelling the adverse effect of ω_φ/ω_d, and this is shown in the pole/zero plot of Fig. 36 for Configuration E. The effect of "overdriving" the crossfeed (and thus moving the Dutch roll zero below the pole) is not appreciable because of the relatively high gain yaw rate loop closure accomplished by the pilot. The motivation for using a crossfeed is to approximately decouple the controls so that aileron (with rudder crossfeed) produces

mostly roll, and rudder mostly yaw rate. Although Configurations C and E are the only ones requiring such a crossfeed, it was found that the pilot also used a crossfeed with "B" (which already exhibited a pole/zero cancellation for the Dutch roll mode). The reason for this may be explained by the pilot learning that a crossfeed was desirable after the failure for better performance, and that a crossfeed with "B" didn't appreciably affect performance. These results offer the type of support for the graceful degradation hypothesis that was sought in this investigation.

These results and examination of the time histories yielded a number of more general observations which are illustrated by Figs. 29-34:

- The pilot used the rudder to control yaw rate with all of the configurations, even though it was not needed in prefailure Configuration A. This suggests that the pilot was trying to reduce the dynamic effect of the failure by modifying his prefailure control, which tends to support the graceful degradation hypothesis.

- According to pilot comments and the response data, the cue that was used to determine that a hardover failure had occurred was the increased rate at which the turn needle moved. Thus, when the error <u>rate</u> exceeded some threshold value, the pilot assumed a hardover failure had occurred and he responded by applying a large rudder step.

- For hardover failures the magnitude of the first yaw rate error peak was only a measure of the pilot's time delay prior to applying a rudder step. This resulted from $\dot{r}$ being approximately a constant (r was a ramp) during the time between augmenter failure and the end of the retention phase.

- The yaw rate control task was apparently more difficult than the bank angle task. This is based on the fact that the pilot frequently used relatively small amounts of aileron (compared to rudder activity) and still had no difficulty controlling bank angle to an acceptable level of error. This is illustrated in Fig. 33.

- Bank angle control was only slightly affected by the failure. This is based on the observation that the bank angle errors before and after failure did not differ substantially regardless of the prefailure configuration. The bank angle errors did not increase during the transition. This is shown in Figs. 29-34.

22

- The yaw rate amplitudes show that Configuration C gives better performance in steady state than "E", "B" better than "C", and "A" better than "B", as would be expected. The magnitude of the steady-state yaw rate amplitudes with "E" appeared to be independent of the prefailure configuration. These results influence both the graceful degradation considerations and the revised transition response model, as shown subsequently.

C. GRACEFUL DEGRADATION CONSIDERATIONS

The primary intent of the multiple-loop experiments was to generate data that could be used to test the validity of the graceful degradation hypothesis. As stated in Section I, this hypothesis asserts that the degradation in performance immediately following a step change in controlled element dynamics increases as the change in dynamics increases. This implies that some prefailure control activity by the pilot is preferred to his merely observing that the (automatic) SAS is doing an adequate job.

The data analysis to study graceful degradation was achieved in two ways. The first involved manual analysis of the pen-recorder time traces to determine typical details. The second was a digital analysis of the tape recorded data which yielded averages of the gross characteristics. The results are presented below.

1. Manual Analysis

The data were analyzed manually by measuring typical transition parameters and tabulating these as histograms for comparison of the configurations. The parameters are listed below and illustrated in Fig. 37 for the hard- and soft-failure modes:

r_{MAX} ≡ maximum yaw rate error peak during transition for soft-failures

r_1 ≡ magnitude of first yaw rate error peak for hard-failures

τ_T ≡ transition duration (or total settling time); the transition is considered to last as long as the yaw rate error peaks remain outside the envelope of the postfailure steady-state error peaks

23

N_P ≡ number of significant yaw rate error overshoots during transition

Other parameters shown in Fig. 37 and used subsequently include:

δ_{r_0} ≡ magnitude of first rudder pulse for hard-failures

T ≡ duration of first rudder pulse for hard-failures

τ_F ≡ pilot's retention duration for soft-failures, or his time delay prior to applying the initial rudder pulse for hard-failures

The parameters are defined in terms of the yaw rate, pilot rudder output and SAS rudder output; so only these traces are given in Fig. 37.

Histograms showing the distribution of maximum yaw rate peaks for the soft-failures are given in Fig. 38. It shows that the relative number of runs with yaw rate errors large enough to give an obvious transition region increases as the prefailure dynamics improve. The hard-failure data in Fig. 39 show that Configurations B and C give smaller maximum yaw rates than "A". Both of these results support the graceful degradation hypothesis.

The distribution of transition durations for soft-failures is shown in Fig. 40. This duration requires that the error increases above the postfailure asymptotic level in order to be measured, and this only occurred with the good prefailure dynamics. Since the poor dynamics (Configuration C) did not peak above that level, it strongly supports the graceful degradation hypothesis. The results are inconclusive for the hard-failures, shown in in Fig. 41. Perhaps the duration is affected more by the hardover transient acting as a disturbance (the same in all cases) than it is by the change in dynamics.

The distribution of error overshoots for the soft-failures is given in Fig. 42. The striking thing is that no significant error overshoots occurred for the poor prefailure dynamics while they occurred frequently with the good prefailure dynamics, again supporting the hypothesis.

For the hard-failure data in Fig. 43 the distribution of the number of
yaw rate error overshoots does not lead to a conclusion regarding
graceful degradation.

The results of the manual analysis can be summarized as follows:

> Most of the soft-failure data supports the
> graceful degradation hypothesis of better
> performance being associated with smaller
> changes in the controlled element dynamics.
> This was also true for the maximum error
> peaks of the hard-failures.

> Some of the hard-failure data are inconclusive.

> There was no evidence to support a hypothesis
> contrary to that of graceful degradation being
> associated with smaller changes in the controlled
> element characteristics.

Other trends were noted in the data relating to training and fatigue,
specifically:

> As the subjects became more experienced, the
> degradation in performance following a failure
> became less pronounced, which tended to diminish
> differences between configurations.

> Minor fatigue was evidenced in some of the data
> which showed increases in the asymptotic level
> of error following failure as the end of a day's
> runs was approached. It was not universal, and
> whether it increased more for one configuration
> than another was not evident.

The effects of fatigue, attention, motivation, etc., need to be
investigated more carefully since they are important variables in
this problem area. It was beyond the scope of this program, however,
which concentrated on the highly trained, attentive, and rested
subject.

The preceding results have emphasized system performance and pilot
adaptation following failure. A more subtle aspect of graceful
degradation involves modification in prefailure pilot adaptation
to obtain improved performance immediately following augmenter

failure. Two types of prefailure pilot control action were observed which were not only not required by the configuration being flown at the time, but were slightly detrimental to the control of the prefailure configuration. They did result in improved control immediately after the augmenter failed. The first involved the pilot's using a small amount of rudder control with Configuration A, and the second involved using an aileron-to-rudder crossfeed with Configuration B. Both of these situations were discussed in Subsection B along with the other experimental results. This pilot response phenomenon has been dubbed "conditional adaptation," because it is conditioned or influenced by a future event which is defined probabilistically. There is considerable evidence of conditional adaptation in the data, and further research is needed to relate the adaptation to the probability and severity of failure.

2. Digital Analysis

Digital analyses were made for each type of failure to obtain average results as a function of time. The tape recorded data were digitized at 0.1 sec intervals and computations were made from 10 sec before the failure to 20 sec after the failure. Five runs were selected for analysis for hard- and soft-failures with each of the three configurations (30 runs in all). Each set of five runs formed an ensemble, and averages were made within each ensemble to obtain

- Time-varying mean (at 0.1 sec intervals)
- Time-varying standard deviation (at 0.1 sec intervals)
- Time-varying autocorrelation function (at 1.0 sec intervals)

The computational procedures and equations are given in Appendix C. This was done for the following signals for each run:

- Pilot's rudder output
- Pilot's aileron output
- Displayed yaw rate (error)

26

These calculations over an ensemble produce average results which show gross trends, but they obscure fine detail in the data. Hence, they complement (rather than replace) the preceding manual analysis which in effect considers typical properties of the fine detail.

The yaw rate standard deviation (σ_r) is most pertinent to the question of graceful degradation. For soft-failures the mean value of yaw rate will approach zero as the number of runs in the ensemble increases. However, the standard deviation from the mean is an indication of the yaw rate within a given run. In particular, differences in the magnitude and duration of variability from the mean just after failure for different configurations would be an indication of relative degradation of performance (increased error).

Figure 44 shows the time variation through failure of the yaw rate standard deviation for soft- and hard-failures with Configurations A and C.

Figures 44(a) and (b) are plots of 3 sec averages of σ_r for the period from 10 sec before a soft-failure to 20 sec after the failure. Figure 44(a) shows that with Configuration A there is a region of yaw rate just after a soft-failure which is higher than that in either the prefailure or postfailure steady state. This indicates a period of degraded performance. Figure 44(b) shows that such a situation does not occur with Configuration C (for soft-failures) where the yaw rate appears to increase slowly and monotonically to the postfailure steady-state level. It is noted that this result is consistent with that from the manual analysis where no transition region could be identified for soft-failures from Configuration C.

For hard-failures the results are not as clear. Figures 44(c) and (d) are 3 sec averages of σ_r versus time for hard-failures. For this case both Configurations A and C show a transient increase in σ_r following failure, with the peak value of σ_r for "C" a little bigger than that for "A". The fact that "C" is not considerably better than "A" is probably a result of the hardover transient which causes a large error to occur regardless of the change in the dynamics. This is consistent with the single-axis results, and suggests that (for hardovers) graceful degradation relates more to a question of how bad are the postfailure dynamics than to any relative differences in prefailure and postfailure dynamics.

27

D. TRANSITION RESPONSE MODEL

Considerable insight into the transition model for multiple-loop
situations derives from the results of subsection B, above. The
principal new aspects are the pilot's use of crossfeed and the effect
of conditional adaptation of the pilot's prefailure dynamic response.
Additional understanding of the numerical parameters in the model are
available from digital analyses. These modelling considerations are
reviewed below.

Predictions were made of the multiple-loop transition response prior
to the experiments, based on the prior single-loop results and models
(Refs. 6, 7, and 10). Quasi-linear describing functions were used
for the pre- and postfailure steady state. Time optimal control of yaw
rate was assumed during the nonlinear phase, and response predictions
were made. These time optimal predictions are detailed in Appendix B
and illustrated in the phase plane of Fig. 45. Preliminary analyses in
the course of the experiment showed, however, that the original predictions
for the steady-state phases were substantially in error due to the pilot's
use of crossfeed and conditional adaptation. These findings were confirmed
by mechanizing an analog version of the pilot and adjusting forward loop
and crossfeed gains so that the error envelopes (for example) matched the
pilot data. As a result, these original steady-state predictions are not
included; and the loop closures shown subsequently are based to some extent
on the current results. Hence, they are interpretive rather than predictive.

The assumed and apparent form of the pilot/aircraft/augmenter system
is given in Fig. 46. Pilot control of yaw rate and bank angle is given
by Y_r and Y_φ, respectively. The pilot crossfeed is Y_{CF}. The gust
disturbance input is denoted by β_g. The effective controlled element
for yaw rate control (in steady state) is such that the pilot's adaptation
should be (per Ref. 7) a pure gain plus time delay, i.e.,

$$Y_r = \frac{\delta_{r_r}}{r} \doteq K_r e^{-\tau_r s} \tag{1}$$

28

The predicted form for bank angle control involves a small amount of lead equalization to cancel the roll subsidence time constant, T_R, giving:

$$Y_\varphi = \frac{\delta_a}{\varphi} \doteq K_\varphi (T_R s + 1) e^{-\tau_\varphi s} \qquad (2)$$

The crossfeed is assumed to be a pure gain (based on Ref. 10 data), and of sufficient magnitude to make $\omega_\varphi \doteq \omega_d$, that is:

$$Y_{CF} \doteq \frac{\delta_{r_{CF}}}{\delta_a} \doteq K_{CF} \qquad (3)$$

In addition to these quasi-linear operations the pilot produces remnant which can be thought of as an additive noise injected at the outputs of Y_r and Y_φ.

Time-varying power spectra were computed for pilot rudder output, δ_{r_p}, aileron output, δ_a, and the system yaw rate, r, as described in Appendix C. These were used to estimate the magnitude of Y_r. From Fig. 46 it is seen that:

$$\delta_{r_p} = -Y_r r + Y_{CF}\delta_a + \text{remnant} \qquad (4)$$

If the signals in the system are cross-correlated with the gust input, then the cross-spectra between the gust input and the pilot's rudder output is:

$$\Phi_{\beta_g \delta_{r_p}} = -Y_r \Phi_{\beta_g r} + Y_{CF}\Phi_{\beta_g \delta_a} \qquad (5)$$

This can be rearranged to give

$$Y_r = \frac{-\Phi_{\beta_g \delta_{r_p}} + Y_{CF}\Phi_{\beta_g \delta_a}}{\Phi_{\beta_g r}} \qquad (6)$$

If the crossfeed, Y_{CF}, is a pure gain, then it is a simple matter to compute Y_r using cross spectra and Eq. 6. An approximation to $|Y_r|$ was obtained by using the available power spectra in place of the cross spectra.* Of course, the presence of any pilot remnant reduces the accuracy of the estimate and phase angle information is not available.

The amplitude ratio of Y_r was computed via this technique using 1 sec time averages of the power spectra. This gave $|Y_r|$ as a function of time as well as frequency with one data point per second. Only the two lowest frequency points of the spectra were used. Plots of $|Y_r(t)|$ from 10 sec before failure to 15 sec following failure were made for soft-failures of all three prefailure configurations. These are presented in Figs. 47 to 49, and the approximate steady-state results are summarized below. For any given configuration the data

CONFIGURATION	APPROXIMATE $|Y_r|$	
	dB	linear
A	−5	0.55
B	2.5	1.3
C	4	1.6
E	3	1.4

show a constant amplitude ratio (gain) for frequencies up to about 9 rad/sec. The ratios of pilot gains for the various configurations are:

$$E : C \ = \ 1 : 1.1$$
$$E : B \ = \ 1 : 0.9$$
$$E : A \ = \ 1 : 0.4$$

For comparison, the ratios for the pilot models estimated via Ref. 15 were:

$$E : C \ = \ 1 : 0.8$$
$$E : B \ = \ 1 : 0.8$$
$$E : A \ = \ 1 : 0.2$$

---

*Although preferred, the cross spectra require several times as much computation; an effort that was beyond the scope of this program.

The fact that E:C was greater than E:B in the data is attributed to the crossfeed. The present ratios based on power spectral estimates were all higher than the Ref. 7 results derived from cross spectra and this is attributed to the presence of remnant.

The preliminary estimates for the steady-state loop closures were revised based on these spectral results and the observations of sub-section B. The pilot yaw rate loop closures for Configurations A, B, C, and E are given in Figs. 50−52, respectively. Configurations B and C are the same because of the use of compensating crossfeed in the latter. The pilot closures for this "outer" roll loop for A, B, C, and E are given in Figs. 53−55. Again, B and C are combined. The estimated parameters from Figs. 50−55 are summarized in Table IV.

The pilot model for the hard-failures can be summarized in the following way (see the block diagram of Fig. 46). Prior to failure the pilot's yaw rate control is $\delta_{rr_1} = K_{r_1} e^{-\tau_r s} r$ (a pure gain with time delay). He may also use a crossfeed of rudder proportional to aileron deflection, depending on the prefailure dynamics. It is assumed that the pilot will use just enough crossfeed to give $\omega_\varphi/\omega_d = 1.0$. His bank angle control is $\delta_a = K_\varphi (T_R s + 1) e^{-\tau_\varphi s} \varphi$.

The increased speed of the turn needle at $t = t_0$ signals a hardover failure.* After his time delay, τ_F, the pilot responds in a nonlinear manner; that is, at time $t_1 = t_0 + \tau_F$ he applies a temporary feedforward rudder step of magnitude δ_{r_0} to bring the yaw rate back to a level that he can maintain via linear control. When the yaw rate returns to this lower level, he removes the rudder step. At time $t_2 = t_0 + \tau_F + T$ the pilot's yaw rate control becomes $\delta_{rr_2} = K_{r_2} e^{-\tau_r s} r$ and he uses an aileron-to-rudder crossfeed such that $\delta_{r_{CF}} = K_c \delta_a$.

After the failure transient the pilot does not adapt immediately to the postfailure dynamics. He may make a rapid change in the _form_ of his adaptation, but there is a gradual adjustment period as he brings the errors down to some asymptotic level. Thus, during the adjustment

---

*These times are defined in Fig. 37.

TABLE IV

SUMMARY OF ESTIMATED LOOP CLOSURE PARAMETERS

LOOP	PILOT FORM	CONFIG.	τ_r or τ_φ (sec)	T_R (sec)	K_r or K_φ	PHASE MARGIN (deg)	GAIN MARGIN (dB)	ω_c $\left(\dfrac{\text{rad}}{\text{sec}}\right)$	REMARKS
Yaw Rate $\dfrac{r}{\delta_r}$	$K_r e^{-\tau_r s}$	A	0.15		-0.2	90	26	0.018	A very low gain closure
		B and C	0.15		-0.8	73	13	3.6	A compromise between a very sensitive root locus and a real root at too low a frequency
		E	0.15		-1.0	47	10	4.1	This closure gave a maximum phase margin
Crossfeed	K_c	C			-1.25				Assumed to make $\omega_\varphi = \omega_d$
		E			-0.625				
Bank Angle $\dfrac{\varphi}{\delta_a}$	$K_\varphi(T_R s + 1)e^{-\tau_\varphi s}$	A	0.20	0.20	-0.3	60	10-1/2	2.6	These loops looked like a K/s when the pilot used a crossfeed and a lead; they were closed to give about a 60 deg phase margin according to Ref. 7
		B and C	0.20	0.20	-0.3	60	10-1/2	2.6	
		E	0.20	0.20	-0.3	57	10-1/2	2.8	

Note: The values of τ_r and τ_φ were based on Ref. 7.

phase the pilot is acting as an adaptive control system. For numerical modelling purposes this adjustment phase is sometimes neglected and the postfailure steady-state phase is assumed to follow the nonlinear phase immediately.

The pilot model for soft-failures differs from the hard-failure model only in the deletion of the nonlinear phase of transition. This was the case with the current simulation because the retention phase dynamics were not highly unstable, and errors did not build up rapidly enough to motivate the pilot to resort to nonlinear control. This was partly due to conditional adaptation which resulted in pilot use of rudder even when it was not required for good steady-state performance.

In conclusion, the basic results of the single-loop model regarding the transition phases and their form still apply. The principal refinements relative to the multiple-loop case can be summarized as follows.

- The pilot uses crossfeed to decouple and simplify the yaw rate and bank angle control tasks

- The pilot uses conditional adaptation to improve failure performance

- The failure only affects the axis of control in which it occurs

- The pilot produces a nonlinear step feedforward to cancel the hardover

- The soft-failures did not exhibit a nonlinear control phase, and the retention phase was considerably longer

These results are combined with the single-loop results in Section V.

33

SECTION IV

IMPLICATIONS FOR FLIGHT CONTROL SYSTEM DESIGN

The combined results of the single- and multiple-loop experiments lead to several considerations pertinent to flight control system design. These are summarized in the following paragraphs.

The graceful degradation hypothesis is supported by the experimental results. Therefore, a flight control system design that gives less change in effective controlled element following a failure will give better transition performance.

The transition performance with hardover failure was relatively invariant with the amount of change in the dynamics at failure. The performance with soft-failures tended to vary as a function of the change in dynamics, but it was generally better than that for hardovers. The relative invariance of the hardover failures is a consequence of the retention times being about the same due to alerting. It suggests that if alerting can be "designed" into (or accompany) soft-failures, performance will be improved.

For soft-failures the crux of the entire graceful degradation situation lies in the closed-loop system stability during the retention phase; that is, the stability of the prefailure pilot model, Y_{p_1}, controlling the postfailure vehicle, Y_{c_2}. If $Y_{p_1}Y_{c_2}$ is stable, closed-loop, then a critical situation generally does not develop after a failure.

A flight control (e.g., stability augmentation) system should be designed to keep the pilot in the loop prior to a failure rather than to allow (or require) him to merely monitor the controller/vehicle system activity. This might be accomplished by giving the pilot the task of controlling a simultaneous model of the actual system. One payoff for this is obvious — the pilot will have a shorter retention period. For example, a pilot who has his feet on the pedals at the time of failure because he is "in the loop" will have a shorter time delay prior to initial rudder input than a pilot who is merely an observer and has his feet on the floor. For some kinds of failure a long retention period or delay would be catastrophic.

A pilot tends to use conditional adaptation, which means that his prefailure control activity is a function of the probability of failure and the severity of the transition. If $Y_{p_1}Y_{c_2}$ closed-loop (or Y_{c_2} alone) presents difficult control characteristics, then the pilot will anticipate a failure by modifying his prefailure adaptation, Y_{p_1}, to improve $Y_{p_1}Y_{c_2}$. This will be something other than the stationary values appropriate for Y_{c_1}. Consequently, a control system should not only make prefailure flight control available, but it should be designed so that considerably improved $Y_{p_1}Y_{c_2}$ stability is possible with simple modifications in prefailure control activity (as was the case in the multiloop experiments).

When Y_{c_2} was very unstable, hardovers were indistinguishable in performance from soft-failures. Conversely, when the change in controlled element was small, and/or Y_{c_2} was good, the hardovers were substantially different from the soft-failures because the response to the transient was dominant.

A point to consider along with flight control system design is pilot training. During the training of pilot subjects in the experimental tasks, performance following a failure improved rapidly as the number of practice runs increased. Even hardover failures gave little performance degradation when encountered regularly. Any failure can be difficult if it represents a significant change from recent experience (as was found during early failure practice runs following only steady-state control of each configuration). The implication of this experience is that pilots should have frequent refresher training to keep them current with regard to flight control system failure situations. As an example, it might be desirable for the pilot to practice a few failures enroute (on a simulated model) prior to an instrument landing.

SECTION V

COMPOSITE PILOT TRANSITION MODEL

A composite pilot model for step changes in controlled element dynamics has resulted from the single- and multiple-loop experiments. These experiments were run with skilled subjects in practiced situations. The salient features of the model can be expressed in terms of a single-loop tracking task. The single-loop model is also applicable to the failed loop in a multiple-loop situation if only one loop involves a significant change in the controlled element dynamics.

As might be expected, the composite model is quite like the single-loop model in Section II. It divides the transition into phases with respect to time, each of which has certain distinguishing characteristics:

- Prefailure steady-state; stationary compensatory tracking, with the possible use of conditional adaptation

- Retention; prefailure pilot describing function plus the postfailure controlled element dynamics operating closed-loop

- Nonlinear control; large control actions (sometimes time-optimal) which stabilize the system and reduce the error to some acceptable level

- Adjustment phase; pilot describing function has same form as that for postfailure steady-state phase, but parameter values are being adjusted to minimize system error

- Postfailure steady-state; stationary compensatory tracking

The retention phase starts at the failure. Its end is defined as the point in time when an abrupt change in pilot control output begins. It is most evident in transitions where the nonlinear control phase can be clearly seen.

The nonlinear control phase (if present) starts at the end of retention and continues until the pilot control output has been reduced (approximately) to within the postfailure steady-state envelope. Time-optimal control with fixed bang amplitudes is an appropriate limiting case. The nonlinear control phase may include a learned response that is merely triggered by the failure (such as a feedforward step). For soft-failures with some systems the

36

nonlinear phase is not present. It is present only when required, i.e., when linear control is inadequate to maintain reasonable system errors.

The postfailure steady-state phase starts at the end of the nonlinear control phase, to a first approximation. In some cases, the envelope of system error decays gradually following the nonlinear control phase. This corresponds to an adjustment phase wherein the pilot's steady-state adaptation is being achieved by a relatively long term (e.g., $5-10$ sec) optimization process.

Block diagrams of the various phases of the model are given in Fig. 60. The several combinations of pilot control during the nonlinear phase are described in Table V, together with a summary of known applicability.

On the basis of the experimental results it is apparent that the general form of model given in Ref. 6 is still valid with a few extensions and modifications:

- Numerical estimates are now available for the retention duration, when this phase exists.

- Hardover failures have shorter retention durations than soft-failures, except for the most difficult postfailure controlled elements where there is no difference.

- The pilot compensates for failure transients (hardovers, etc.) during the nonlinear control and postfailure steady-state phases. In some cases this appears to be a feedforward signal which cancels the failure transients, although this was not apparent for the most difficult postfailure controlled elements. An alternative is to treat the transient as an initial condition to nonlinear control, and then produce a trim bias in post-failure steady state.

- Time-optimal control alone during the nonlinear phase is still a valid idealization for the soft-failures, as an attainable limiting case. However, some suboptimal control mode is more typical.

- Postfailure steady-state error characteristics were generally larger than that predicted by an optimized quasi-linear model. This suggests that any adjustment (optimization) phase is relatively long term and does not end immediately following the nonlinear phase.

- Prefailure conditional adaptation may be present. This means that the pilot may use an adaptation prior to failure which is not a steady-state optimum but which will improve the system performance immediately after failure (such as a modified gain or a crossfeed).

37

TABLE V

PILOT CONTROL FORM DURING NONLINEAR PHASE OF TRANSITION

TYPE OF PILOT CONTROL MODEL[*]	WHEN APPROPRIATE
Linear controller alone	This form of control is not applicable to this phase because it represents a case in which there is <u>no</u> nonlinear phase present. (An example of a case where no nonlinear phase occurred was the soft-failure with the multiple-loop Configuration C.)
Nonlinear controller alone	This is appropriate for hard- <u>and</u> soft-failures when $Y_{p_1}Y_{c_2}$ is unstable, such as for $K \rightarrow K/s^2$.
Linear controller plus feedforward controller	This is appropriate for hardover failures when $Y_{p_1}Y_{c_2}$ is well behaved (stable), such as with the multiple-loop Configuration C. For this case the signal fed forward is likely to resemble a delayed (due to retention) replica of the hardover transient.
Nonlinear controller plus feedforward controller	Although this may appear appropriate to the hardover case with unstable $Y_{p_1}Y_{c_2}$, the response is probably indistinguishable from that of the nonlinear-controller-alone situation. Therefore, whichever model is easier to mechanize is appropriate.

[*]Combinations of controllers not listed are inappropriate models.

SECTION VI

CONCLUSIONS AND RECOMMENDATIONS

Single-axis and multiple-axis compensatory tracking task experiments were carried out with skilled subjects. The controlled element dynamics were changed abruptly during the tracking, and the pilot's response was recorded and analyzed.

A. CONCLUSIONS

The experimental results indicate that the graceful degradation hypothesis is valid. Thus, an improvement in tracking performance can be expected during a transition in controlled element dynamics if the change in dynamics is diminished. More detailed implications for design are given in Section IV.

A previous model for human pilot dynamic response during controlled element transitions (Ref. 6) was verified and extended. The verification shows that the following transition response phases do exist in general:

- Prefailure steady-state
- Retention
- Nonlinear control
- Postfailure steady-state

The extensions relate to the existence of hardover (deterministic) signals in the system and occur in the nonlinear control and postfailure steady-state phases. Amplifying details are given in Section V.

B. RECOMMENDATIONS

The study of pilot response to controlled element transitions is far from complete. Areas where additional work is required are summarized below.

Motion cues. The effect of motion cues on transition response should be examined in order to quantify the differences between fixed- and moving-base.

Operator loading. Pilot response and performance with simultaneous transitions in more than one control loop should be studied. The effect of additional tasks (e.g., lateral and longitudinal control) on pilot response (with a transition in one loop) should be considered.

39

Conditional adaptation. The effect of transition probability and severity on the prefailure pilot adaptation and response should be investigated.

Display transitions. Important changes in the effective controlled element dynamics can occur via the display. Examples include the transition from IFR to VFR at breakout in an instrument approach, and the use of head-up and head-down displays in terrain-following or air-to-ground attack. Another class involves transitions from pursuit to compensatory display content. These should be studied.

REFERENCES

1. Sheridan, Thomas B., *Time-Variable Dynamics of Human Operator Systems*, AFCRC-TN-60-169, Mar. 1960.

2. Sadoff, Melvin, *A Study of a Pilot's Ability to Control During Simulated Stability Augmentation System Failures*, NASA TN D-1552, Nov. 1962.

3. Young, Laurence R., David M. Green, Jerome I. Elkind, and Jennifer A. Kelly, *The Adaptive Dynamic Response Characteristics of the Human Operator in Simple Manual Control*, NASA TN D-2255, Apr. 1964.

4. Elkind, Jerome I. and Duncan C. Miller, *Adaptive Characteristics of the Human Controller of Dynamic Systems*, AFFDL-TR-66-60, July 1966.

5. Elkind, Jerome I. and Duncan C. Miller, *On the Process of Adaptation by the Human Controller*, Paper Presented at Third Congress of the International Federation of Automatic Control, London, 20-25 June 1966.

6. Weir, David H., and Anil V. Phatak, *Model of Human Operator Response to Step Transitions in Controlled Element Dynamics*, NASA CR-671, Jan. 1967.

7. McRuer, Duane, Dunstan Graham, Ezra Krendel, and William Reisener, Jr., *Human Pilot Dynamics in Compensatory Systems: Theory, Models, and Experiments with Controlled Element and Forcing Function Variations*, AFFDL-TR-65-15, July 1965.

8. Washizu, Kyuichiro and Katsuyuki Miyajima, "Controllability Limit of a Human Pilot," *AIAA Journal*, Vol. 3, No. 5, May 1965, pp. 941-947.

9. Elkind, J. I., *Human Operator Response to Changing Controlled Element Dynamics*, Bolt Beranek and Newman Inc., May 1963.

10. Stapleford, R. L., D. T. McRuer, and R. Magdaleno, *Pilot Describing Function Measurements in a Multiloop Task*, NASA CR-542, Aug. 1966.

11. Landphair, Lee C., *Stability and Control of the X-14 VTOL Research Airplane*, Bell Aircraft Corp., Rept. No. 68-978-002, 5 Sept. 1958.

12. Pauli, Frank A., *A System to Vary the Stability and Control of a Deflected-Jet Fixed-Wing VTOL Aircraft*, AIAA Paper No. 64-194, May 1964.

13. Rolls, L. Stewart, and Fred J. Drinkwater, III, <u>A Flight Determination of the Attitude Control Power and Damping Requirements for a Visual Hovering Task in the Variable Stability and Control X-14A Research Vehicle</u>, NASA TN D-1328, May 1962.

14. Pauli, Frank A., Daniel M. Hegarty, and Thomas M. Walsh, <u>A System for Varying the Stability and Control of a Deflected-Jet Fixed-Wing VTOL Aircraft</u>, NASA TN D-2700, Mar. 1965.

15. Hill, J. A., <u>A Piloted Flight Simulation Study to Define the Handling Qualities Requirements for a Lunar Landing Vehicle</u>, North American Aviation Rept. No. NA 62H-660, 13 Sept. 1962.

16. Greif, Richard K., Emmett B. Fry, Terrence D. Gossett, and Ronald M. Gerdes, "Simulator Investigations of Various Control Systems for VTOL Aircraft," <u>Conference on V/STOL and STOL Aircraft</u>, Ames Research Center, Moffett Field, California, NASA SP-116, Apr. 4-5, 1966.

17. Von Alven, William H., J. M. Evans, W. B. Reese, <u>Failure Rates and Failure Modes of Small Rotary Electrical Devices</u>, ARINC Res. Corp. Pub. No. 160-2-269R, Nov. 1961.

18. Tribken, E. R., and S. J. Sandler, <u>Final Technical Report on the Principles of Adaptive Reliability</u>, Sperry Rand Report No. L5-1262-0205, Mar. 1963.

19. <u>Preliminary Investigation of the Reliability and Possible Malfunctions of the Ryan Model 69 Aircraft Flight Control System</u>, Control Specialists, Inc. Rept. CSI-4, 13 Sept. 1954.

20. Evans, J. M., <u>Failure Rates and Failure Modes of Airborne Rotary Devices, Relays, and Other Electrical Parts</u>, ARINC Res. Corp. Pub. 204-1-336, 31 Dec. 1962.

21. Ashkenas, I. L., <u>A Consolidation of Lateral-Directional Handling Qualities</u>, AIAA Paper No. 65-314, July 1965.

22. Ashkenas, Irving L., and Duane T. McRuer, <u>Approximate Airframe Transfer Functions and Application to Single Sensor Control Systems</u>, WADC TR 58-82, June 1958.

23. Johnston, D. E., and D. T. McRuer, <u>A Summary of Component Failure Rate and Weighting Function Data and Their Use in Systems Preliminary Design</u>, WADC TR 57-668, Dec. 1957.

24. Johnston, D. E., and D. H. Weir, <u>An Assessment of Operational and Cost Tradeoff Factors for a Typical High Performance AFCS</u>, STI TR 119-1, June 1962.

25. Johnston, Donald E., Keith A. Ferrick, and Edward L. Alexander, A Compilation of Component Field Reliability Data Useful in Systems Preliminary Design, WADC TR 60-330, Supplement 1, AD 270-462, Nov. 1961.

26. Rabinowitz, Charles and S. S. Patti, Self-Contained Electronic Flight Control System, Final Report No. 4, Kaman Aircraft Corp. Rept. G-166, 6 Oct. 1961.

27. Bullard, E. C., F. E. Oglebay, W. H. Munk and G. R. Miller, BOMM: A System of Programs for the Analysis of Time Series, Univ. of California, La Jolla, Jan. 1966.

28. Bendat, Julius S. and Allan G. Piersol, Measurement and Analysis of Random Data, John Wiley and Sons, Inc., N. Y., 1966.

29. Blackman, R. B. and J. W. Tukey, The Measurement of Power Spectra, Dover Publications, Inc., N. Y., 1958

APPENDIX A

DETAILS OF THE SINGLE-AXIS EXPERIMENTS

VEHICLE SELECTION AND DESCRIPTION

The stated objective of the first experimental series was to study transitions in a single-axis compensatory tracking task among controlled elements of the approximate form K, K/s, and K/s^2. It appeared that roll control in a hovering VTOL with either rate or rate plus attitude augmentation would provide a means of obtaining these controlled elements in the frequency range of interest, and would give a realistic experimental situation in terms of control system characteristics and failure modes.

A number of vehicles were considered including the Bell X-14A, the LTV XC-142, and a helicopter. The selection criterion was based on the availability of airframe dynamic data, control system data and diagrams, failure data, and loop closures and system surveys. The Bell X-14A (roll axis) was found to be most suitable on balance, and was chosen as the subject vehicle.

The X-14A is described in Ref. 11. The roll dynamics of the basic airframe in hover are approximately a pure inertia, neglecting the small aerodynamic effects. Reaction control jets at the wingtips provide for roll control.

FLIGHT CONTROL SYSTEM DESCRIPTION

A variable stability control system (described in Refs. 12 – 14) has been added to the X-14A to permit variations in the control power and roll rate damping. It was mechanized in the simulation to provide a roll-rate damping inner loop. It consists of a rate gyro and associated electronics driving an electric servomotor which positions the reaction nozzles. It was mechanized in series with the pilot for simulation purposes, although the airplane has it in parallel.

A roll attitude feedback system operating in series with the pilot's control output was also desired in order to obtain an approximately pure

gain controlled element over a nominal frequency range. Such a system was synthesized analytically for purposes of this study using a vertical gyro and associated electronics driving the nozzle servo. The roll rate feedback functioned as an inner loop. The control system mechanization is shown in block diagram form in Fig. 1.

Selection of the sensor, actuator, and airframe dynamics completed the specification of the augmentation system. The characteristics of the rate gyro installed in the X-14A were not known. Representative transfer functions for the dynamic lags of both gyros were chosen, consistent with the assumed constraints of light weight and low cost. These are shown in Fig. 2. The nozzle servo dynamics were estimated from step response data for the X-14A system given in Ref. 13. A second-order form was used for simplicity, although the overshoot characteristics suggest that a third order might have been a slightly better approximation at high frequency. The airframe was a simple inertia. A roll power of 0.8 rad/sec^2 was selected from the data of Ref. 13 to correspond with good pilot opinion. The effect in the roll axis of gyroscopic coupling due to the engines was assumed to be negligible.

Gains shown in the rate and attitude loops of Fig. 2 were set as high as possible consistent with sensor and actuator lags. The object was to select the broadest practicable frequency region of what was effectively a pure gain controlled element with both loops operating, and an integration, K/s, controlled element with only the inner loop. Note that this use of high gains was not necessarily consistent with the rate and attitude loop gains which yielded optimum pilot opinion in a series of hover task simulation studies where the task was to either hover or perform maneuvers (Refs. 13, 15, 16). The feedback loop gains shown in Fig. 2 resulted in the effective controlled element dynamics (near the region of crossover) given in Table A-I. Some of the higher frequency lags have been omitted in Table A-I, because they have a negligible influence on pilot control activity.

FAILURE CHARACTERISTICS

Performance of the transition/degradation experiments involved failing the augmentation system shown in Fig. 1 in various ways and observing

EFFECTIVE CONTROLLED ELEMENT DYNAMICS
FOR THE SINGLE-AXIS STUDY

AUGMENTATION	EFFECTIVE CONTROLLED ELEMENT
Rate plus attitude	$\dfrac{1.72}{\left[s^2 + 2(.6)(5.1)s + (5.1)^2\right]}$
Rate only	$\dfrac{320}{s(s + 18.6)\left[s^2 + 2(.66)(10.4)s + (10.4)^2\right]}$
Attitude only	$\dfrac{.715}{\left[s^2 + 2(-.2)(3.3)s + (3.3)^2\right]}$
None	$\dfrac{.8}{s^2}$

pilot response. To do this in the most realistic way, it was necessary
to know the relative failure rates and mode of failure of the various
components in the controlled element.

The relative failure rates were found by first establishing the
absolute failure rates from typical reliability data, and then noting
the fractional contribution of each component. Several in-house sources
of reliability data yielded the failure rate estimates of Table A-II.
The nozzle servo is included in Table A-II to show its contribution to
the total system failure rate. It was not failed during the simulation,
of course, since it operates in a serial way on the total pilot output
as shown in Fig. 1, and its failure would have resulted in complete
loss of control.

A detailed investigation of the mode of failure of the augmentation
system components was made, using information from several sources including
Refs. 17 through 20. The results are summarized in Table A-III. The
component output at time of failure is shown as one of several types of steps
or as a ramp. When the probability of a given failure mode is greater than
90 to 95 percent, it is shown as 100 percent in Table A-III for simplicity.

TABLE A-II

COMPONENT FAILURE RATES

COMPONENT	FAILURE RATE (PER 10^6 HRS)	DATA SOURCE
Control Console: Connector　　　1 Wire wound pot 20 Rotary switch　35	56	Ref. 23
Power Supply	120	Ref. 24
Nozzle Servo: Motor, tach., 　gear train　　　30 Position FB pot　20 Magnetic amplifier 10 Summing amplifier　30	90	Refs. 17, 25
Preamplifier (each)	30	Ref. 24
Rate Gyro	100	Ref. 24
Vertical Gyro	400	Ref. 24

TABLE A-III

MODES OF FAILURE FOR THE SINGLE-AXIS STUDY

COMPONENT	OUTPUT AT TIME OF FAILURE	PROBABILITY OF OUTPUT
Control Console	Step to zero feedback in both loops	100%
Power Supply	Step to zero feedback in both loops	100%
Rate Loop Preamplifier	Step to zero feedback in rate loop	100%
Attitude Loop Preamplifier	Step to zero feedback in attitude loop	100%
Rate Gyro	Hardover step in rate loop	100%
Vertical Gyro	Hardover step in attitude loop	60%
	Ramp output in attitude loop	40%

47

Combining the relative failure rates from Table A-II with the probability of mode of failure in Table A-III yielded the set of transition/degradation situations of Table A-IV. These situations defined the procedure for the simulation/experimental series. The presentation sequence of the situations was randomized and they occurred with the probabilities shown in Table A-IV.

TABLE A-IV

FAILURE SITUATIONS IN THE SINGLE-AXIS STUDY

SITUATION	PROBABILITY OF OCCURRENCE
Both loops fail to zero feedback	24%
Rate loop fails hardover	14%
Attitude loop fails hardover	32%
Attitude loop fails ramp	22%
Rate loop fails to zero feedback	4%
Attitude loop fails to zero feedback	4%

PILOT TRANSITION RESPONSE PREDICTIONS

Predictions were made prior to the experiments of the expected pilot response before, during, and after the failure. This involved application of the original pilot transition response model derived in Ref. 6 and summarized in Section II of the main text.

The first step in response prediction was to estimate the quasi-linear pilot describing functions under the stationary conditions existing before and after the failure. The various controlled elements were given in Table A-I. The pilot describing functions were estimated using the modeling techniques of Ref. 7, and these plus the characteristic closed-loop roots are shown in Table A-V. A compact notation for polynomial factors is used in this table and elsewhere in the report, i.e.:

$$\text{denote } (s + a) \text{ by } (a)$$
$$\text{denote } \left[s^2 + 2\zeta\omega s + \omega^2\right] \text{ by } \left[\zeta, \omega\right]$$

TABLE A-V

STEADY-STATE CHARACTERISTICS OF THE SINGLE-AXIS SYSTEM

AUGMENTATION	EFFECTIVE CONTROLLED ELEMENT	PILOT DESCRIBING FUNCTION	CHARACTERISTIC* CLOSED-LOOP ROOTS	REMARKS
Rate Plus Attitude	$\dfrac{1.72}{[.6, 5.1]}$	$\dfrac{8(3.0)}{(.05)}e^{-.4s}$	$(1.87)[.16, 3.6][.86, 13.4]$	
Rate Only	$\dfrac{320}{(0)(18.6)[.66, 10.4]}$	$17.25e^{-.24s}$	$[.15, 3.4][.57, 14.6][.95, 25]$	
Attitude Only	$\dfrac{.715}{[-.2, 3.3]}$	$-12.5e^{-.1s}$	$(13)(25.2)[.17, 1.54]$	K_p negative
		$6.25(.2)e^{-.1s}$	$(10.5)(67.3)[.51, 5.2]$	K_p positive
None	$\dfrac{.8}{(0)(0)}$	$4.05(.2)e^{-.39s}$	$(.213)(22.6)[.11, 3.76]$	Low frequency closed-loop root is cancelled by pilot's lead.

*Two closed-loop roots are due to the second-order Padé approximation to $e^{-\tau s}$.

The relatively high frequency dynamic lags due to the gyros and control nozzles were included in the loop closures of Table A-V, even though they are not shown in the effective controlled elements column or Table A-I. The steady-state describing functions and closed-loop dynamics define the "boundary conditions" on both sides of the transition response (as discussed in Section II).

The transition response of the pilot immediately following the failure contained two distinct phases, according to the original model in Section II. The first of these was the "retention phase" which usually lasted less than a second and involved the prefailure pilot (describing function) adaptation in control of the postfailure controlled element. The next phase of the transition response had been dubbed the "optimal control phase." It involved large, rapid, stick deflections to stabilize the system and reduce the accumulated error; often in a nearly time optimal manner for a single-axis fixed-base task.

Retention phase predictions were made by combining the closed-loop dynamics of the prefailure pilot (Y_{p_1}) and the postfailure controlled element (Y_{c_2}). The various failure situations are summarized in Table A-VI, together with the retention phase dynamics and characteristic closed-loop roots.

Comparing the closed-loop roots in Tables A-V and A-VI shows that each type of failure results in an unstable quadratic pair which dominates the initial response following failure and causes the system to diverge. This divergence in the displayed error allows the pilot to detect and (at least) partially identify the failure. He then switches to a mode of control which stabilizes the system and reduces the error.

Predictions of pilot response during the optimal control phase had been made in Ref. 6 using phase plane techniques; assuming the time optimal model to be valid. These predictions related more to "form" than to specific quantitative results; i.e., the minimum number of pilot stick reversals and the bang durations could be determined, but numerical values of the bang amplitudes and threshold levels for detection and switching to postfailure steady-state operation could not be predicted

50

TABLE A-VI

RETENTION PHASE DYNAMICS, SINGLE-AXIS STUDY

PREFAILURE AUGMENTATION	FAILURE (EFFECTIVE TRANSITION)	RETENTION PHASE LOOP DYNAMICS, $Y_{p_1}Y_{c_2}$	RETENTION PHASE CHARACTERISTIC CLOSED-LOOP ROOTS*
Rate	Rate Loop, $.16/s \rightarrow .8/s^2$	$\dfrac{13.8e^{-.24s}}{(0)(0)}$	$(10.8)[-.35, 3.5]$
	Attitude Loop, $.061 \rightarrow .16/s$	$\dfrac{2560(3.0)e^{-.4s}}{(0)(.05)(18.6)[.66, 10.4]}$	$(3.8)(19.5)[-.28, 1.96][.65, 11.7]$
Rate Plus Attitude	Both Loops, $.061 \rightarrow .8/s^2$	$\dfrac{6.4(3.0)e^{-.4s}}{(0)(0)(.05)}$	$(2.3)(6.0)[-.61, 2.6]$
	Rate Loop, $.061 \rightarrow \dfrac{.715}{[-.2, 3.3]}$	$\dfrac{5.72(3.0)e^{-.4s}}{(.05)[-.2, 3.3]}$	$(1.23)(3.6)[-.43, 3.6]$

*One closed-loop root is due to the first-order Padé approximation to $e^{-\tau s}$.

51

very precisely at that writing. As a result, no predictions other than those in Ref. 6 were made for this phase.

SIMULATION MECHANIZATION

The simulation was mechanized on GEDA analog computers in conjunction with a P-51 cockpit containing a center stick controller and a horizon line (inside-out) roll display. A random-appearing command input, φ_i, was used with a cutoff at 1.5 rad/sec. The flight control system was failed in various ways by the experimenter using switching logic. The failures were presented in a random sequence during the experiments with relative frequency derived from Table A-IV. The recorded data consisted of time histories of the various signals in the loop. Mean-square errors were measured to determine the training level of the subject. Amplifying details on the mechanization and setup are given in succeeding paragraphs.

The analog diagram is given by Fig. 3. It shows the switching, scaling, and cockpit connections. A hold circuit was used to terminate the problem if the roll motions become too large. A squared error circuit provided an error score which was used to measure the subject's performance.

The forcing function was an approximately Gaussian, random-appearing, roll command consisting of a sum of six equal amplitude sinusoids. The six input frequencies (in rad/sec) were: .157, .262, .393, .602, .969, and 1.49. They were chosen to be nonharmonically related, and to have their sum and difference frequencies nonharmonically related. The amplitudes were scaled to give an rms bank angle on the CRT display of 5 deg. Two additional sine waves were present in some of the experiments at 2.54 and 4.03 rad/sec, respectively. These had one-tenth the amplitude of the lower frequency components and their effect on the response characteristics was assumed to be negligible (in accordance with past experience).

A limiter was placed at the output of the automatic loops to restrict their authority following failure (relative to that of the pilot), thereby permitting the pilot to fly the failed vehicle and to produce a control bias to counter a hardover. The limit occurred at ±3 in. of equivalent pilot stick deflection (of the ±5 in. available). The hardover failures

resulted in a step bias equivalent to 1-1/2 in. of equivalent stick
deflection. The ramp also terminated at 1-1/2 in. equivalent stick
after 2 sec. The effective controlled element dynamics changed for
very large roll angles because of the limiter, and this occurred
occasionally during the hardover failure conditions (where a pilot
bias was required). This nonlinearity did not appear to have a sig-
nificant effect on the results of the experiments as they related to
transition models or the graceful degradation hypothesis.

SUBJECT BACKGROUND AND TRAINING PROCEDURES

The principal subject for the experiments (ROB) was a 33 year old
commercial pilot with 1700 hours of flight experience, including F-86D,
F-84F, F-102, and Boeing 707 aircraft. He is an engineering psychologist
who has participated in that technical capacity in other programs related
to human operator response and manual control displays. His duties in
connection with this study were strictly those of a pilot subject, however,
and he was not familiar with the experimental details, purposes, or any
anticipated outcomes. He had not had much prior experience as a subject
in simulated tracking tasks, and about 10 hours of practice (180 trials of
3 to 4 minutes) were used to familiarize him with the problem and to
obtain an asymptotic level of performance. One other subject (JDM) whose
describing function and performance had been measured in similar tasks
in the past was used occasionally during the training period in order
to help "calibrate" the principal subject.

Initial training consisted of practicing each of the various controlled
element dynamics as a stationary tracking task. The subject was told that
"he was controlling the roll degree of freedom in a hovering VTOL, to keep
the wings level, and to minimize the bank angle tracking error." He was
not told what the controlled element dynamics were nor what his control
technique should be. After an apparently asymptotic level of performance
with the stationary dynamics was obtained, the failure situations were
practiced. The subject was told "we are going to fail the FCS in various
ways, the failures will occur at random and without warning, and you will
not know what the failure is." The subject was not instructed in the

53

desired control technique, nor was he familiar with current models of pilot transition response.

It became apparent after about 6 hours (120 trials) of practice, that the subject's performance was poorer than that of other past subjects in similar stationary and failure situations, although a "stable" level of performance had been reached. Since it was apparent that he was not going to improve, steps were taken to ascertain his tracking "performance criteria," because this was a likely source of discrepancy. Questioning revealed that his technique was to: halt the upset (divergence), stabilize the aircraft at the resultant bank angle, and then return it to wings level. It appeared that he was giving considerable weight to minimizing bank angle rate, angular acceleration, and possibly control activity—not to bank angle error alone. Following a discussion with the subject of the implications of minimum mean-square error (and further practice) his performance improved significantly as measured by (1) mean-square error in stationary tasks, and (2) transition times following FCS failure. Furthermore, his performance was more comparable to that of other subjects in past experiments.

EXPERIMENTAL PROCEDURE

Following training, 160 experimental runs were made to obtain single-axis transition response data. This included 100 runs where the prefailure controlled element dynamics were approximately a gain (rate plus attitude augmentation of the vehicle) and 60 runs with K/s prefailure controlled element dynamics (rate augmentation only). The numbers and types of data runs are summarized in Table A-VII. The two different types of prefailure controlled element dynamics were not mixed in any given experimental session. For example, in an afternoon session involving 2 hours of experiments, the prefailure dynamics would always be either a gain or K/s (not a mixture). In addition, the order of presentation of the various failure situations was randomized.

Each experimental session began with a 10 to 15 minute warmup period consisting of both stationary tracking and failure situations. Each data run lasted 3 to 4 minutes, and the failure occurred at a random

time 1 to 3 minutes after the start. A one minute rest period was taken
between runs. After a series of runs lasting about 20 minutes the subject
was given a longer rest period where he got out of the cockpit. Typically,
15 to 20 runs were made in the course of a morning or afternoon. The cock-
pit cover was closed during the runs (the subject could see only the display)
to minimize distractions and alerting which might have been caused by actions
of the experimenter.

TABLE A-VII

SUMMARY OF SINGLE-AXIS EXPERIMENTAL RUNS

PREFAILURE AUGMENTATION	POSTFAILURE AUGMENTATION	FAILURE MODE	NUMBER OF RUNS
Rate $\left(Y_{c_1} \doteq \dfrac{K}{s}\right)$	None $\left(Y_{c_2} \doteq \dfrac{K}{s^2}\right)$	Soft	43
		Hard	17
Rate Plus Attitude $(Y_{c_1} \doteq K)$	Rate $\left(Y_{c_2} \doteq \dfrac{K}{s}\right)$	Soft	4
		Ramp	22
		Hard	32
	Attitude $\left(Y_{c_2} \doteq \dfrac{K}{|\zeta,\omega|} \; ; \; \zeta \text{ neg.}\right)$	Soft	4
		Hard	14
	None $\left(Y_{c_2} \doteq \dfrac{K}{s^2}\right)$	Soft	24

APPENDIX B

DETAILS OF THE MULTIPLE-AXIS EXPERIMENTS

VEHICLE SELECTION AND DESCRIPTION

The stated objective of the second experimental series was to study transitions in a multiple-axis compensatory tracking task. The task selected was that of lateral control of a fixed-wing aircraft. Certain dynamic characteristics of the airframe-plus-augmenter system were desired for this case in order to properly exercise the graceful degradation hypothesis. It was decided that a good lateral example would have the following properties.

(1) $\omega_\varphi/\omega_d > 1$, airframe alone

(2) ζ_d, $\zeta_\varphi < 0$, airframe alone

(3) Good $r \longrightarrow \delta_r$ augmenter loop

This gives a case that the pilot can and must fly with manual rudder plus aileron in the event of rudder-axis augmenter failure. The augmenter gain can be adjusted to give either optimum ζ_d' or just so-so ζ_d' before the failure, in order to examine the effect of differential Y_c. To obtain well-defined levels of relative degradation, rather unusual sets of vehicle dynamics and yaw-rate damper characteristics were required. As a result, the specific vehicle was a hybrid, with the yaw damper similar to that used in the F-106. The desired bare-airframe characteristics,[*] as defined in terms of the vehicle transfer function factors, are presented in Table B-1. Using the approximate factors in Ref. 22 along with these desired dynamic characteristics led to the set of stability derivatives given in Table B-2.

---

[*]With the exception of the dutch roll characteristics, these characteristics lead to good handling qualities (Ref. 21). The subsequent selections of control effectiveness values were also made to be as near optimum as possible.

TABLE B-I

BARE-AIRFRAME CHARACTERISTICS

PARAMETER	VALUE	REMARKS
$\dfrac{1}{T_s}$	$\doteq 0$	A neutrally stable spiral mode was desired.
$\dfrac{1}{T_R}$	5 sec^{-1}	Good rolling characteristics were desired.
$\dfrac{\omega_\varphi}{\omega_d}$	1.15	Bad Dutch roll characteristics were desired to force the pilot to close a yaw-rate-to-rudder loop.
ζ_d	$-.15$	An unstable Dutch roll was desired in order to make the control task difficult.
ζ_φ	$-.15$	
$\dfrac{\omega_r}{\omega_d}$	$.2$	This permitted a good $r \rightarrow \delta_r$ augmenter loop to be closed.
ω_d	2 rad/sec	The pilot must be able to control the Dutch roll mode.
$\left\lvert \dfrac{\varphi}{\beta} \right\rvert_{DR}$	2.5	This kept the Dutch roll mode from being merely a "snaking" motion.

TABLE B-II

STABILITY DERIVATIVES FOR THE BARE AIRFRAME

$N'_\beta = 4$	$L'_\beta = -25$	$Y_v = 0$
$N'_r = .6$	$g/U_o = .032$	$N'_{\delta_a} = -2$
	$L'_p = -5$	$L'_{\delta_a} = -40$
	$N'_p = .032$	$N'_{\delta_r} = -3.2$
	$L'_r = 0$	

The above value of g/U_O corresponds to an airplane traveling at 1,000 ft/sec (or about 682 miles per hour). To be moving that fast, and yet have a dutch roll frequency of only 2 rad/sec, is an unusual situation. Rather than trying to pinpoint the altitude and airplane structural geometry consistent with the above characteristics, it will merely be noted that the dynamics are not wholly unreasonable, and that they accentuate the appropriate qualities desired in the simulation.

The pertinent open-loop transfer functions resulting from the above derivatives are given below for reference.

$$\frac{\varphi}{\delta_a} = \frac{-40\left[s^2 + 2(-.13)(2.29)s + (2.29)^2\right]}{(s - .024)(s + 5)\left[s^2 + 2(-.14)(2)s + (2)^2\right]}$$

$$\frac{r}{\delta_r} = \frac{-3.2(s + 5)\left[s^2 + 2(-.04)(.2)s + (.4)^2\right]}{(s - .024)(s + 5)\left[s^2 + 2(-.14)(2)s + (2)^2\right]}$$

AUTOMATIC FLIGHT CONTROL SYSTEM DESCRIPTION

The only automatic control device used in this simulation was a yaw rate augmenter. Its function was to add damping to the dutch roll mode to give the pilot a better airplane to fly. To keep the augmenter from opposing the pilot in steady turns, the yaw rate signal from the rate gyro was "washed out" before being fed to the rudder actuator. Figure 23 presents the relationships among system elements for the multiple-loop control task.

By closing the $r \rightarrow \delta_r$ augmenter loop at several gains, it is possible to generate various levels of improved dutch roll characteristics. A root locus plot of the washed-out $r \rightarrow \delta_r$ loop closures is shown in the sketch on the next page. A washout time constant of .25 sec was chosen as a result of a compromise between good dutch roll damping and turn-entry dynamics. It was found that the closure of the yaw rate damper loop alone did not provide all of the desired configurations. Therefore, the stability derivative N'_r and one of the control

$$\left(\frac{r}{\delta_r}\right)\left(\frac{Ks}{s+.25}\right) \text{ Loop Closure}$$
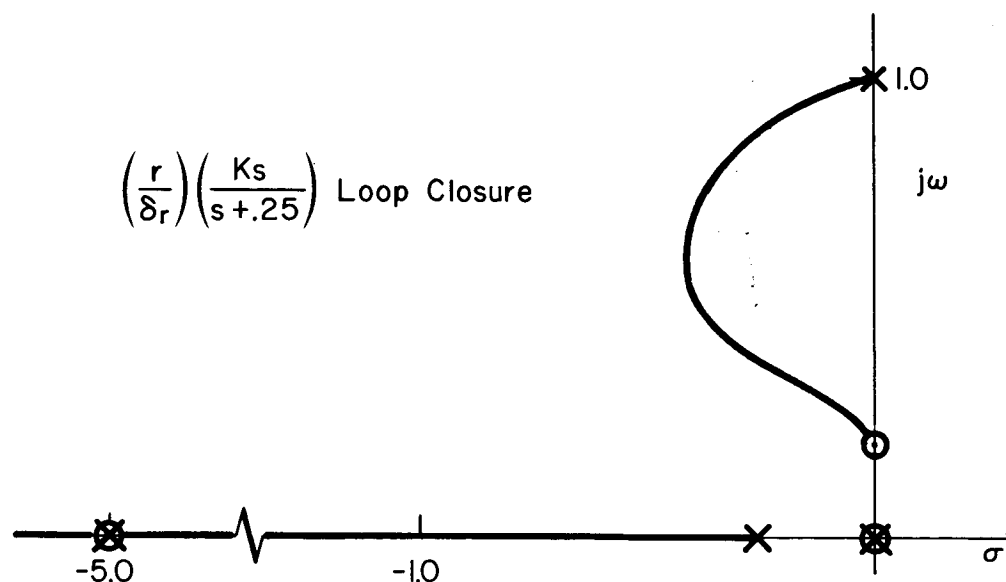
Sketch. Root Locus Plot of a Washed-Out $r \rightarrow \delta_r$ Loop Closure

effectiveness derivatives, N_{δ_a}', were changed as the damper loop was closed. They were changed back instantaneously when a configuration was failed to the basic airframe alone. These added changes allowed ω_φ/ω_d and ζ_φ and ζ_d to be varied independently of any other parameters.

To generate data pertinent to the graceful degradation hypothesis, it was decided to use three prefailure airplanes: one with good-to-optimum dutch roll damping (Configuration A), and two with only slight dutch roll damping. The two with only slight dutch roll damping differed in that one had a value of ω_φ/ω_d equal to unity (Configuration B), and the other had a value of ω_φ/ω_d equal to 1.3 (Configuration C). The two values of dutch roll damping were obtained via two values of gain in the yaw damper loop closure, while the values of ω_φ/ω_d were determined by the stability derivative N_{δ_a}'.

In Case A (with $K_{r\delta_r}$ optimum) the pilot can use aileron-only control before the failure, but __must__ use the rudder after the failure. In Case B the pilot may occasionally use the rudder before the failure if the dutch roll is excited by a disturbance input. In Case C some manual rudder control is always required before failure in order to avoid destabilizing the dutch roll. Failures were both hard and soft. (An occasional fail-operational situation with a cockpit failure warning light being energized showed the pilot to be ignoring the light.)

59

It was desired to have the three prefailure airplanes as different from each other as possible (so that a pilot could recognize which configuration he was controlling) as well as different from the postfailure airplane (Configuration E). In this way it was hoped to maximize any differences in the failure data for the various configurations. The unaugmented airplane and the three augmented versions selected were rated (Cooper scale) as an 8, 6, 4, and 2, respectively, by a pilot experienced in rating airplanes. The dynamic characteristics and stability derivatives for these configurations are given in Table B-I. From the values given in Table B-III it is seen that the closed-SAS loop dynamics for bank angle control (without the pilot closing a rudder loop) are given by:

Configuration A (good):

$$\left(\frac{\varphi}{\delta_a}\right)_{r \to \delta_{r_{SAS}}} \doteq \frac{-40(s + .31)\left[s^2 + 2(.70)(1.80)s + (1.80)^2\right]}{s(s + .52)(s + 5)\left[s^2 + 2(.70)(1.65)s + (1.65)^2\right]}$$

Configuration B (fair, $\omega_\varphi \doteq \omega_d$):

$$\left(\frac{\varphi}{\delta_a}\right)_{r \to \delta_{r_{SAS}}} \doteq \frac{-40(s + .26)\left[s^2 + 2(.16)(1.96)s + (1.96)^2\right]}{s(s + .29)(s + 5)\left[s^2 + 2(.15)(1.95)s + (1.95)^2\right]}$$

Configuration C (poor, $\omega_\varphi > \omega_d$):

$$\left(\frac{\varphi}{\delta_a}\right)_{r \to \delta_{r_{SAS}}} \doteq \frac{-40(s + .26)\left[s^2 + 2(.13)(2.52)s + (2.52)^2\right]}{s(s + .29)(s + 5)\left[s^2 + 2(.15)(1.95)s + (1.95)^2\right]}$$

AUTOMATIC FLIGHT CONTROL SYSTEM FAILURES

The multiple-loop block diagram in Fig. 23 can be expanded to show the detailed mechanization of the yaw damper loop. This is done in Fig. 24. The yaw damper loop features a dual redundant valve and actuator with sufficient logic to give a fail operational capability under certain circumstances. The remaining SAS components are not dual. The control console and electrical power supply are shown because they

60

SUMMARY OF DYNAMIC CHARACTERISTICS AND STABILITY DERIVATIVES

	"E"	"C"	"B"	"A"
$\dfrac{1}{T_s}$	−.024	0	0	0
$\dfrac{1}{T_{WO}}\bigg\|_{\triangle}$	—	.29	.29	.52
$\dfrac{1}{T_{WO}}\bigg\|_{\frac{\varphi}{\delta_a}_{NUM}}$	—	.26	.26	.31
$\dfrac{1}{T_R}$	5.0	5.0	5.0	5.0
ω_d	2.00	1.95	1.95	1.65
ζ_d	−.14	.15	.15	.70
ω_φ	2.29	2.52	1.96	1.80
ζ_φ	−.13	.13	.16	.70
Y_v	0	0	0	0
L'_β	−25	−25	−25	−25
N'_β	4	4	4	4
$\dfrac{g}{U_o}$	.032	.032	.032	.032
L'_p	−5	−5	−5	−5
N'_p	.032	.032	.032	.032
L'_r	0	0	0	0
N'_r	.6	0	0	0
L'_{δ_a}	−40	−40	−40	−40
N'_{δ_a}	−2	−4	0	0
N'_{δ_r}	−3.2	−3.2	−3.2	−3.2
K from $\left(\dfrac{-.25Ks}{s+.25}\right)$	0	−.80	−.80	−3.2

contribute to the reliability and failure mode analyses. Representative values of the valve-actuator and rate gyro dynamics were used. The washout circuit characteristics were tailored to suit the selected airframe dynamics.

The failure modes and rates of failure for the SAS components shown in Fig. 24 are summarized in Table B-IV. These failure rates derive

TABLE B-IV

RELIABILITY AND FAILURE MODE SUMMARY FOR LATERAL AIRPLANE

COMPONENT	FAILURE RATE (per 10^6 hours)	FAILURE RATE DATA SOURCE	FAILURE MODE	
			SAS TRANSIENT	PROBABILITY
Control Console	56	Ref. 23	Step to zero feedback	100%
Power Supply	120	Ref. 24	Step to zero feedback	100%
Rate Gyro	100	Ref. 24	Step* hard-over rudder	100%
Preamplifier	30	Ref. 24	Step to zero feedback	100%
Washout Circuit	78	Ref. 24	Step to zero feedback	100%
Servoamplifier	30	Ref. 24	Step to zero feedback	100%
Dual Redundant Valve and Actuator	1070	Ref. 24	None, operational	41%
		Ref. 24	Hold position (of feedback signal)	59%

*Not a true step because it is filtered through the washout.

from a study of the flight control system in the A-4C aircraft, Ref. 24. The failure mode transients and probabilities shown are based on analyses made during the Case I study, Refs. 23–25, plus data on valves and actuators given in Ref. 26. When one failure mode was dominant it was assumed (for simplicity) to have a 100 percent likelihood of occurrence.

Combining like SAS transients from Table B-IV in proportion to failure rates (or probabilities of occurrence) leads to the overall failure mode summary in Table B-V. Although reasonable for actual failures, the

TABLE B-V

SUMMARY OF FAILURE MODES OF SAS COMPONENTS

SAS TRANSIENT	PROBABILITY
None, operational	30%
Hold position	42%
Step to zero feedback	21%
Step hardover	7%

above percentages were not practical for the purposes of this simulation study. Preliminary tests showed the pilot to be ignoring a failure warning light. Thus, he was essentially oblivious to the fail-operational situation. In addition, the transient associated with the step-to-zero-feedback failure produced a step rudder change that resembled the transient from the hardover rudder situation (to the extent that both caused the turn needle to "jump"). Due to the similarity of the failure symptoms, the step-to-zero-feedback failures were combined with the hardover-rudder-signal failures. Then it was decided to omit the fail-operational cases. This left two types of failure transients: the soft failure (hold position of signal to actuator) and the hard failure (with a washed-out rudder step[*]). These were presented to the pilot with equal frequency and in a random sequence.

PREDICTION OF PILOT TRANSITION RESPONSE

Prediction of pilot transition response involves several analytical steps. The pilot's describing functions appropriate to the prefailure and postfailure steady-state dynamics must be estimated using the techniques and crossover model of Ref. 7. The operator's control response

---

[*]A washed-out step is a step attenuated by a factor of e^{-at}.

following retention is estimated using a time optimal model. The former is straightforward, while the time optimal response is relatively unique as shown in the discussion given below.

The yaw-rate-to-rudder transfer function following failure is given approximately by:

$$\frac{r}{\delta_r} \doteq \frac{Ks}{\left[s^2 + \omega^2\right]}$$

The corresponding differential equation during switching (when the rudder is moved) is:

$$\ddot{r} + \omega^2 r = K\dot{\delta}_r$$

Integrating over an arbitrarily short time interval yields the following finite difference equation ($\triangle$ denotes an incremental change):

$$\triangle\dot{r} = K\triangle\delta_r$$

which is applicable immediately after switching. This shows that a step change in rudder, $\triangle\delta_r$, causes a step change in yaw rate, $\triangle\dot{r}$.

Between switches (when the rudder is motionless) the differential equation becomes

$$\ddot{r} + \omega^2 r = 0$$

which has the solution

$$r = A \sin(\omega t + \alpha)$$

Adding the squares of ωr and $\dot{r}$ gives

$$\dot{r}^2 + \omega^2 r^2 = A^2\omega^2 \; ,$$

which shows the coasting trajectories to be circles on the phase plane of of $\dot{r}$ versus ωr.

64

Combining the coasting and switching trajectories gives the phase plane portrait of the sketch. Clearly, the optimum time to switch is when $r = 0$, as this is the only time that the origin is directly approached (for the zero damping case).
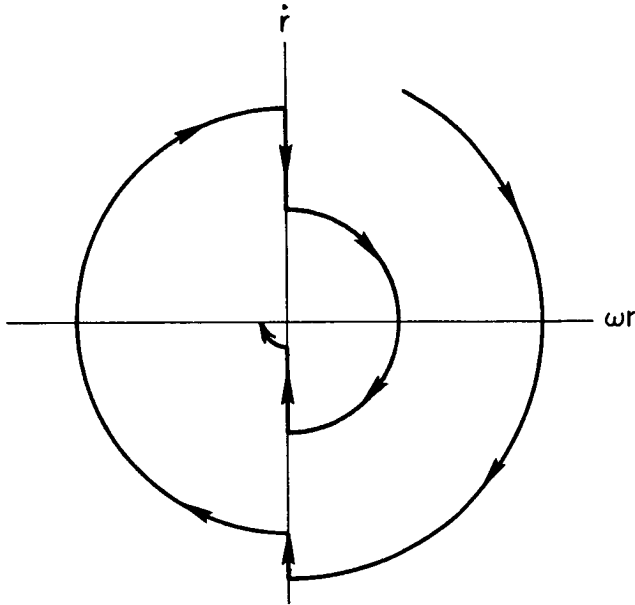
Sketch. Phase Plane Portrait of Time Optimal Yaw Rate Damping

An actual phase plane plot was generated during the simulation experiments. The result is presented in Fig. 45.

SIMULATION DETAILS

Using the stability derivatives given above, the equations of motion for the simulated airplane are:

$$
\begin{bmatrix} s & -.032 & 1 \\ 25 & s(s+5) & 0 \\ -4 & -.032s & s - N_r' \end{bmatrix} \begin{bmatrix} \beta \\ \varphi \\ r \end{bmatrix} = \begin{bmatrix} 0 \\ -40 \\ N_{\delta_a}' \end{bmatrix} \delta_a + \begin{bmatrix} 0 \\ 0 \\ -3.2 \end{bmatrix} \delta_r
$$

where the values of N_{δ_a}' and N_r' are determined by the configuration being simulated, and the rudder deflection is the sum of two components (from

65

the pilot and the SAS). Thus,

$$\delta_r = \delta_{r_p} + \delta_{r_{SAS}}$$

Per the earlier discussion of the yaw damper, the rudder deflection due to the SAS is given by

$$\delta_{r_{SAS}} = -K\left(\frac{.25s}{s + .25}\right)r$$

where the value of K is determined by the configuration being simulated. Combining the last two relations with the equations of motion leads to:

$$
\begin{bmatrix}
s & -.032 & 1 \\
25 & s(s+5) & 0 \\
-4 & -.032s & \left(1 - \frac{.8\,K}{s + .25}\right)s - N'_r
\end{bmatrix}
\begin{bmatrix}
\beta \\
\varphi \\
r
\end{bmatrix}
=
\begin{bmatrix}
0 \\
-40 \\
N'_{\delta_a}
\end{bmatrix}
\delta_a
+
\begin{bmatrix}
0 \\
0 \\
-3.2
\end{bmatrix}
\delta_{r_p}
$$

This set of equations was simulated on an analog computer via the analog mechanization shown in Fig. 25.

The equipment used in the simulation is most conveniently presented via the following listing:

- Gedas (two linear racks and one nonlinear rack), bank of comparators (for switching), function generator and demodulator (producing a sum of sine waves) used to produce a random-appearing gust input to the airplane

- P-51 cockpit with a two-gun CRT (for generating a display) and miscellaneous meters (in addition to center stick and rudder pedals)

- Strip recorder

- FM tape recorder

The cockpit layout is described as a conventional seat, stick, and pedal arrangement. Because this is a fixed-base simulator, there were

66

no motion cues available to the pilot. The primary displays of bank
angle and turn rate were generated on a two-gun CRT located roughly
at eye height and about 12 in. from the pilot. In addition, a meter
was set up to resemble the "ball". This meter was wired to indicate
a lagged sideslip, and responded quite like a conventional ball in
kerosene. One additional display was utilized in that the "doughnut"
on an angle-of-attack indexer was wired to light up when a failure had
occurred. The CRT and ball displays were arranged as shown in the sketch.
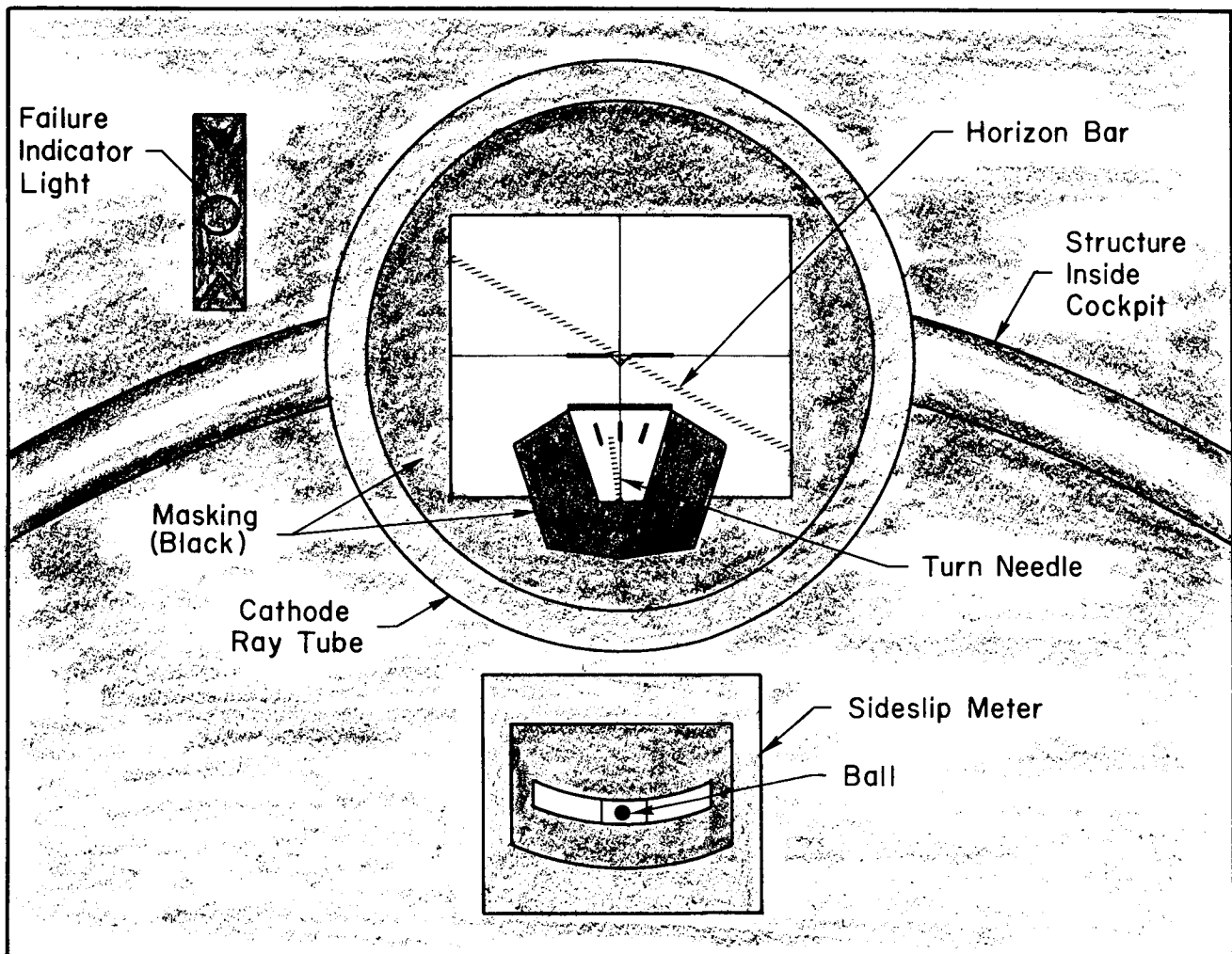
Sketch. Cockpit Display (Indicating Coordinated Left Turn)

One gun of the CRT was used to simulate a horizon bar. This bar (or
line) was made to rotate through an angle equal to the airplane bank angle.
With the airplane model painted on the CRT face, this resembles a conven-
tional attitude gyro presentation. The other CRT gun was used to generate
a turn needle which operated exactly as a conventional turn needle.

67

The switching (during a simulated failure) of the yaw-damper gain, the transient input, and the change of N'_{δ_a} were accomplished with a bank of comparators wired as shown in Fig. 26. The cockpit failure light was also controlled via these comparators.

The airplane was disturbed by a simulated gust input. Because the gusts were filtered by the airplane dynamics, this modified the effective displayed bandwidth. The random-appearing gusts were actually a sum of nine sine waves (obtained from a function generator) as shown in Table B-VI. The gusts were applied to the airplane as sideslip gusts having an rms value of 1.4 deg.

TABLE B-VI

DESCRIPTION OF SINE WAVES USED TO SIMULATE GUST DISTURBANCE

FREQUENCY (rad/sec)	RELATIVE AMPLITUDE
0.3142	1.0
0.5027	1.0
0.7540	1.0
1.1938	1.0
1.9478	1.0
3.2044	1.0
5.1522	0.2
13.1319	0.1
19.9806	0.1

A strip recorder was used to record the gust input, bank angle, and yaw rate, the aileron and rudder deflections, and the yaw-damper output. These same variables were also recorded on an FM magnetic tape recorder.

PILOT SUBJECTS

Two subjects were used during the experiments. One (CWC) is a high-time (several thousand hours) military fighter pilot as well as a commercial airline copilot (instrument rated), and the other (WES)

is a 160-hour private pilot (not instrument rated). Both are about 30 years old. Neither pilot was familiar with the experimental details or the ultimate objectives.

The specific instructions to the pilot were:

> "Minimize bank angle and yaw rate as well as you can throughout the run. Try to never lose control of the vehicle after a failure. If at any time you feel tired, we would like you to stop and take a rest so we can get consistent data from an alert pilot."

Because no "desired" control strategy was given in the instructions, the pilot was forced to evolve his own strategy to minimize errors.

The training procedures for this simulation were quite simple. Each pilot spent about a week (at two hours per day) practicing controlling all of the various configurations as stationary tracking tasks. When an asymptotic level of proficiency with each configuration was reached, failures were then interjected. After practicing the various failures for a few days (approximately 200 trial failures), the experimental runs were made. Subsequent to the initial learning, no substantial differences between the two pilots were evident.

EXPERIMENTAL PROCEDURE

The equipment was checked each morning with an analog pilot that gave zero closed-loop damping. Then a series of five two-minute (approximately) runs was done with the subject controlling a given prefailure configuration. During the runs the cockpit cover was closed so he could see only the display. The subject would rest for several minutes prior to going through five more two-minute runs with a different prefailure configuration. Such a sequence was carried out twice a day for about two hours each time. Longer rest periods were periodically interjected into the above schedule to keep from tiring the subject. A total of ninety runs was made with CWC during the final experiments, with the failure occurring 65 sec into each run.

The configurations were presented in a (somewhat) random sequence, as were the types of failures simulated. The failures for a series of

five runs were chosen (in order) from a master list of failure-sequence. The master failure-sequence used for the final experiments is given in Table B-VII. By using the master sequence it was possible to retain the relative expected failure rates in the simulation. The final ninety experimental runs were distributed as shown in Table B-VIII.

TABLE B-VII

MASTER SEQUENCE OF FAILURES
Soft
Soft
Hard
Soft
Hard
Hard
Soft
Soft
Hard
Hard

TABLE B-VIII

DISTRIBUTION OF EXPERIMENTAL RUNS

PREFAILURE CONFIGURATION	TYPE OF FAILURE	NUMBER OR RUNS
A	Soft	15
	Hard	15
B	Soft	15
	Hard	15
C	Soft	15
	Hard	15

70

APPENDIX C

DIGITAL ANALYSIS AND RESULTS

Time histories of the various signals in the loop were tape-recorded during the multiple-loop experiments. The following signals were recorded:

- Sideslip gust disturbance, β_g
- Roll angle, φ
- Pilot aileron output, δ_a
- Yaw rate, r
- Pilot rudder output, δ_{r_p}
- Yaw rate augmenter output, $\delta_{r_{SAS}}$

This was done for 15 runs of each of the six multiple-loop failure situations (90 runs in all). The data were digitized at a rate of 10 samples per second. The basic 2 min. runs were truncated at 30 sec (10 sec before failure to 20 sec after) to reduce computation costs while retaining the essential portions of the data. Digital analyses were not made on the single-loop results.

The digitized data were analyzed on a CDC 3600 computer using "BOMM, A System of Programs for the Analysis of Time Series" (Ref. 27). Calculations were made over an ensemble of five runs[*] from each of the six failure situations (30 runs in all) to determine the time-varying characteristics before, during, and after failure. The signals analyzed included pilot aileron output, pilot rudder output, and yaw rate. Computations were made of the time-varying means, standard deviations, and power spectra for each of the three signals for the 30 runs, as discussed below.

A. MEAN COMPUTATION

The first step was to compute the time-varying (arithmetic) mean over an ensemble of five runs at 0.1 sec intervals. The failures were "synchronized" to occur at the same time. This involved taking the five data points (one from each run) at any given time interval, adding them algebraically, and

---

[*]Preliminary calculations were made with all 15 runs in the ensemble, but the cost of computation was excessive.

dividing by five. The ensemble can be denoted formally by:

$$\{u_{i,j}\} \quad ; \quad \begin{array}{l} i = 1, \ldots, N \\ j = 1, \ldots, M \end{array}$$

In the case at hand, $N = 5$ members of the ensemble and $M = 300$ samples in time. The time-varying mean over the ensemble of N signals is given by:

$$\bar{u}_j = \frac{1}{N} \sum_{i=1}^{N} u_{i,j} \qquad (C-1)$$

Under stationary conditions or with a soft-failure (i.e., change in augmenter gain only) this should approach zero as the number of ensemble members becomes large.

The next step was to subtract the time-varying mean, $\bar{u}_j$, from each of the N signals. This was done to take out the deterministic and nonstationary effects (associated with the hardovers), leaving only a stationary residual. This had the disadvantage of introducing high frequency variability in each of the signals because of the variability of the mean due to the small sample size. The value of extracting the deterministic pilot output (needed for modeling) was felt to outweigh the disadvantages in this case.

B. STANDARD DEVIATION COMPUTATION

The time-varying run-to-run variability across the ensemble was estimated via the standard deviation (square root of the variance). At any given time, j, each signal (minus the mean) was squared, and the sum of squares was divided by the number of ensemble members, N, less one. The variance is formally denoted by:

$$\sigma_j^2 = \frac{1}{N-1} \sum_{i=1}^{N} \left(u_{i,j} - \bar{u}_j \right)^2 \qquad (C-2)$$

Its square root is the standard deviation.

C. POWER SPECTRUM COMPUTATION

Spectral analysis techniques provide a means of estimating the pilot's quasi-linear describing function and level of control activity. A variety of computational methods have been used in past studies of the human operator

in stationary tasks, almost all involving time-averaging to obtain a single frequency function for a given run. In nonstationary tasks (e.g., dynamic transitions due to failures) the time-varying spectra are of great interest because they show in what way and how fast the pilot adapts to the new dynamics.

At the outset it was desired to compute power spectra for the three signals, δ_{r_p}, δ_a, and r, as well as their cross spectra with the input (to obtain describing functions). The power spectra were ultimately obtained, but the cross spectra were not because of the limited scope of the study. The computational technique described below (adapted from Ref. 28) could be extended easily to cross spectra.

The first step in computing the power spectra was to compute the time-varying autocorrelation "function" (a two-dimensional surface defined at discrete points) for each of the signals in the ensemble $\left\{u_{i,j}\right\}$. The auto-correlation function (surface) for the ith member is a set of K functions defined by

$$R_{i,j,k} = u_{i,j}u_{i,j+k} \quad ; \quad \begin{array}{l} i = 1, \ldots, N \\ j = 0, \ldots, M-k \\ k = 0, \ldots, K-1 \end{array} \qquad (C-3)$$

where K is the number of sample points in the autocorrelation function. Each member of the ensemble $\left\{u_{i,j}\right\}$ is assumed to have the mean removed as described previously. These autocorrelation functions (surfaces) are averaged over the ensemble to obtain a single estimate. This average is denoted formally by:

$$R_{j,k} = \frac{1}{N}\sum_{i=1}^{N} R_{i,j,k} = \frac{1}{N}\sum_{i=1}^{N} u_{i,j}u_{i,j+k} \qquad (C-4)$$

The resultant autocorrelation surface was defined every 0.1 sec in time over a 30 sec period, and for lags at 0.1 sec intervals from 0 through 0.5 sec (K = 6).

The next step was to short-time-average the autocorrelation function (surface) to obtain finite run lengths which would yield spectral points having five degrees of freedom (one for each ensemble member) for the filter bandwidths chosen (by choosing K), see Ref. 29. This turned out to be about

1 sec, and exactly 1 sec was chosen as the short time-averaging interval. The procedure is simply to take the mean of successive groups of 10 in the 300 points in time.* Formally,

$$R_{1,k} \;=\; \frac{1}{10} \sum_{m=0}^{9} R_{n+m,k} \quad ; \quad 1 = 1, 2, \ldots, 30 \qquad (C\text{-}5)$$

where $n = 10(1-1) + 1$, 10 is the number of terms in a given group for unit increase in 1, and $R_{n+m,k}$ derives from Eq. C-4.

The rough power spectrum (surface) was obtained from the autocorrelation function (surface) by Fourier transformation. This is accomplished formally by computing

$$\Phi_{1,q} \;=\; 2\left[R_{1,0} + 2 \sum_{k=1}^{K-2} R_{1,k} \cos \frac{qk\pi}{K-1} + R_{1,K-1} \cos q\pi \right] \qquad (C\text{-}6)$$

where
$$1 \;=\; 1, \ldots, 30-k$$
$$q \;=\; 1, \ldots, K-1 = 1, \ldots, 5$$

The resulting rough power spectrum (surface) was smoothed using a Hanning filter lag window (see Ref. 29) to obtain a better statistical estimate.

D. POWER SPECTRA RESULTS

The time-varying power spectra were computed as described above for the three signals, δ_{r_p}, δ_a, and r, in each of the six failure situations. The δ_a spectra are relatively invariant across the failure and they have not been plotted. The rudder pedal and yaw rate data are of most interest and these are plotted in Figs. 56 through 59 for soft- and hard-failures, respectively. Each spectral point has the units of the basic signals squared, expressed in power decibels (10 $\log_{10}$). Six spectral points were computed in each case (from 0 to 31.4 rad/sec), but only the first

---

*In the actual computations the 30th point in $R_{1,k}$ was disregarded because of errors due to "end effects."

three frequency bands are shown. The higher frequency points were in the asymptotic noise level, and were further contaminated by removal of the ensemble average mean.

Each data point represents an average over 1 sec and 5 ensemble members. The failure occurred between the 10th and 11th seconds. The data for the 30th second have been omitted because they were contaminated by end effects. The first data point in time is also unreliable. The hardover failures occurred to the left and to the right (rudder deflection) in the experimental series. The signs on those to the left were changed before analysis to give all of them the same polarity.

The yaw rate error spectra are shown in Figs. 57 and 59. The prefailure spectral levels are generally in the direction predicted; i.e., Configuration A less than B less than C. The postfailure steady-state levels (all Configuration E) are all the same, as expected. The yaw rate spectra for the transition period (roughly the 10th to 13th second) show the following:

- The Configuration A error level increases abruptly in 1 second for the hard-failure case to a level higher than B or C, as shown in the low frequency data on Fig. 59. The subsequent data are indistinguishable from the steady state indicating the brevity of the transition for hardover.

- The Configuration A power level in the soft case increases gradually from the 10th to 13th second where it becomes higher than B or C, as shown in the low frequency data of Fig. 57. The postfailure steady-state period follows.

- The Configuration B data show the lowest error level during the 11th to 14th second for the hard-failure cases of Fig. 59.

The rudder deflection spectra are shown in Figs. 56 and 58. As expected the power level for Configuration A increases rapidly in the 11th and 12th second. For soft-failures, it actually goes down in the 11th second and then increases, reflecting the longer retention period observed in the soft-failure time histories.

75

The data of Figs. 56—59 are very interesting, but they do not provide strong insight into the mechanism of transition. This is undoubtedly due to the smoothing effect of averaging over both time and the ensemble of 5 runs. The general trends are consistent with the analyses and predictions of the main text. The data are probably most useful in showing the time variation in spectral levels that exist both in steady state and during transition. For rapidly time varying, yet low frequency phenomena of the sort under consideration, the fundamental restriction of uncertainty becomes a barrier in any averaging or fitting process, and individual time histories with their transient insight are generally more useful.
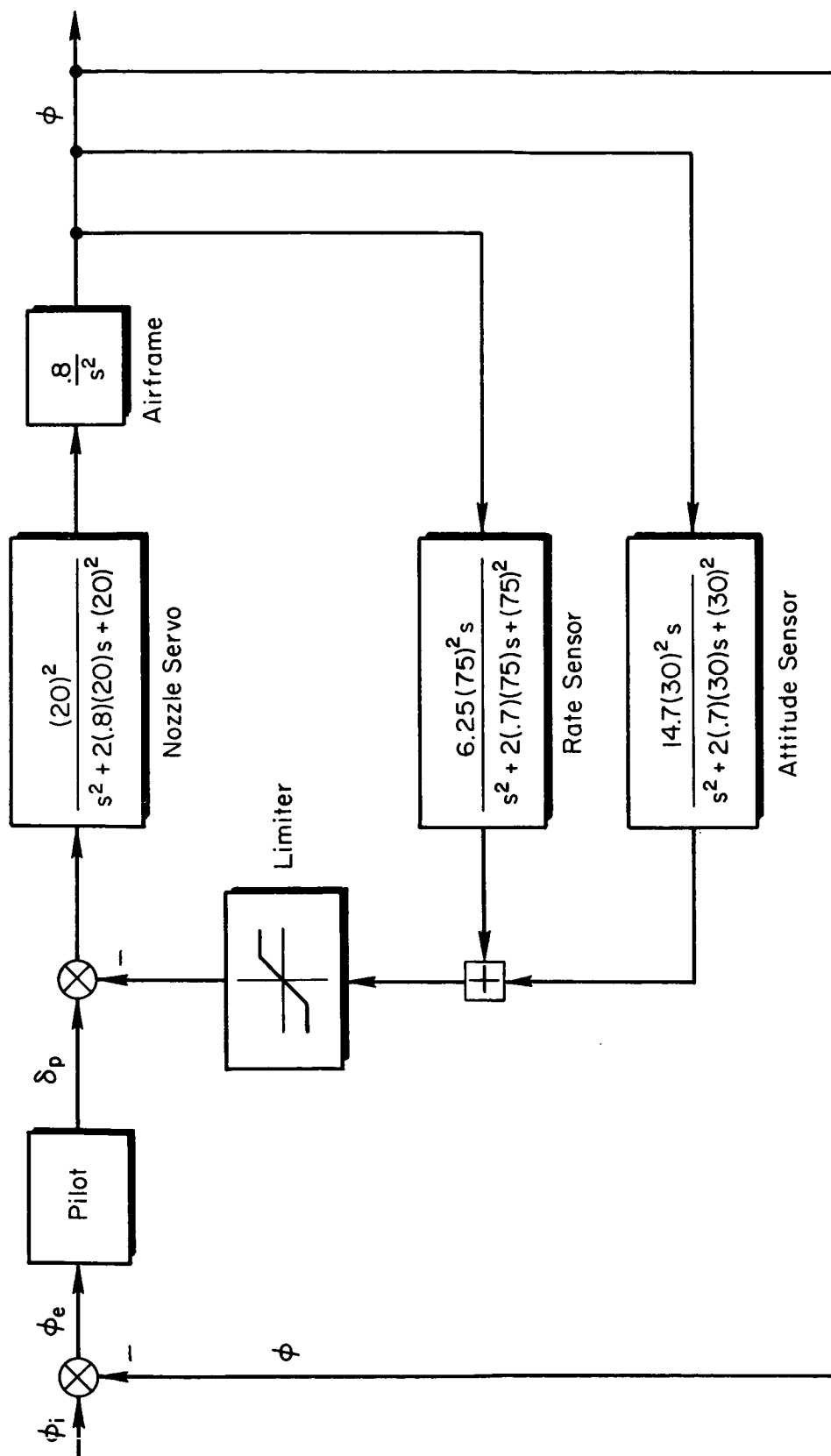
Figure 1. System Dynamics for the Single-Axis Study

77
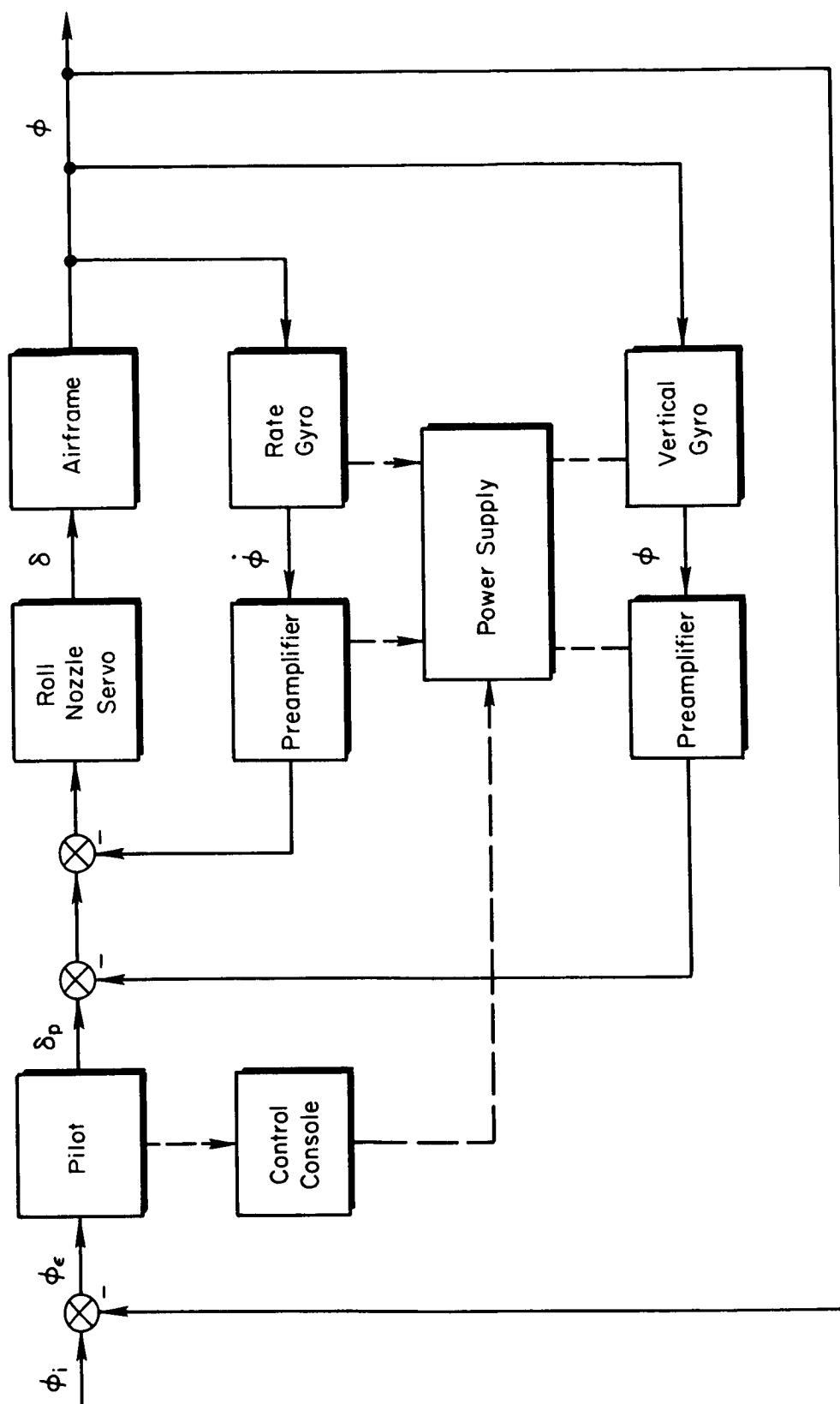
Figure 2. Augmentation System Mechanization for the Single-Axis Study

Figure 3. Analog Mechanization for Single-Axis Experiments
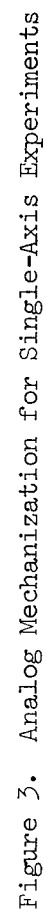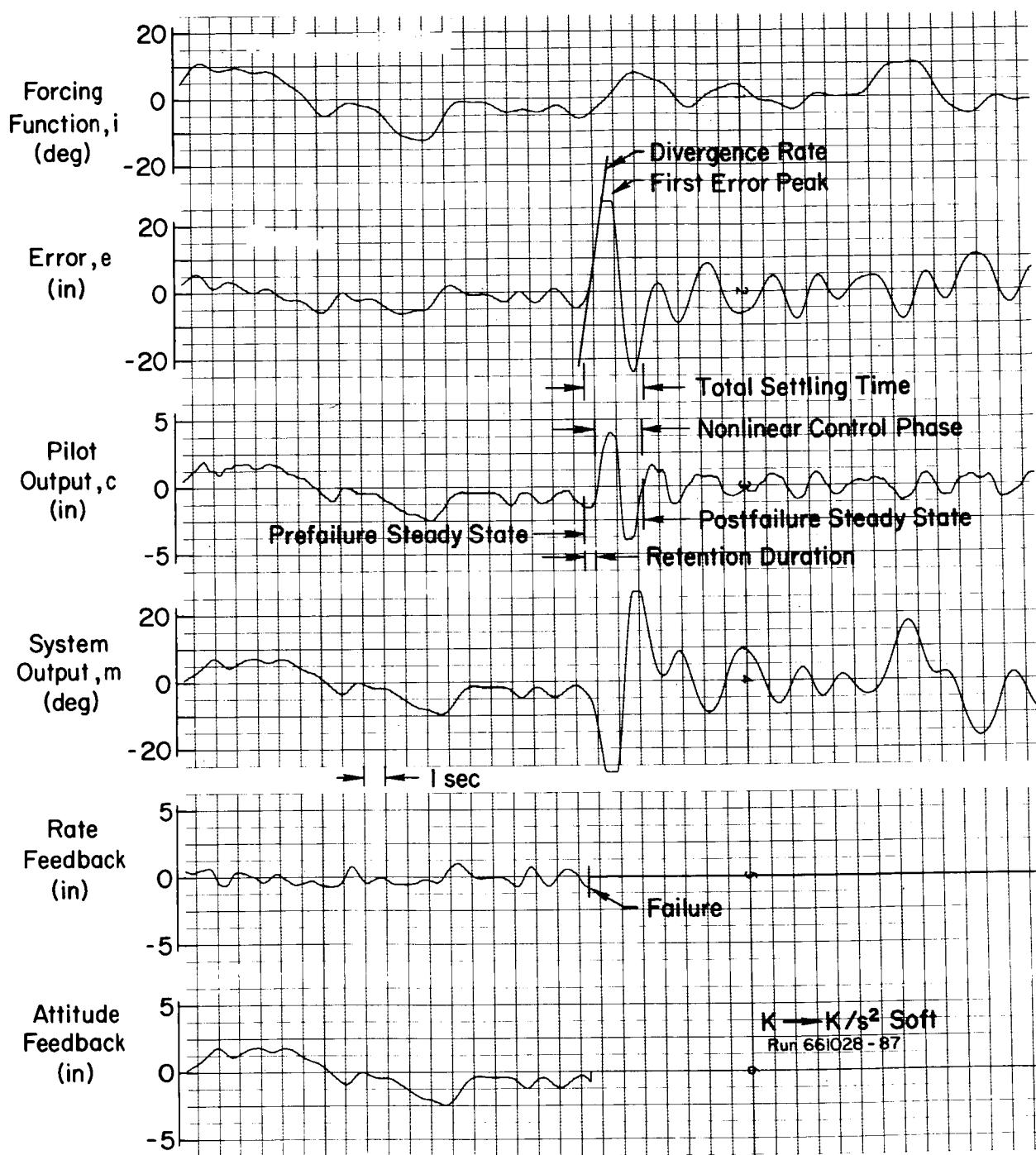
Figure 4. Illustration of Phases and Transition Properties
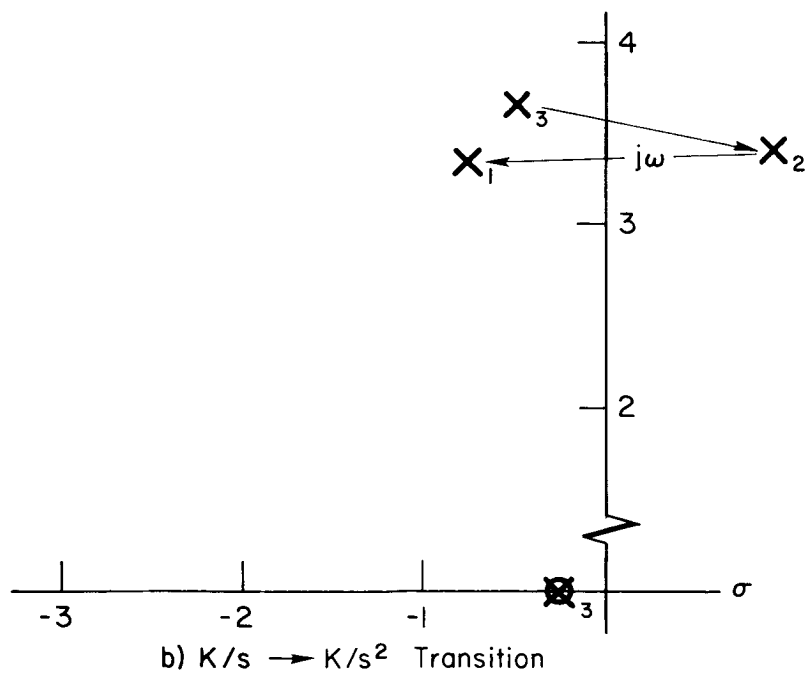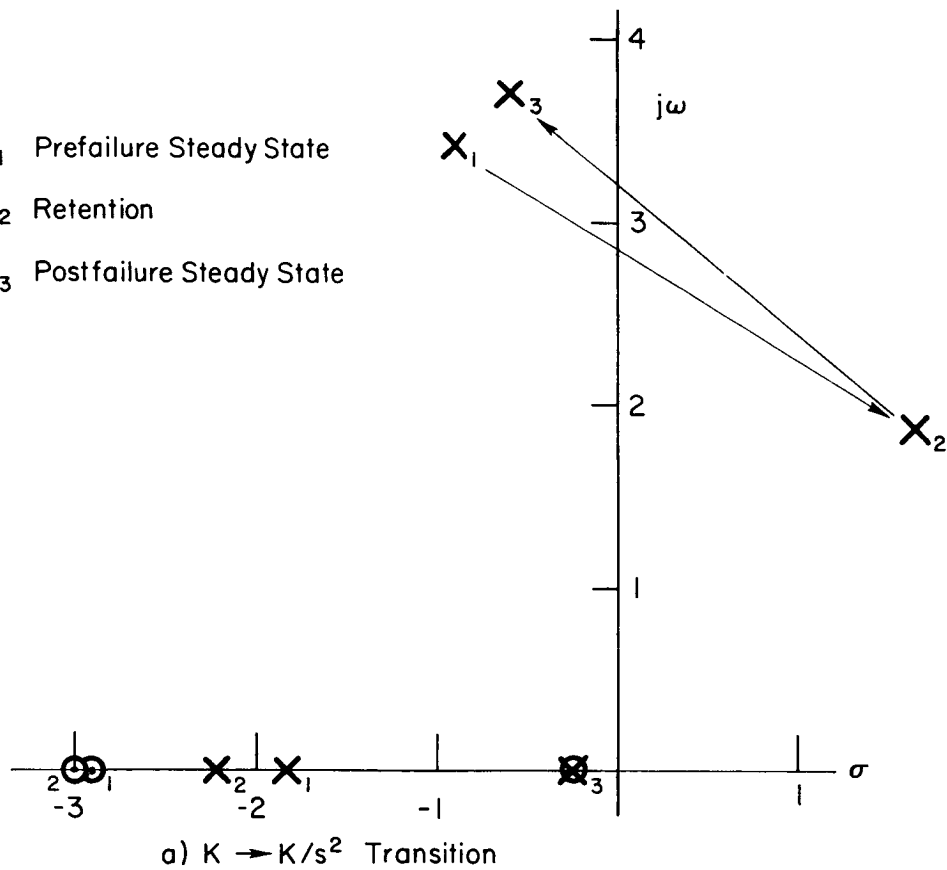
Figure 5. Root Locations for the Approximate System Transfer Function, m/i
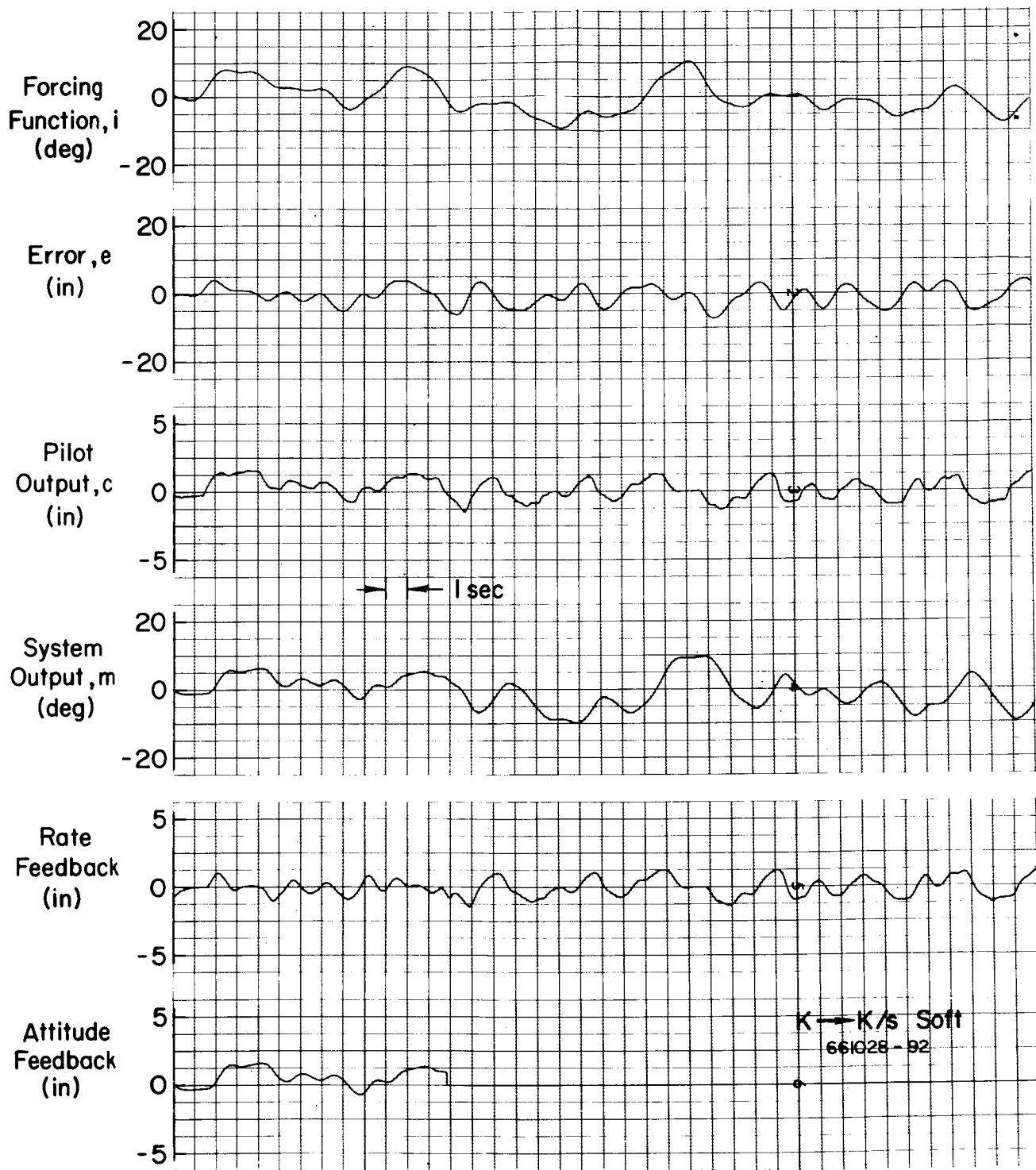
Figure 6. Example of a Soft-Failure from K to K/s
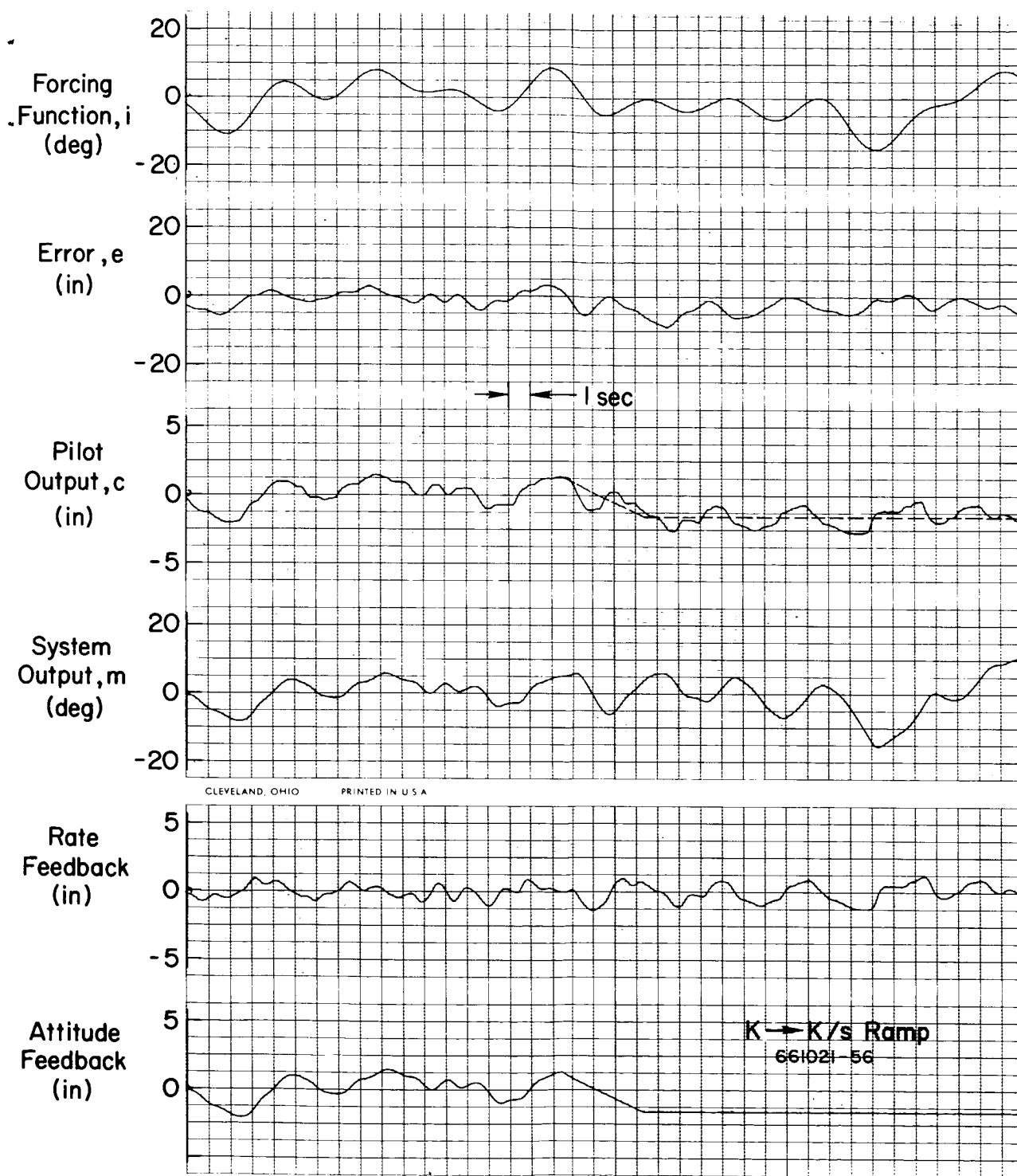
Figure 7. Example of a Ramp Failure from K to K/s
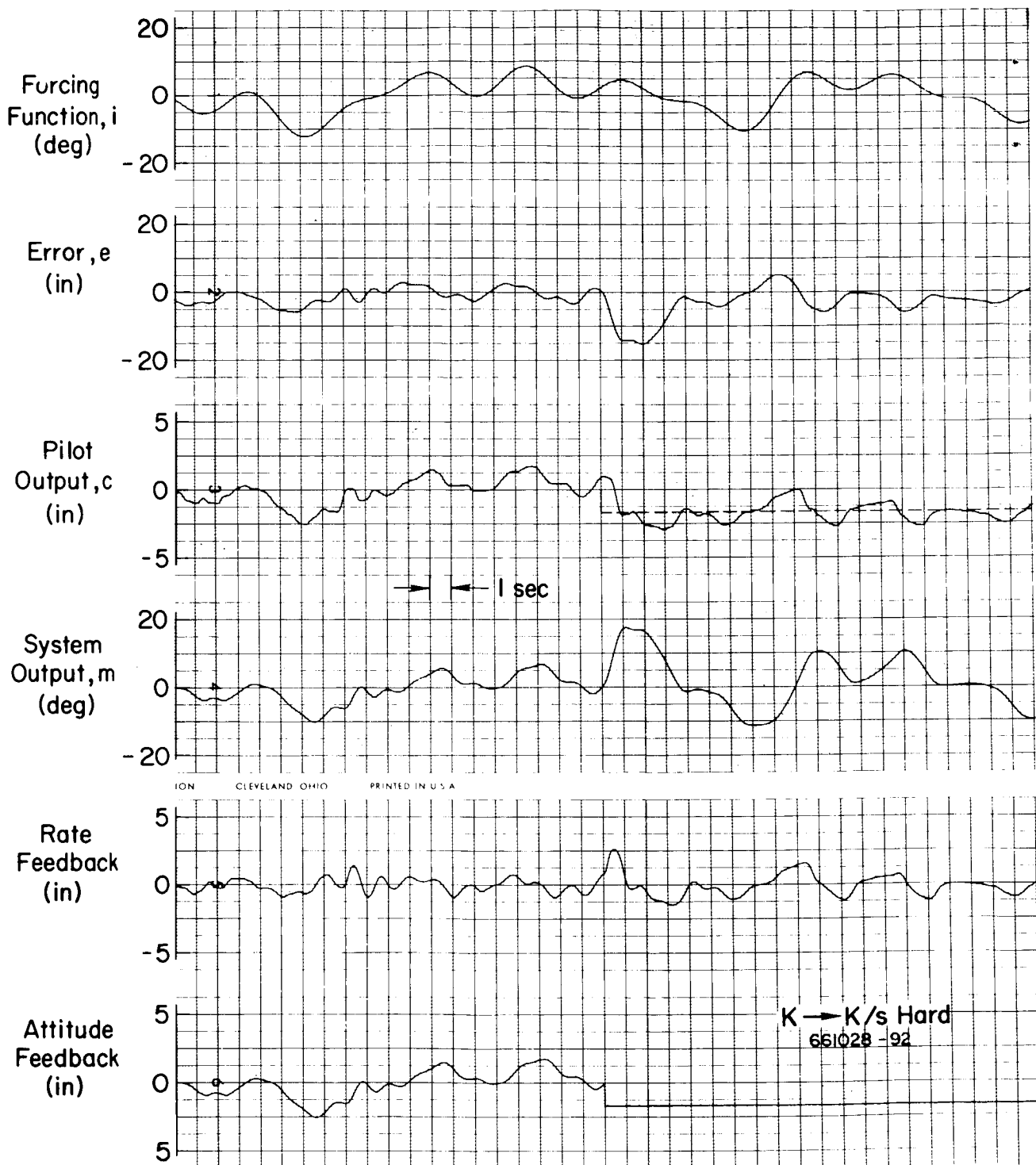
Figure 8. Example of a Hard-Failure from K to K/s

84
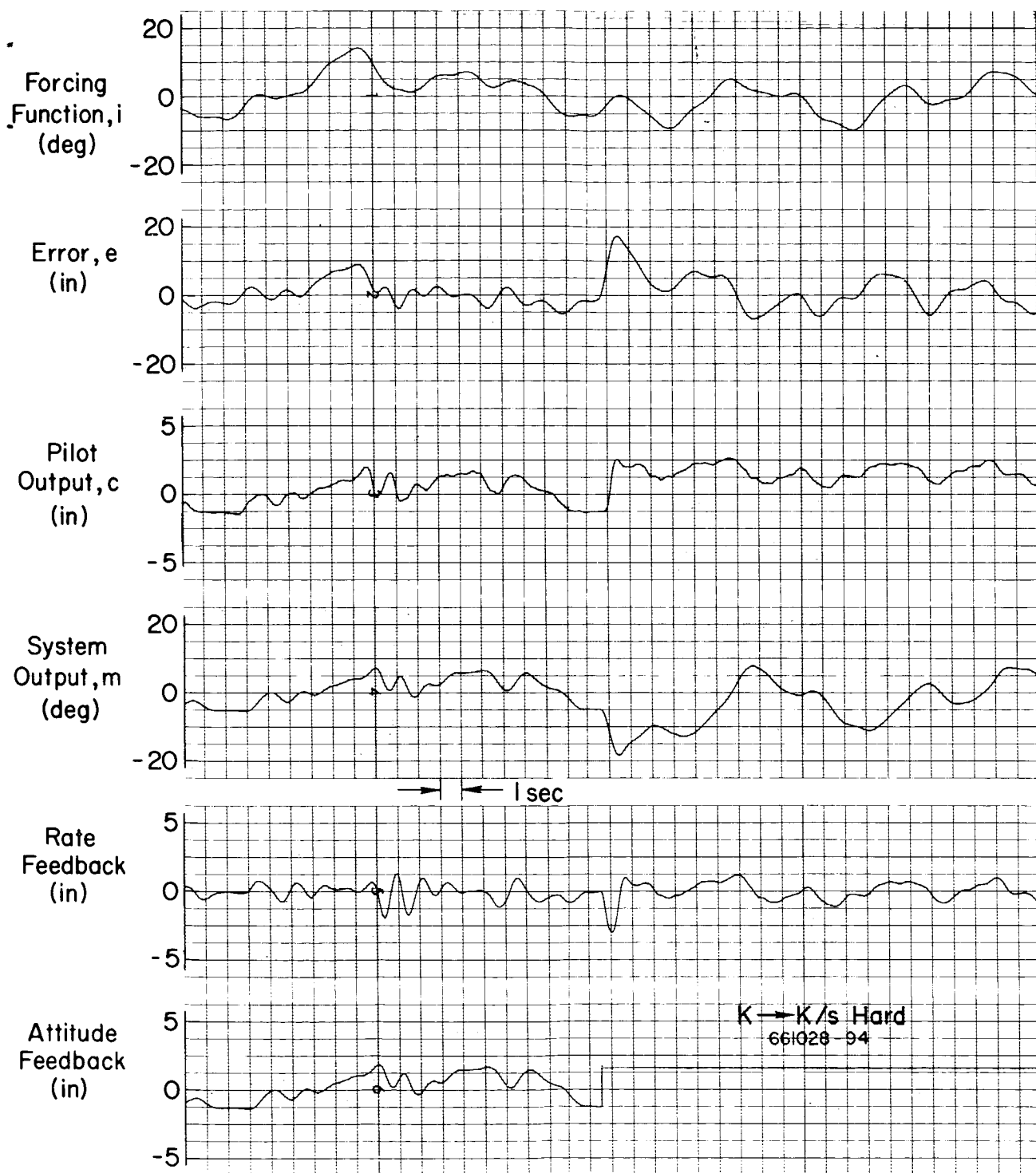
Figure 9. Example of a Hard-Failure from K to K/s

85
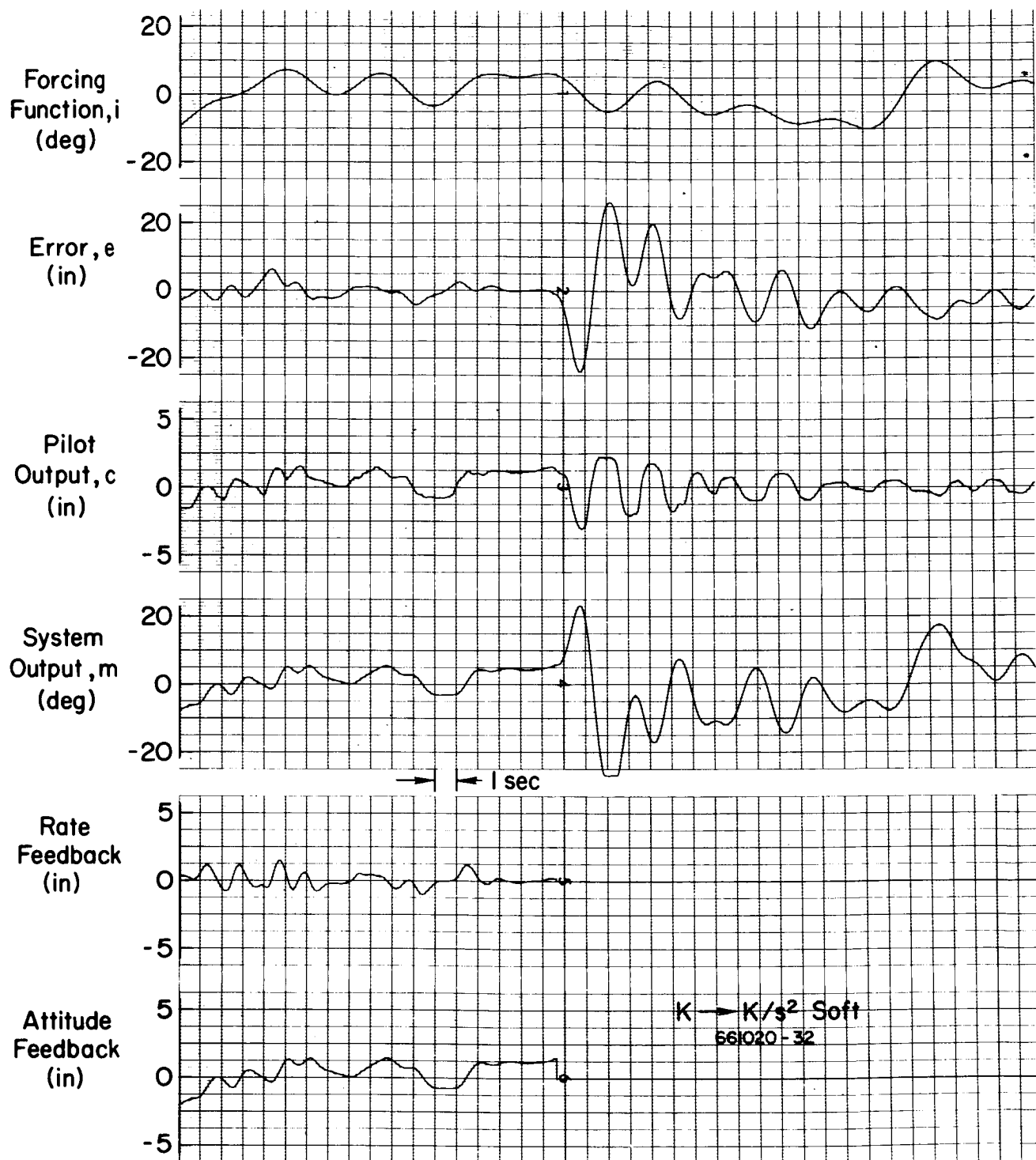
Figure 10. Example of a Soft-Failure from K to K/s^2
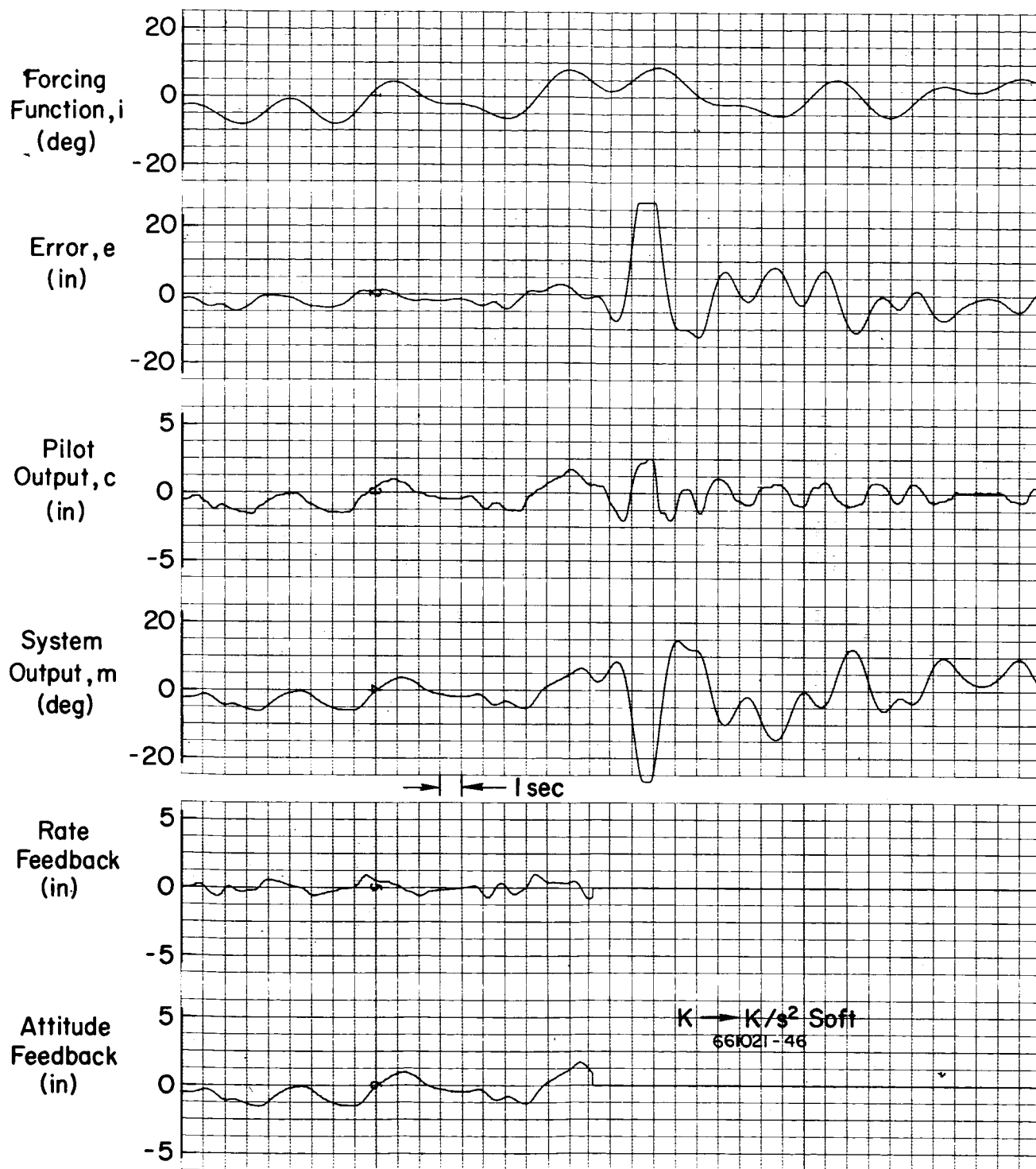
Figure 11. Example of a Soft-Failure from K to K/s^2
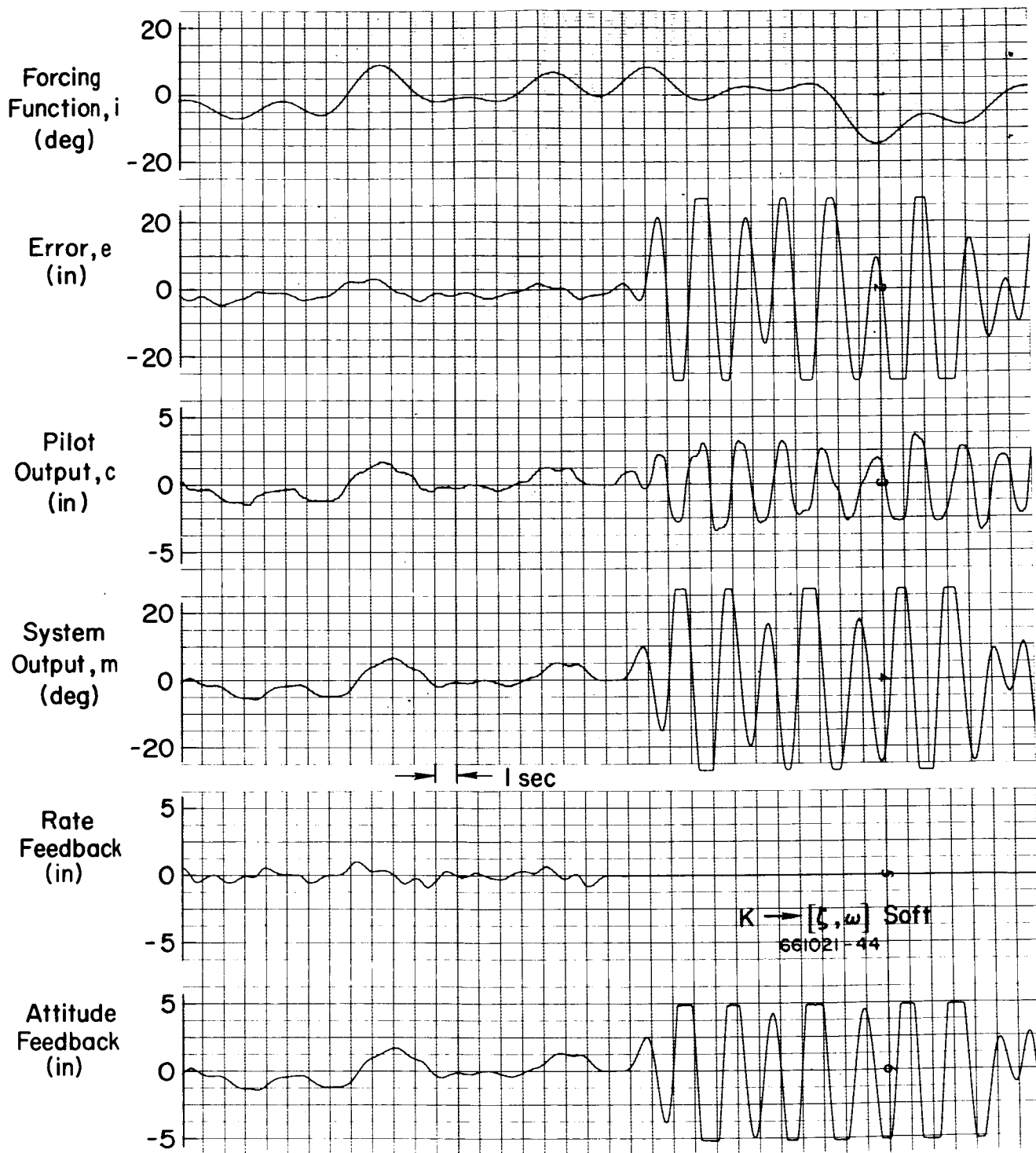
Figure 12. Example of a Soft-Failure from K to $[\zeta, \omega]$

88
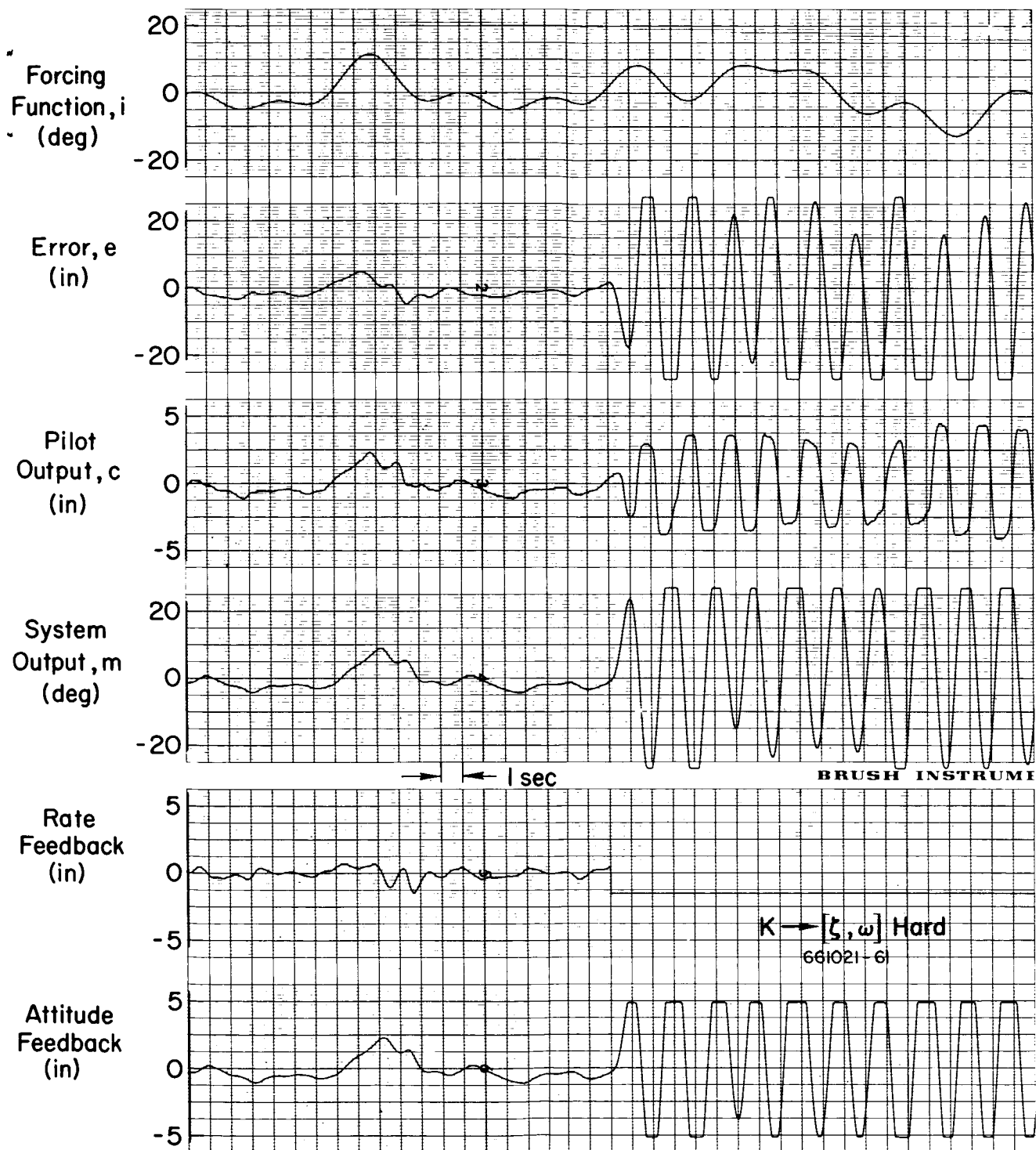
Figure 13. Example of a Hard-Failure from K to $[\zeta, \omega]$

89
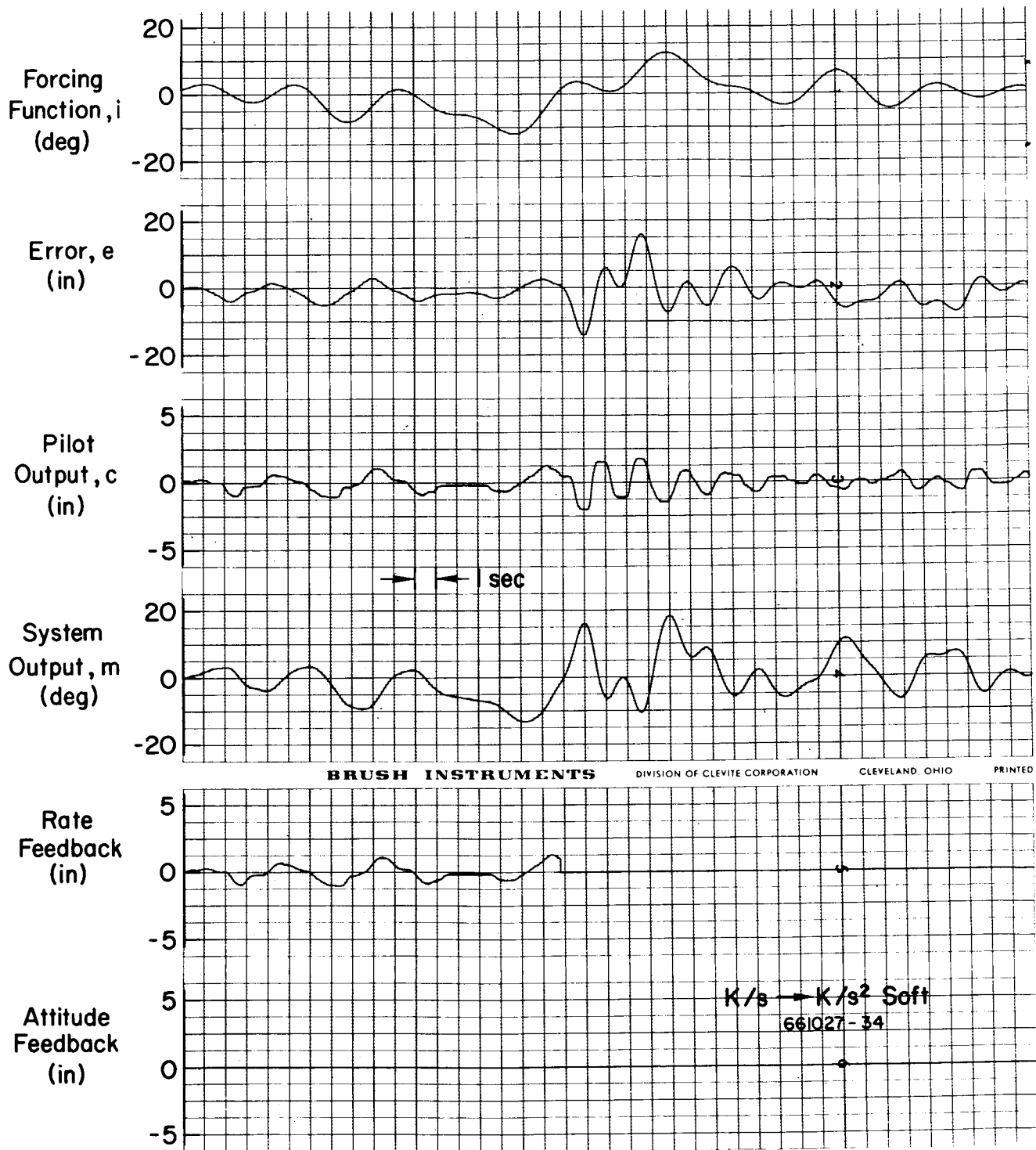
Figure 14. Example of a Soft-Failure from K/s to K/s^2

90
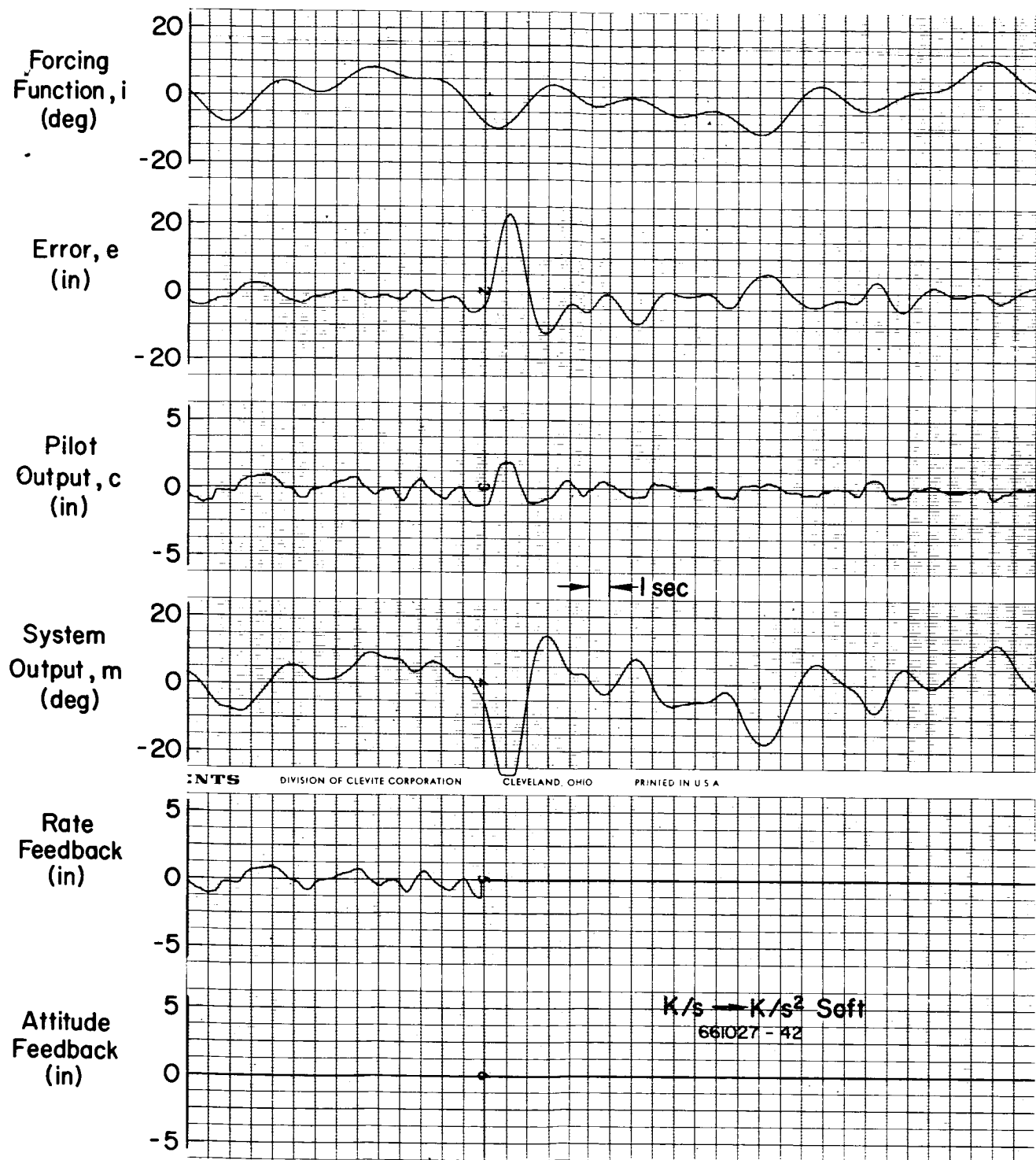
Figure 15. Example of a Soft-Failure from $\dot{K}/s$ to K/s^2
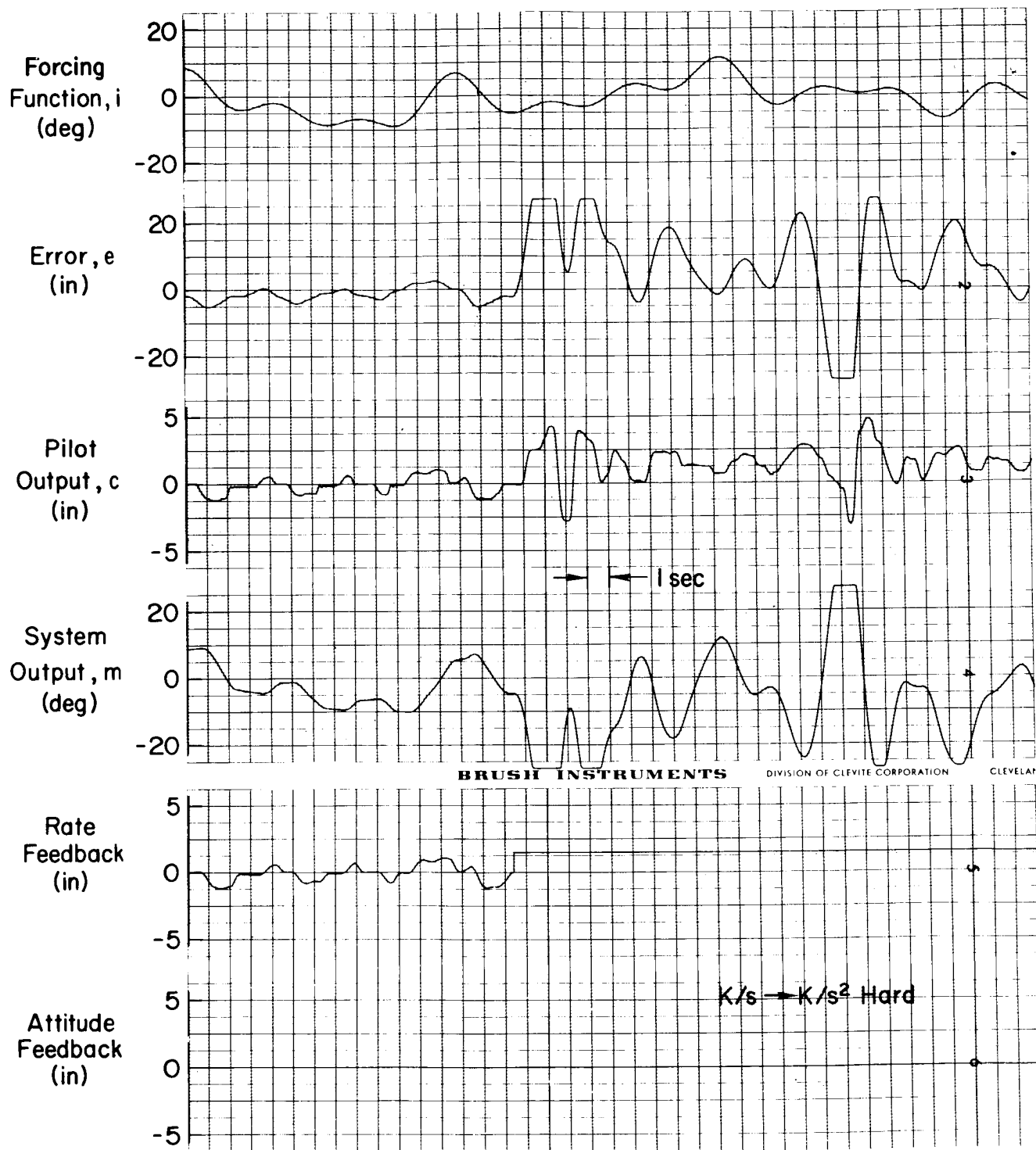
Figure 16. Example of a Hard-Failure from K/s to K/s^2
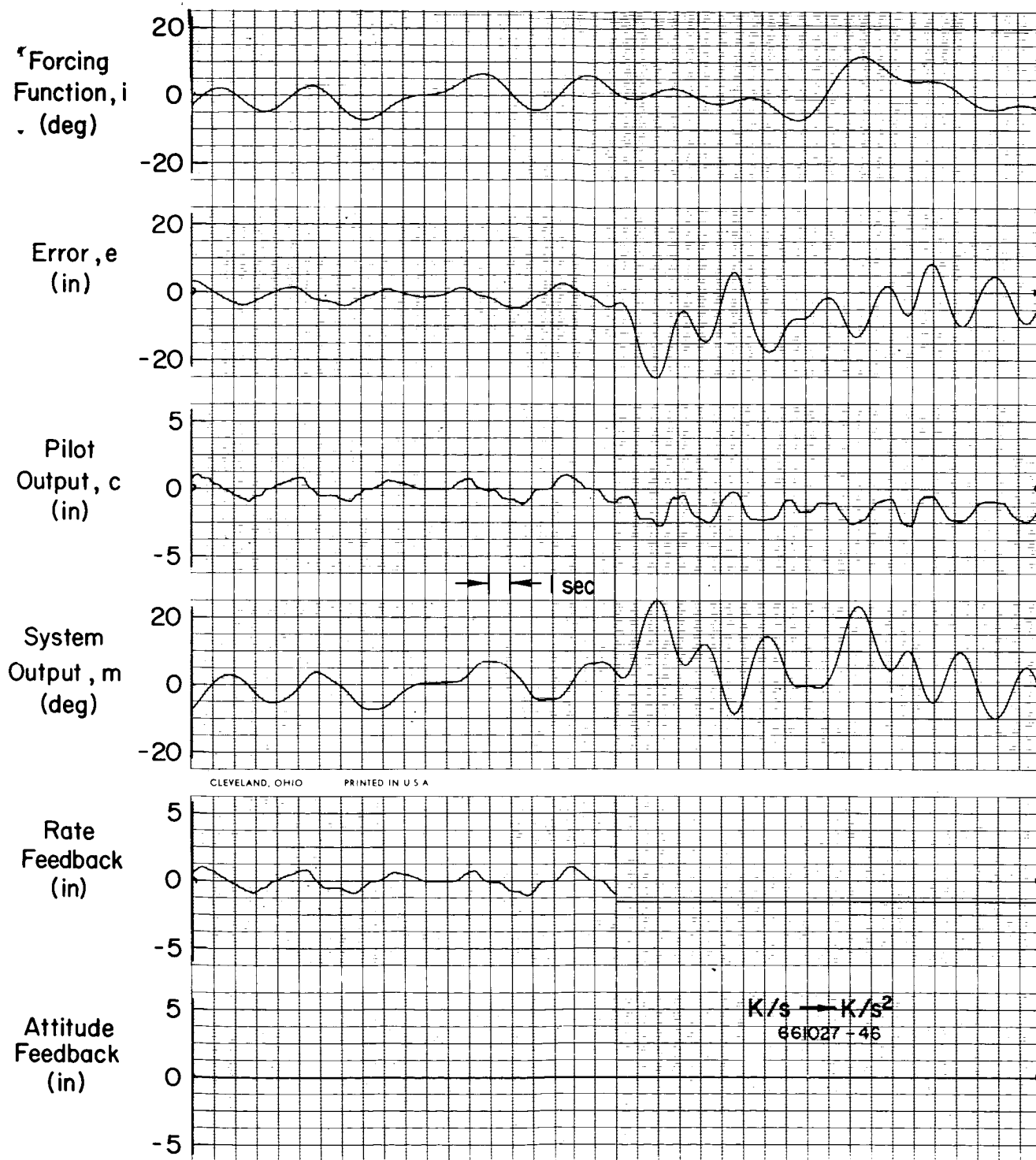
Figure 17. Example of a Hard-Failure from K/s to K/s^2
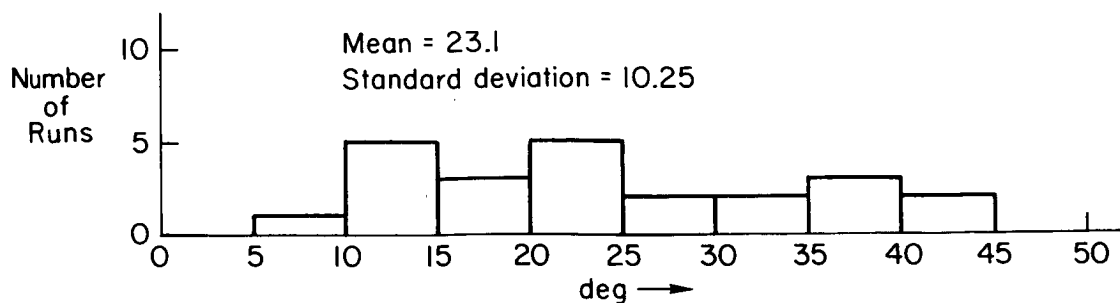
a) $K \rightarrow \dfrac{K}{s^2}$ (soft)

b) $\dfrac{K}{s} \rightarrow \dfrac{K}{s^2}$ (soft)

c) $\dfrac{K}{s} \rightarrow \dfrac{K}{s^2}$ (hard)

Figure 18. Magnitude of First Error Peak

94

Figure 19. Magnitude of Divergence Rate

Figure 20.- Time from Retention to Peak

Mean = 1.0
Standard Deviation = 0.7

a) $K \longrightarrow \dfrac{K}{s^2}$ (soft)

Mean = .95
Standard Deviation = .6

b) $\dfrac{K}{s} \longrightarrow \dfrac{K}{s^2}$ (soft)

Mean = .564
Standard Deviation = .084

c) $\dfrac{K}{s} \longrightarrow \dfrac{K}{s^2}$ (hard)

Figure 21.- Retention Phase Duration

Mean = 5.8
Standard Deviation = 2.56

a) $K \rightarrow \dfrac{K}{s^2}$ (soft)

Mean = 5.12
Standard Deviation = 2.742

b) $\dfrac{K}{s} \rightarrow \dfrac{K}{s^2}$ (soft)

Mean = 6.0
Standard Deviation = 4.4
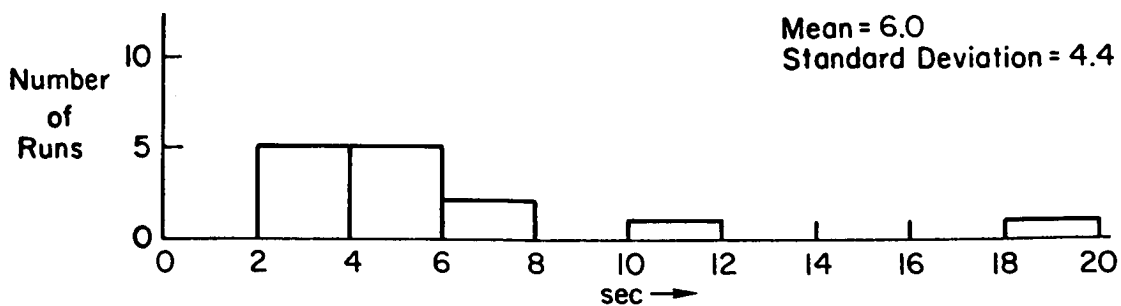
c) $\dfrac{K}{s} \rightarrow \dfrac{K}{s^2}$ (hard)

Figure 22. Total Settling Time

98
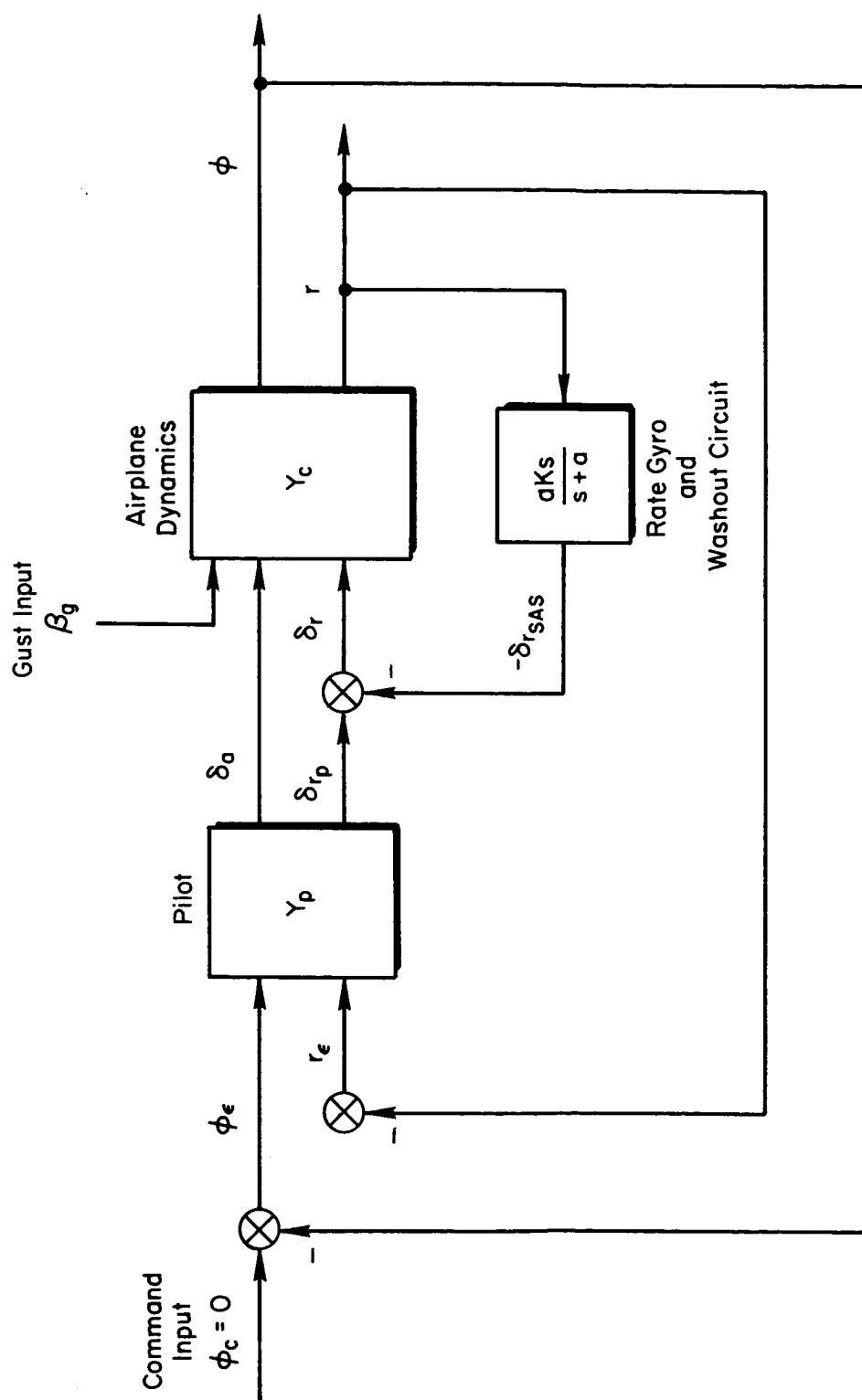
Figure 23. Block Diagram of Multiple-Loop Control Task
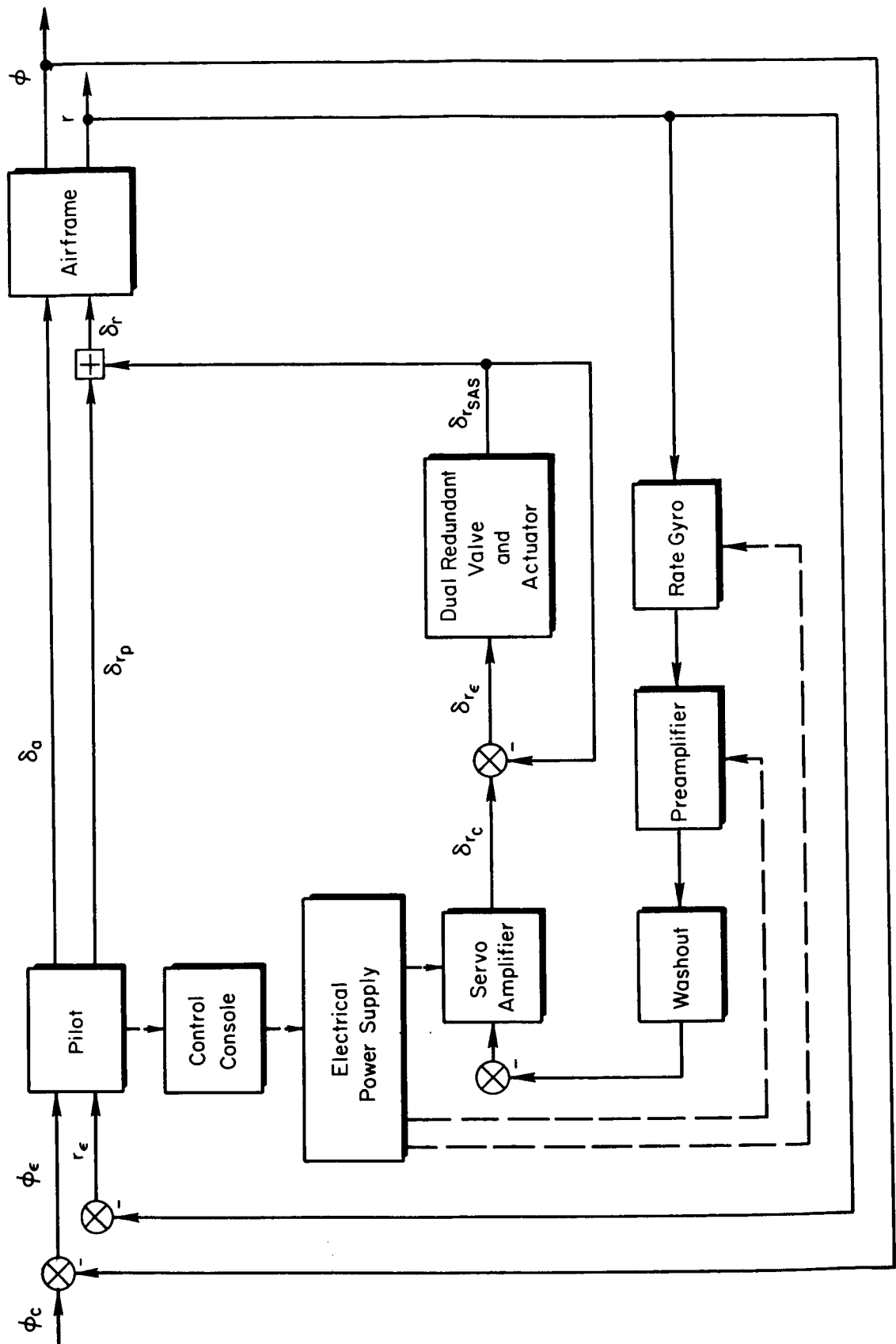
Figure 24. Mechanizational Block Diagram for Multiple-Loop Experiments
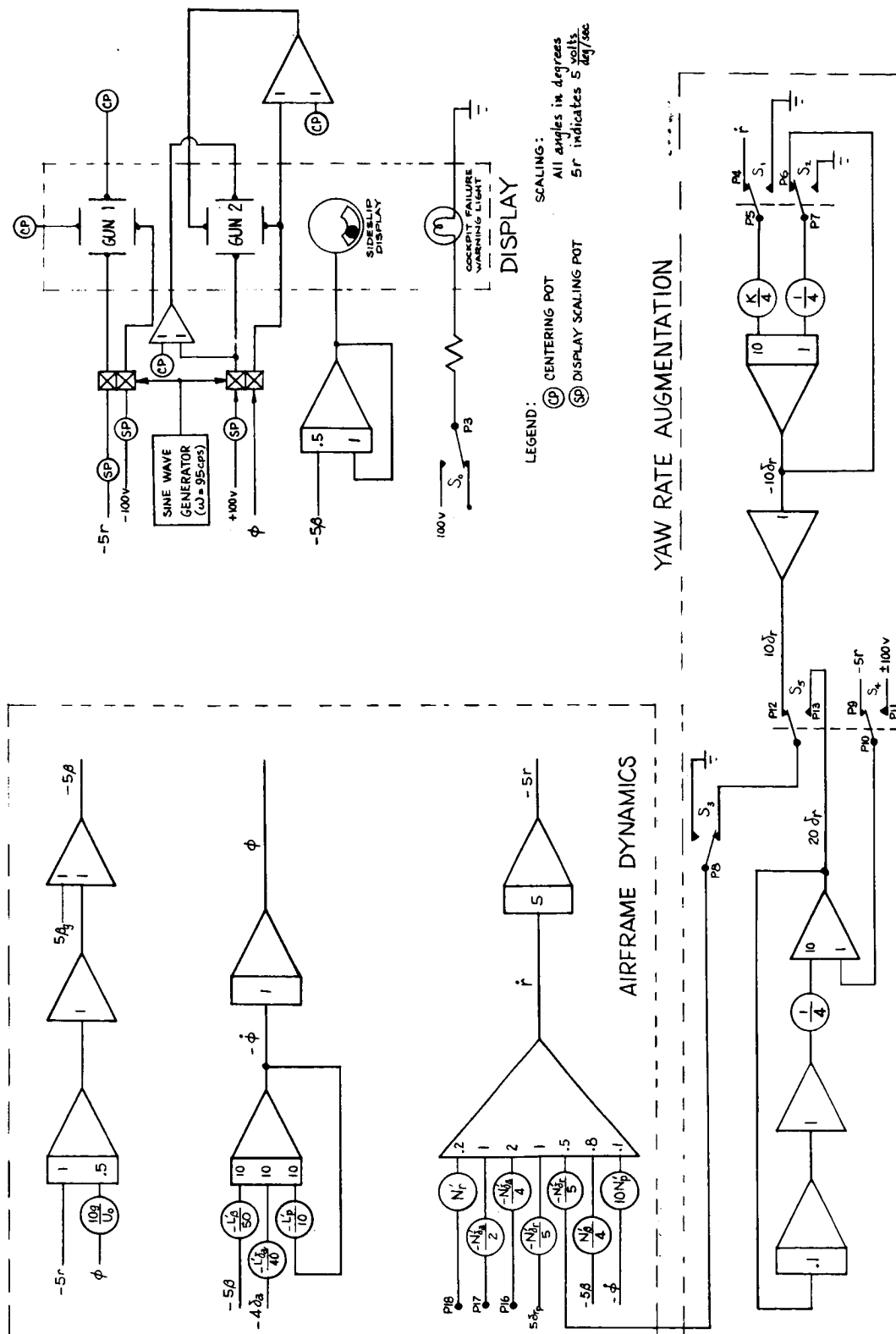
Figure 25. Analog Mechanization for Multiloop Experiments

101

P( ) indicates pin number
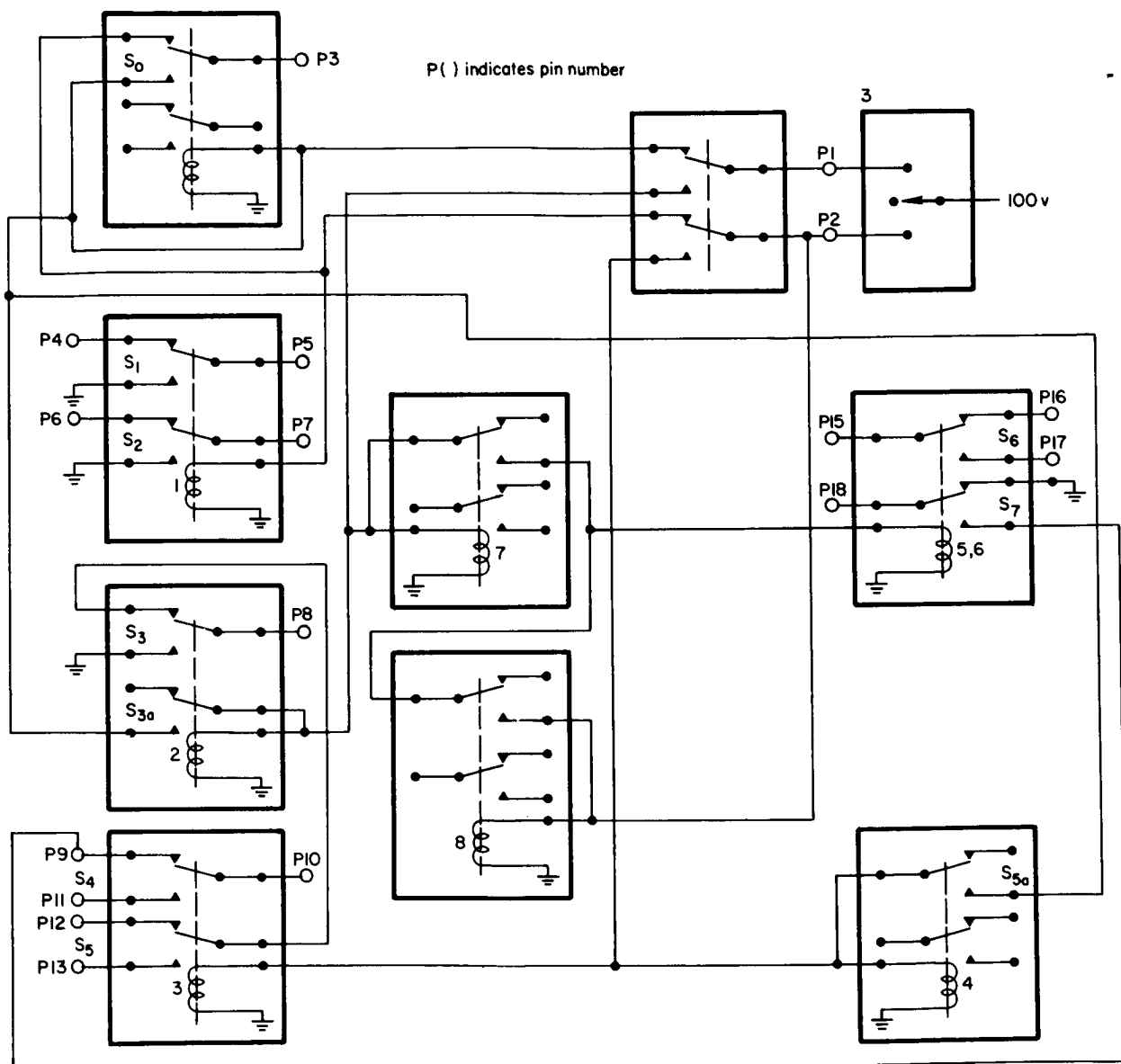
Figure 26. Switching Logic for Multiple-Loop Experiments
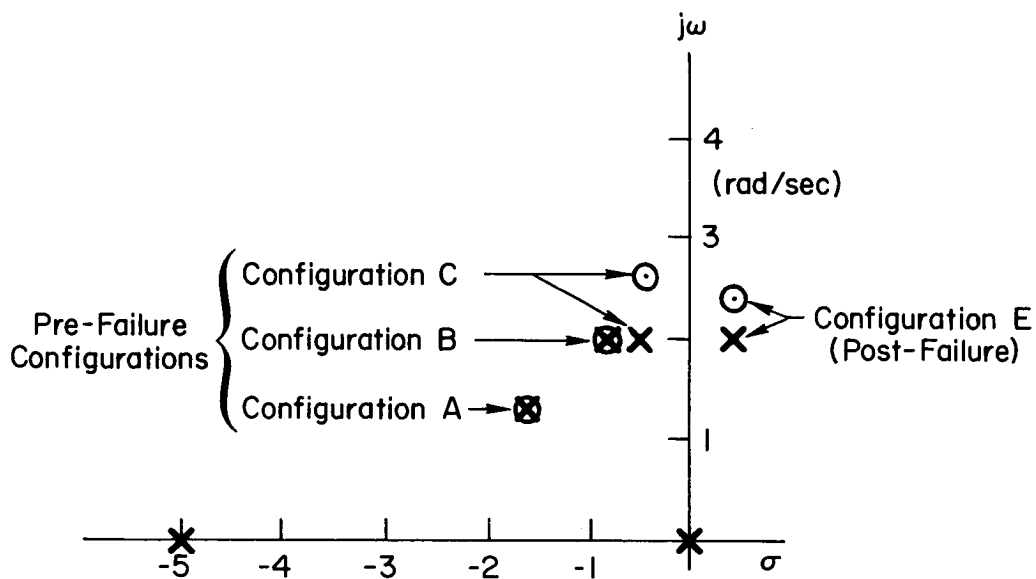
Figure 27. Root Locus Representation
of the Open-Loop φ/δ_a Transfer Functions
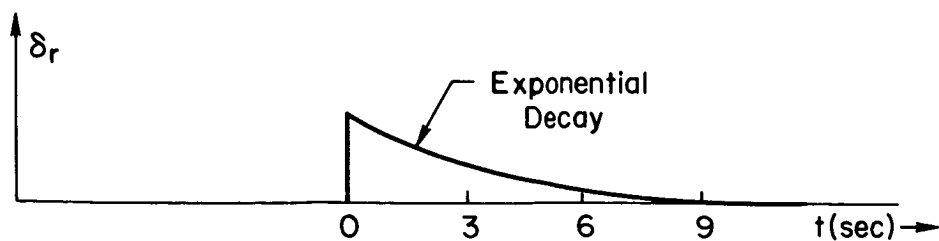
Figure 28. Plot of a Washed-Out Rudder Step
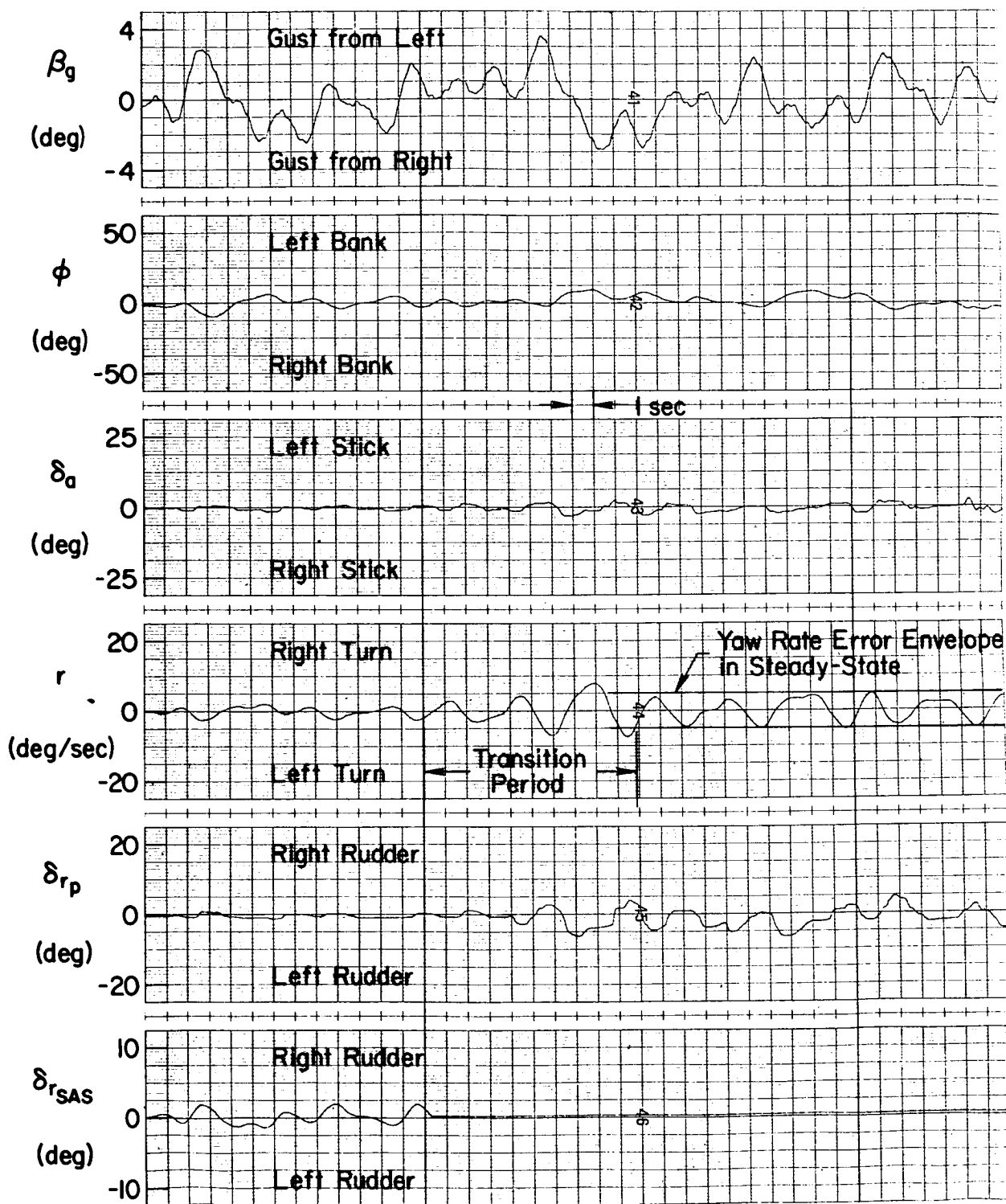
Figure 29. Example of a Soft-Failure with Configuration A

104
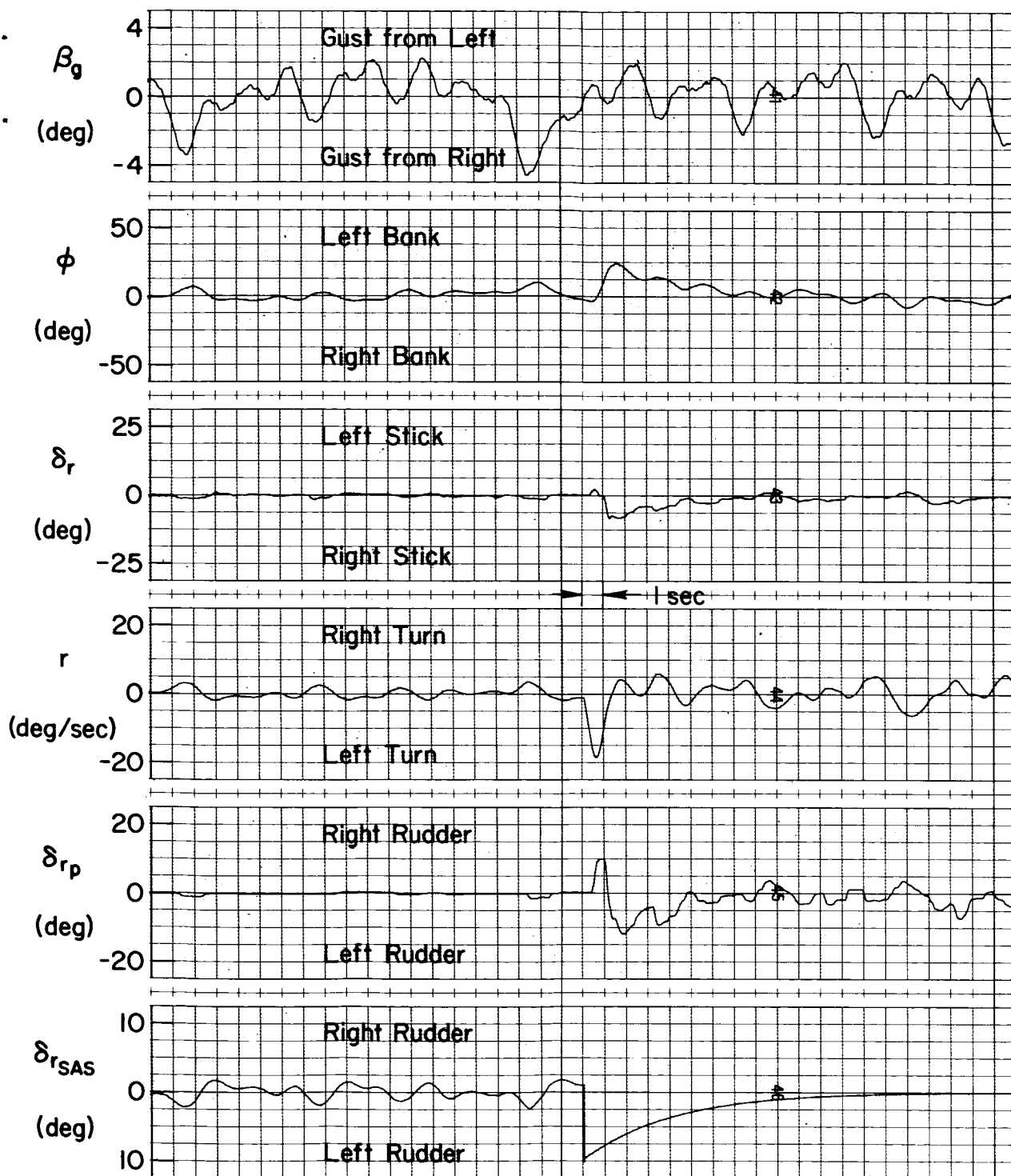
Figure 30. Example of a Hard-Failure with Configuration A

105
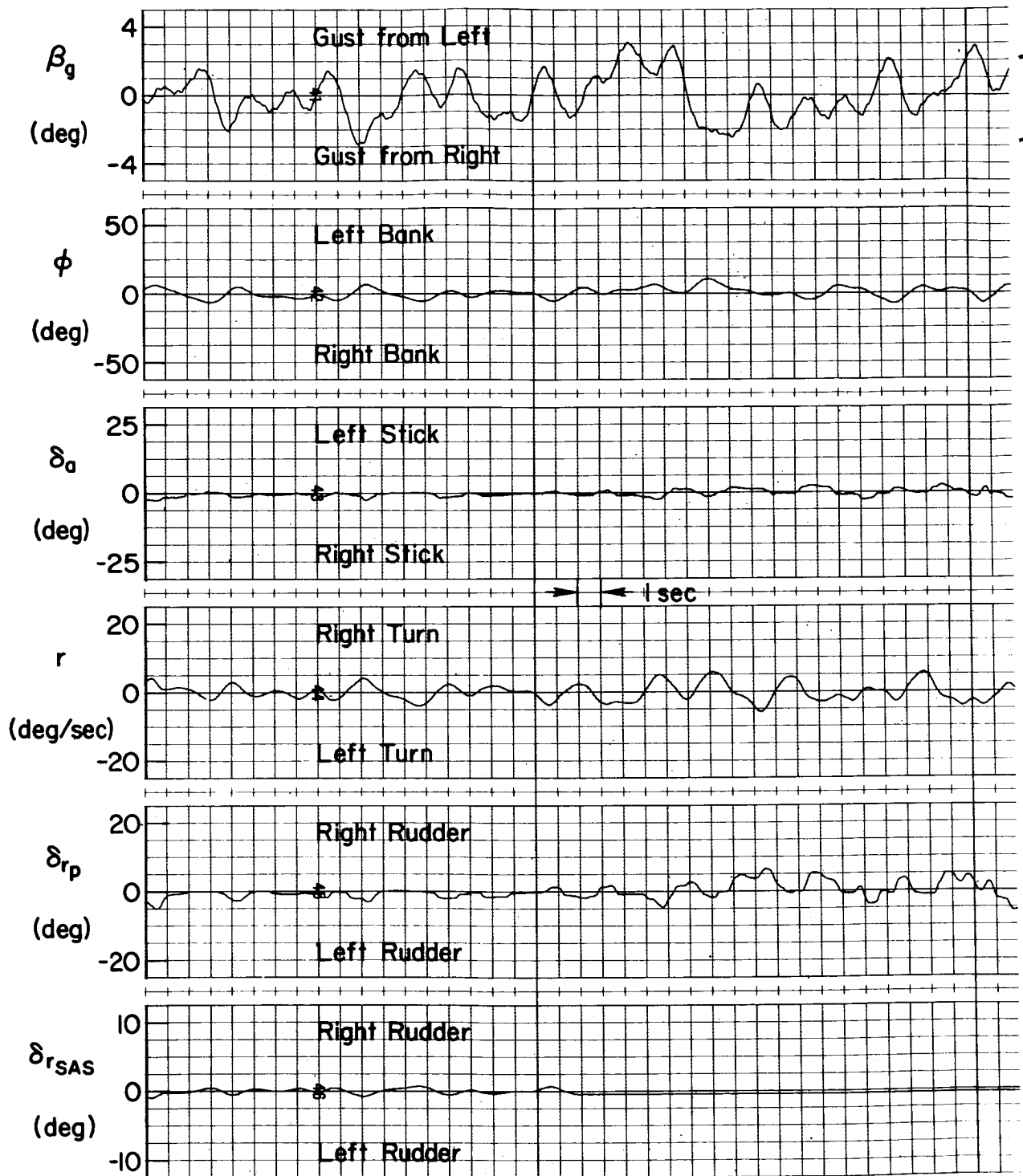
Figure 31. Example of a Soft-Failure with Configuration B

106
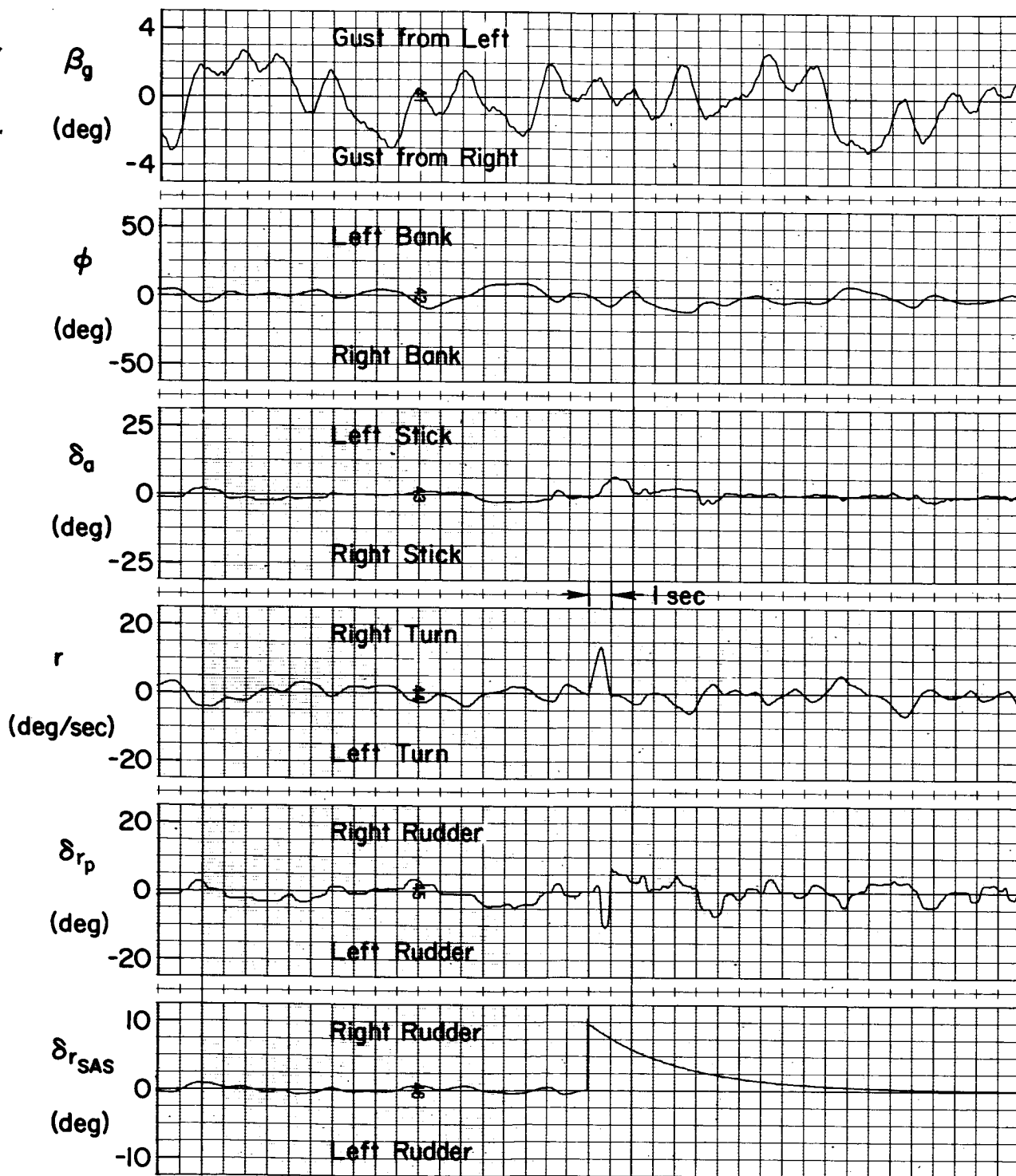
Figure 32. Example of a Hard-Failure with Configuration B
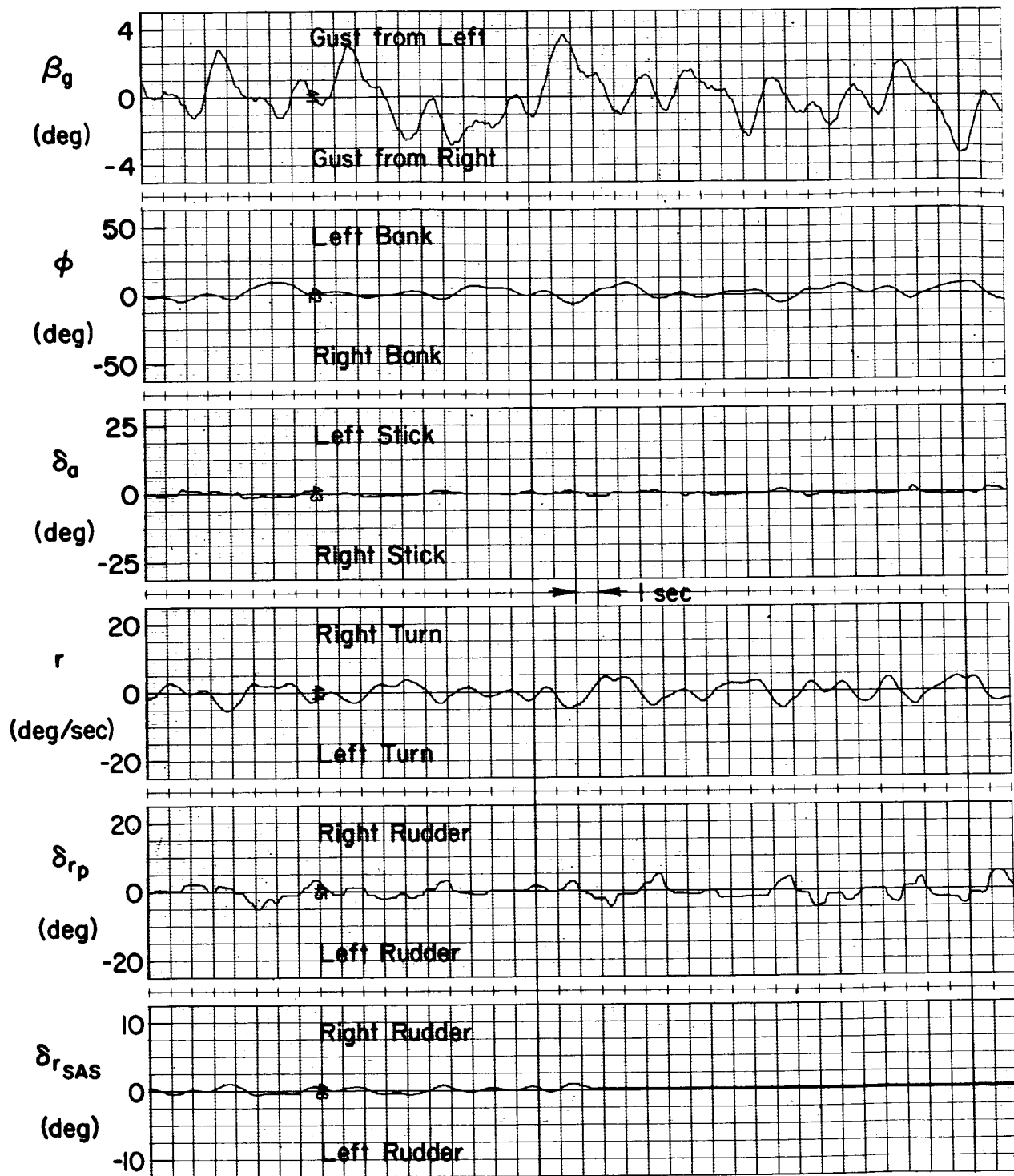
Figure 33. Example of a Soft-Failure with Configuration C

108
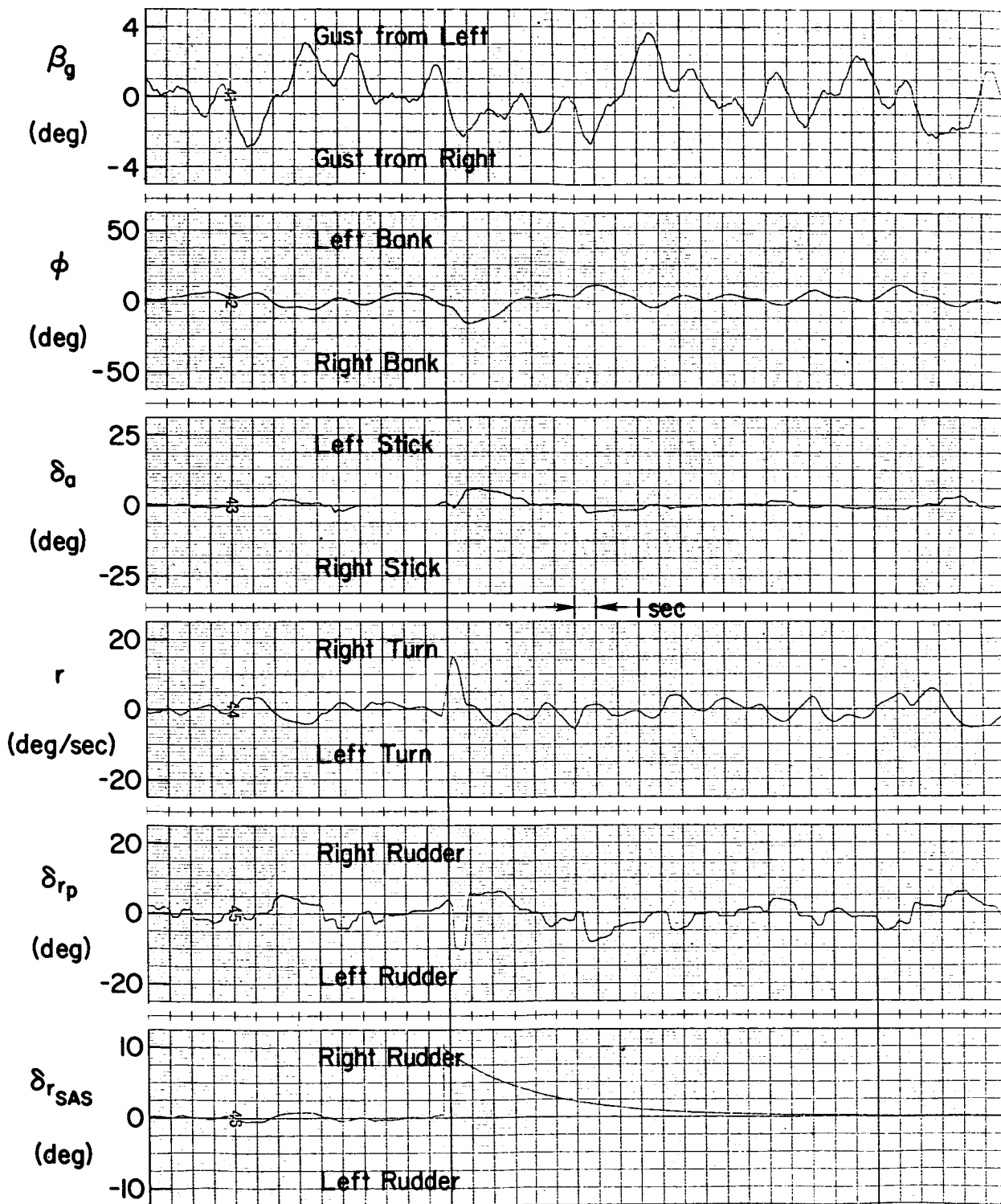
Figure 34. Example of a Hard-Failure with Configuration C

109
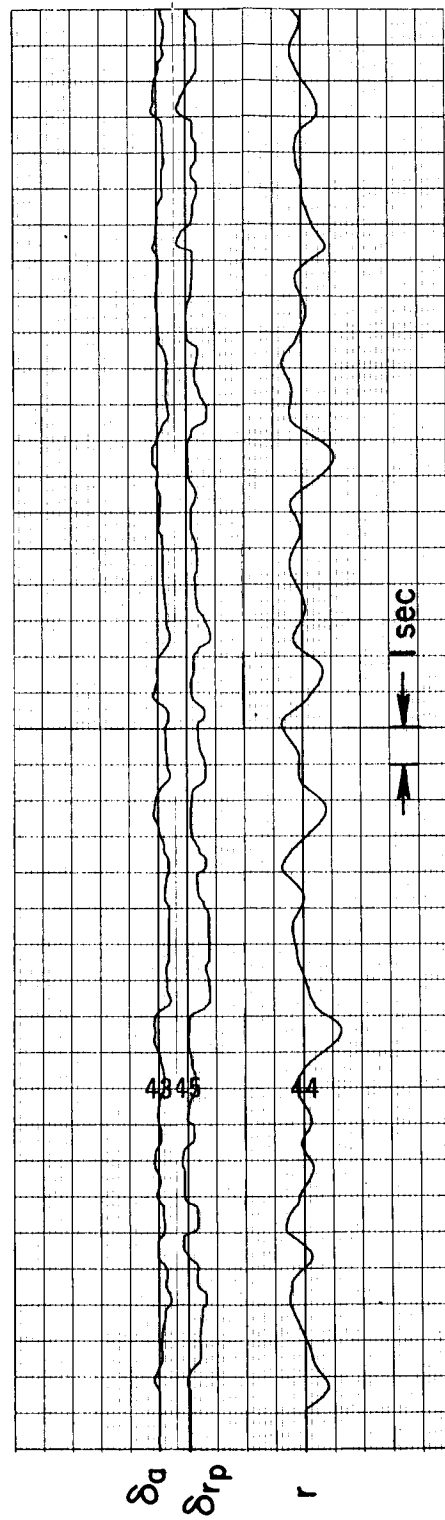
Figure 35. Example of Crossfeed

110
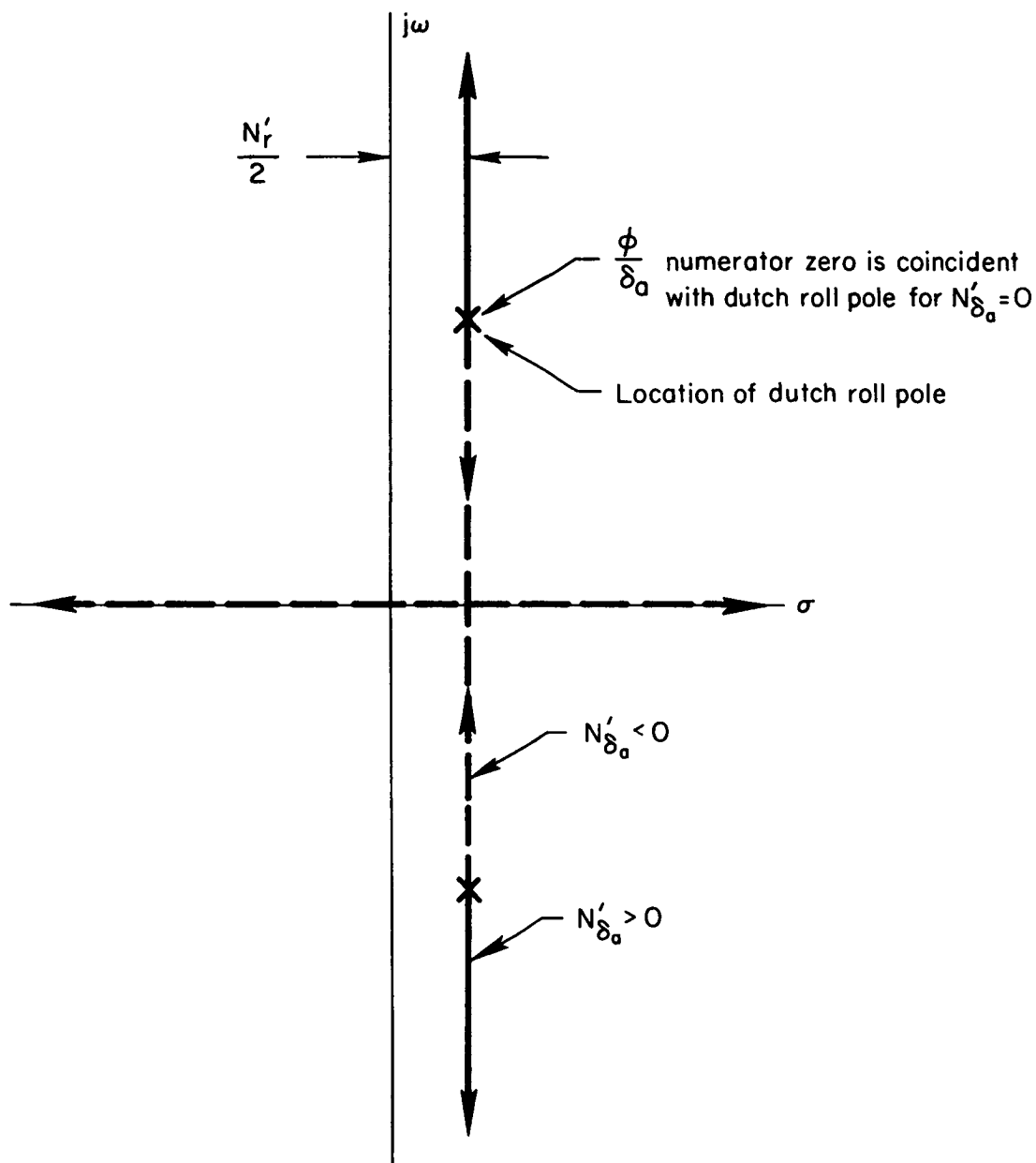
Figure 36. Effect of N'_{δ_a} on the φ/δ_a Numerator Locus, Configuration E
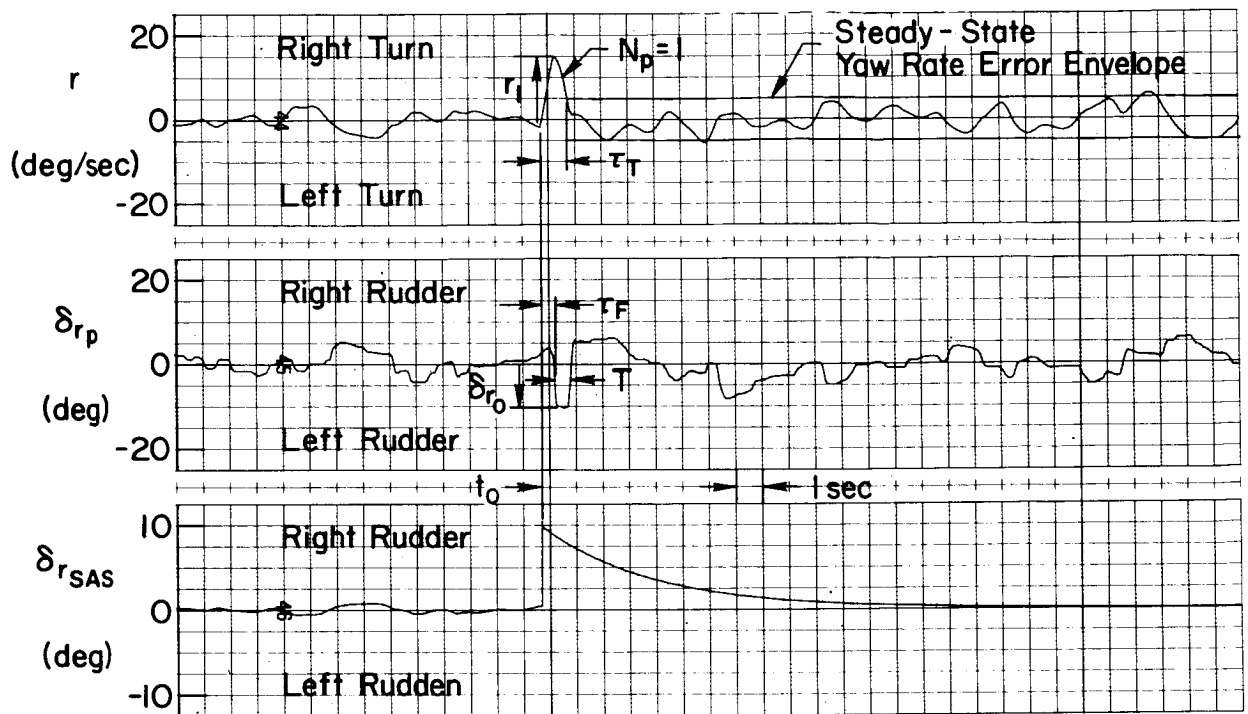
(a) Hard Failure
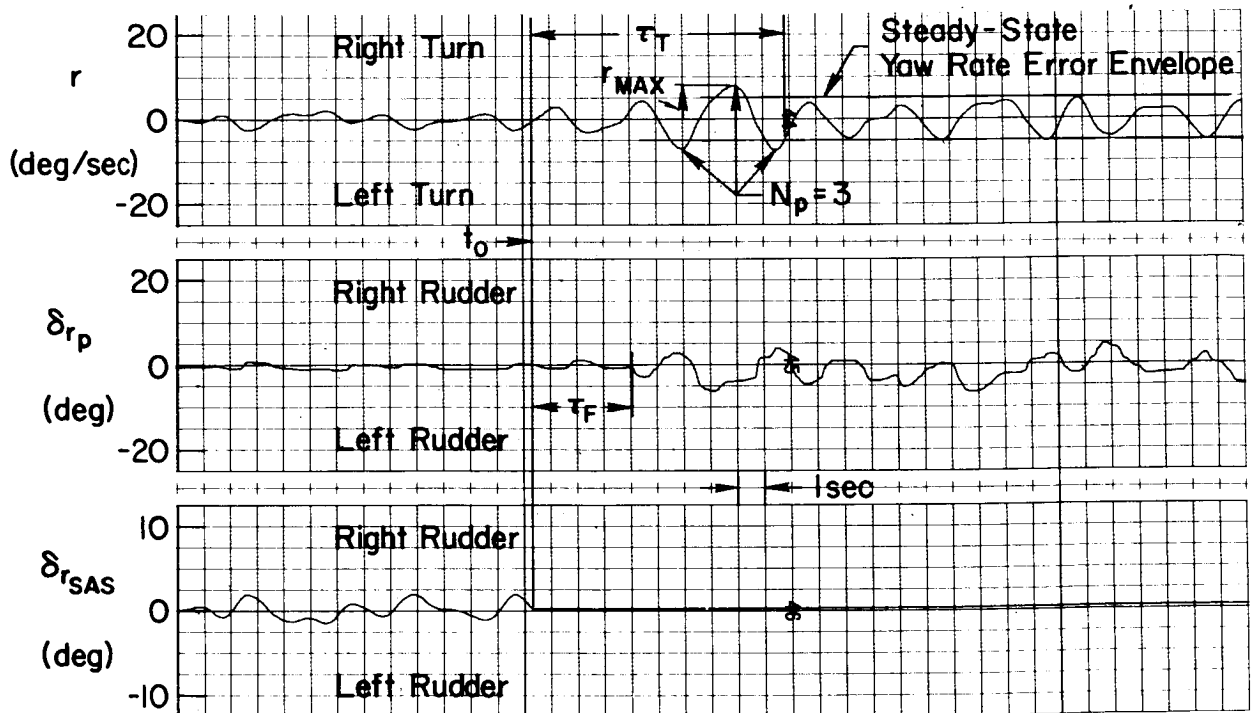
(b) Soft Failure

Figure 37. Definition of Transition Parameters

112

a) Configuration A

b) Configuration B

All 15 runs had no identifiable transition region
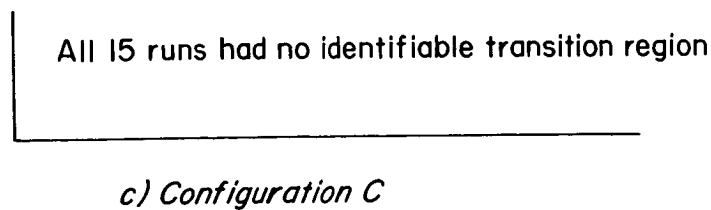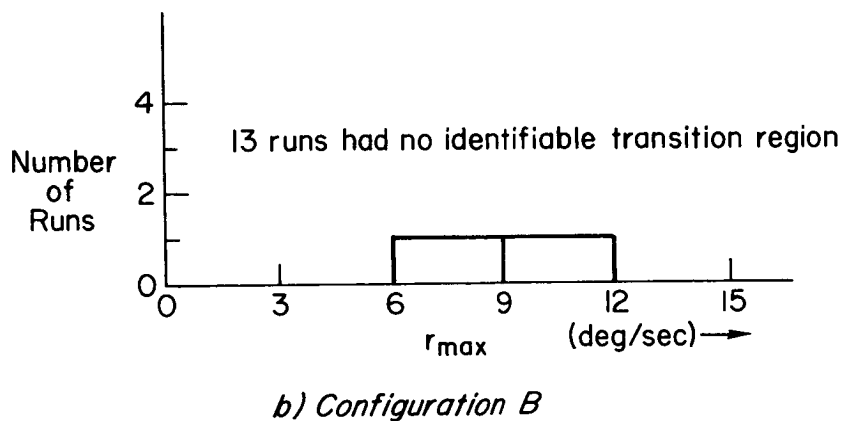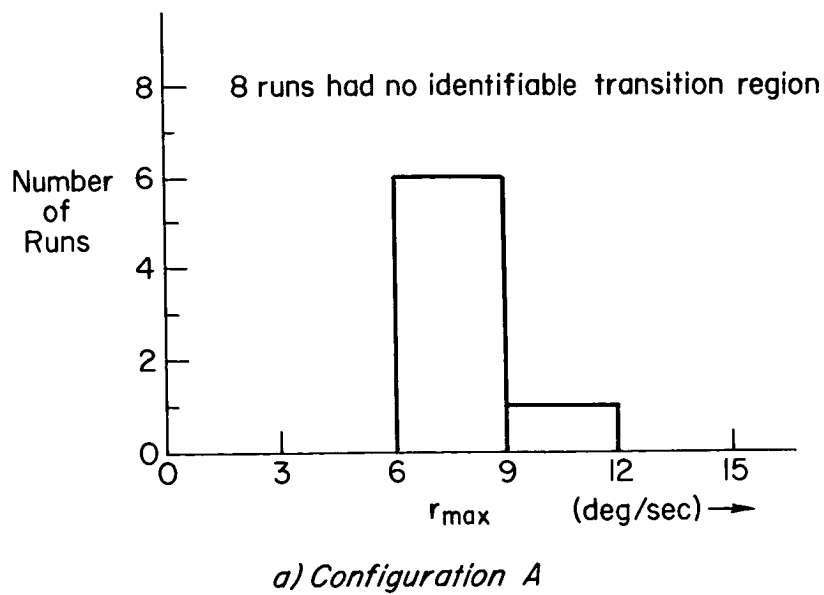
c) Configuration C

Figure 38. Distribution of Maximum Yaw Rate Peaks for Soft-Failures

113
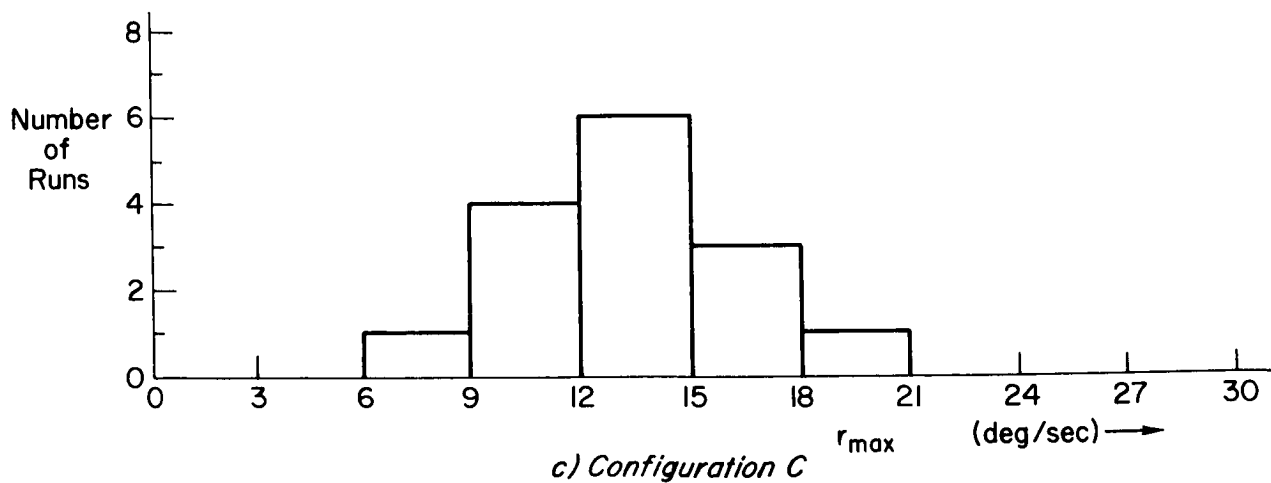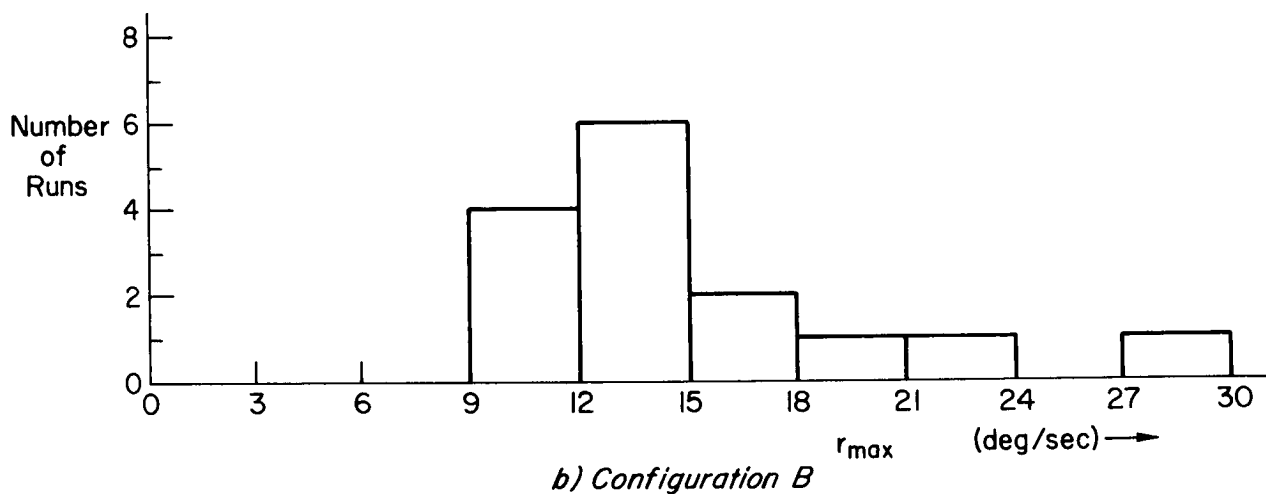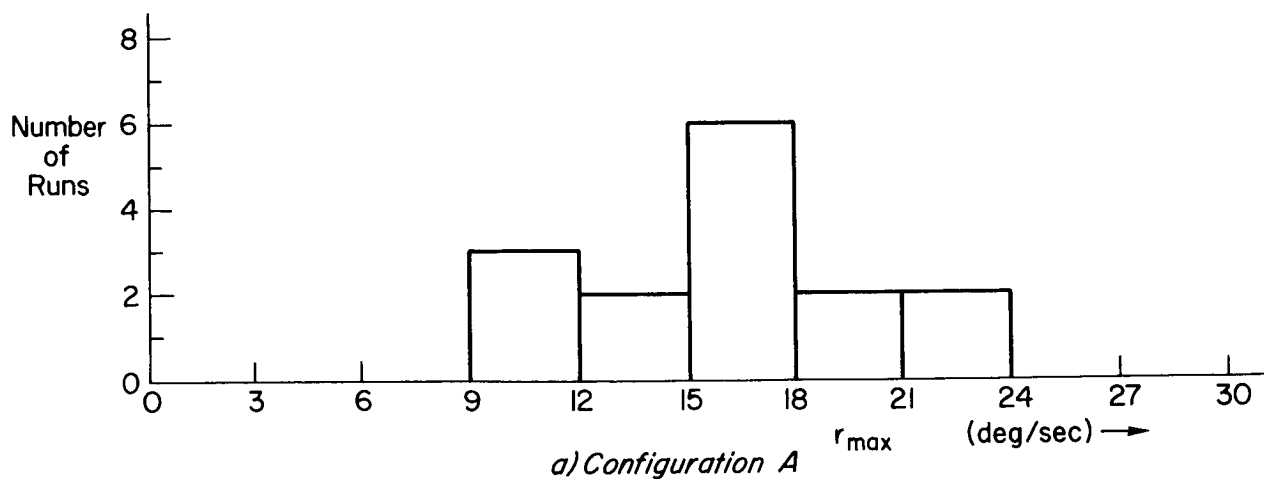
Figure 39. Distribution of Maximum Yaw Rates for Hard-Failures

114

a) Configuration A

b) Configuration B

All 15 runs had no identifiable transition region
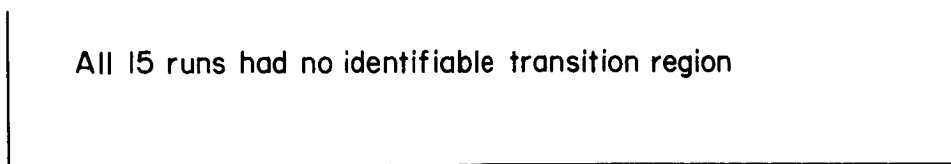
c) Configuration C

Figure 40. Distribution of Transition Durations for Soft-Failures
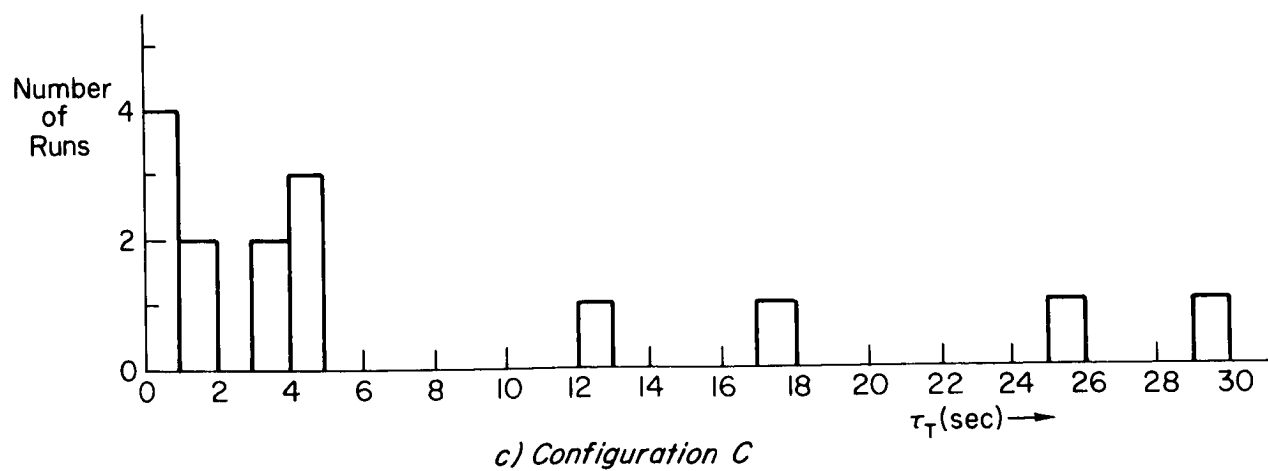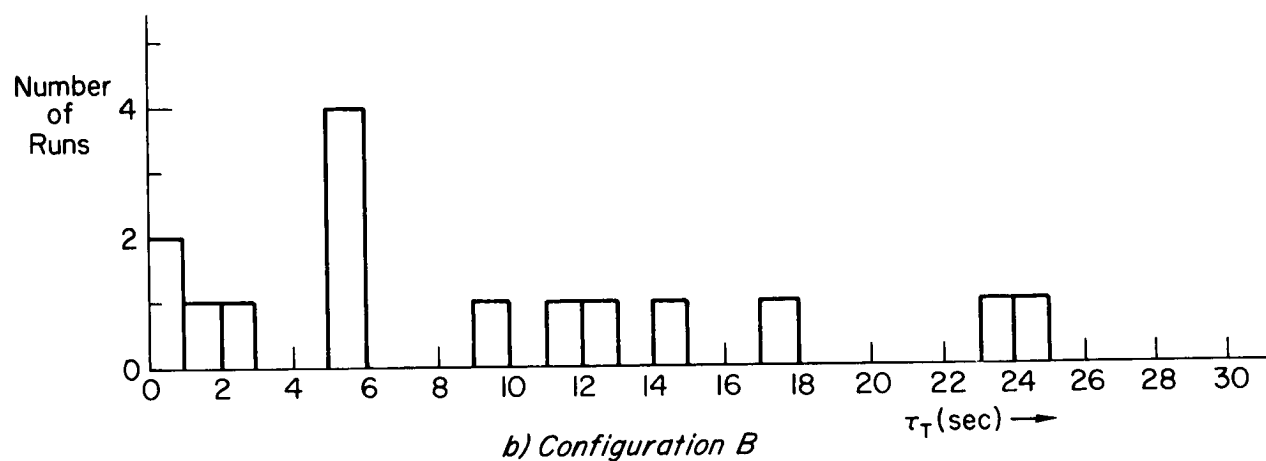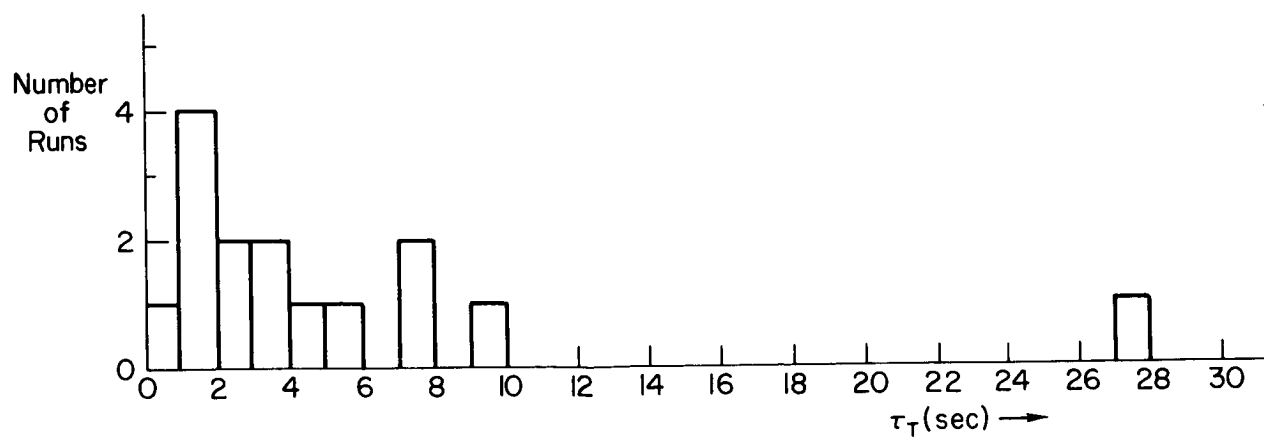
Figure 41. Distribution of Transition Durations for Hard-Failures

116

a) Configuration A

b) Configuration B

All 15 runs had no idetifiable transition region
Mean = "None"

c) Configuration C

Figure 42. Distribution of the Number
of Significant Yaw Rate Error Overshoots for Soft-Failures

117
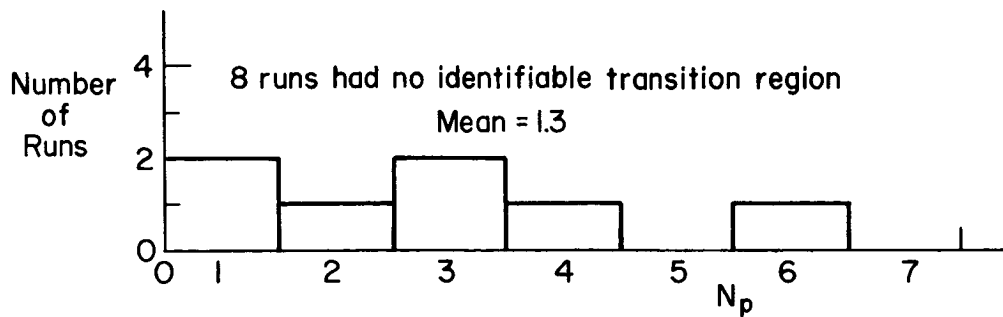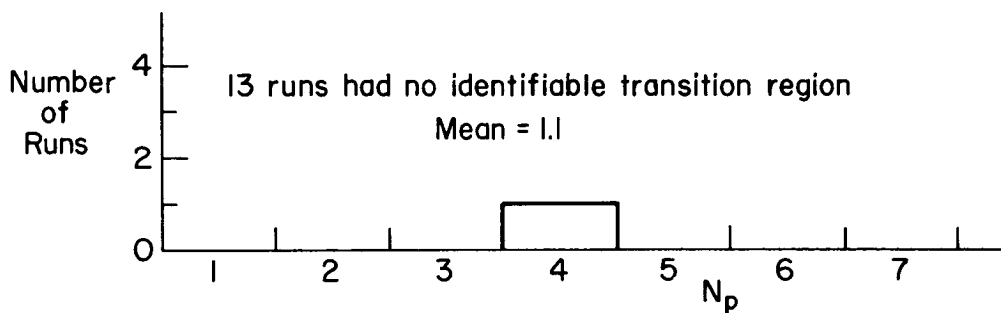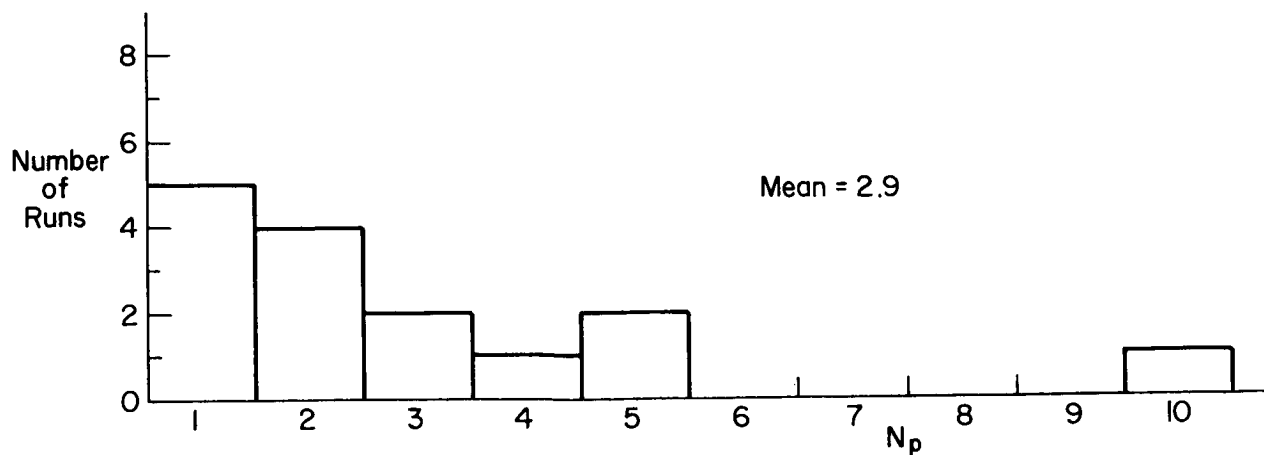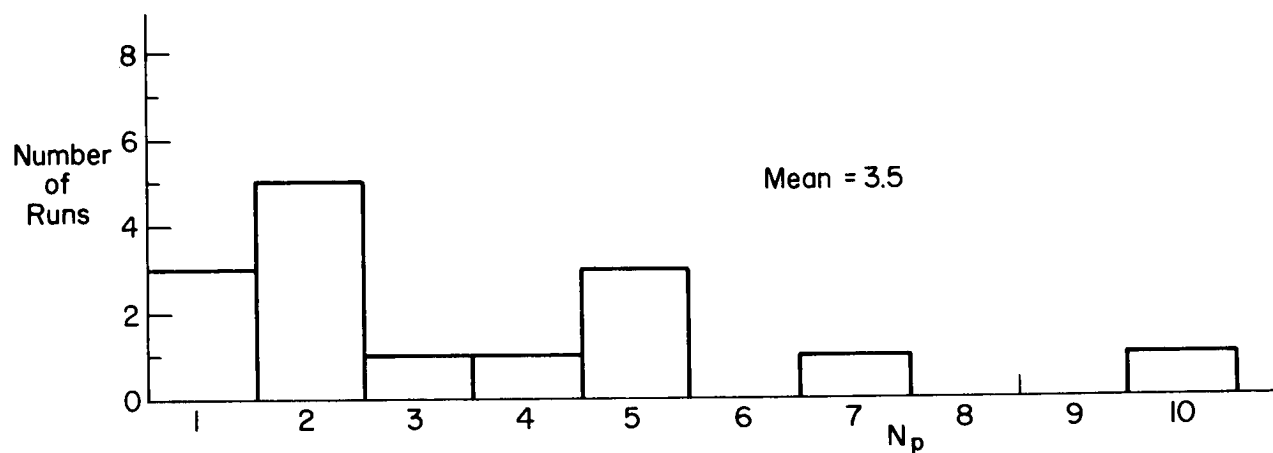
a) Configuration A
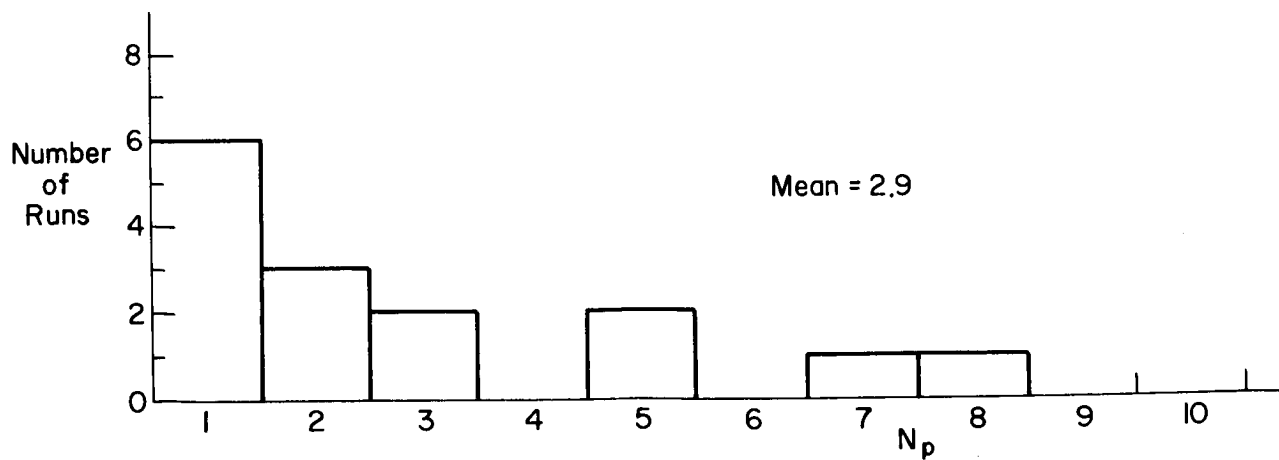
b) Configuration B

c) Configuration C

Figure 43. Distribution of the Number
of Significant Yaw Rate Error Overshoots for Hard-Failures

118
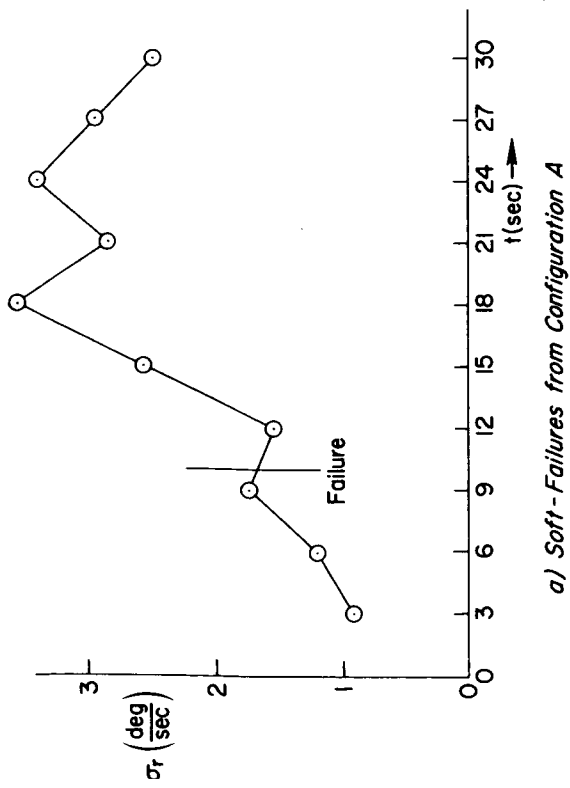
a) Soft-Failures from Configuration A
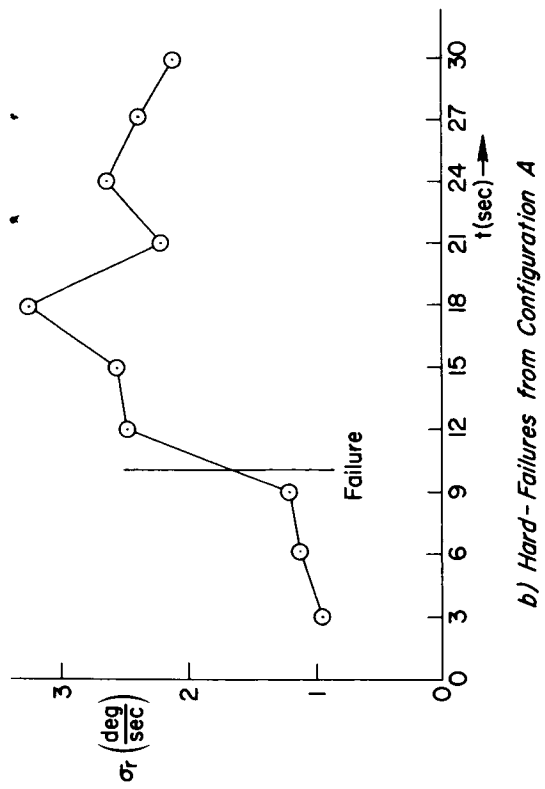
b) Hard-Failures from Configuration A
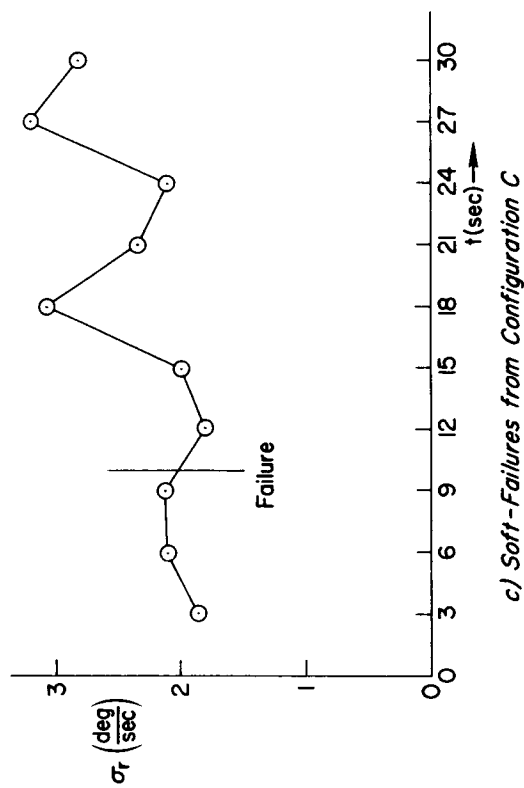
c) Soft-Failures from Configuration C
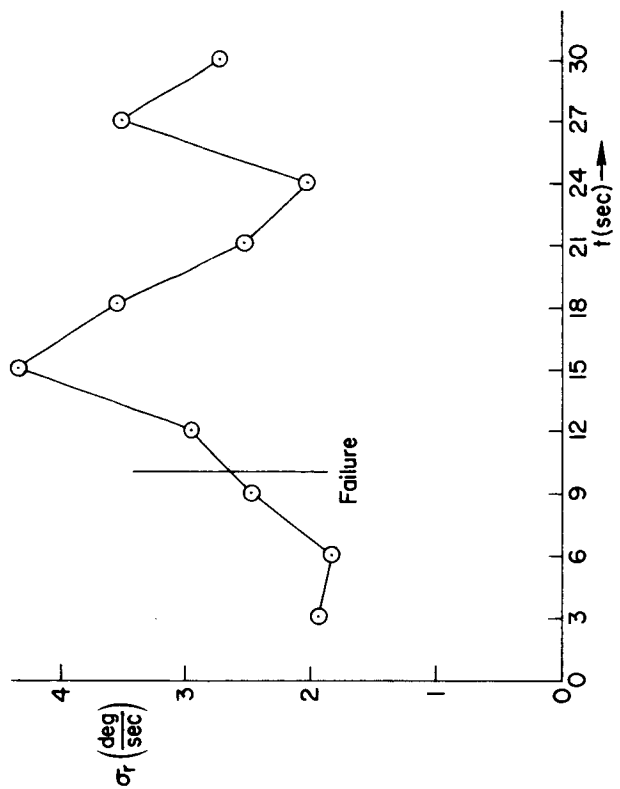
d) Hard-Failures from Configuration C

Figure 44. Yaw Rate Standard Deviations

119
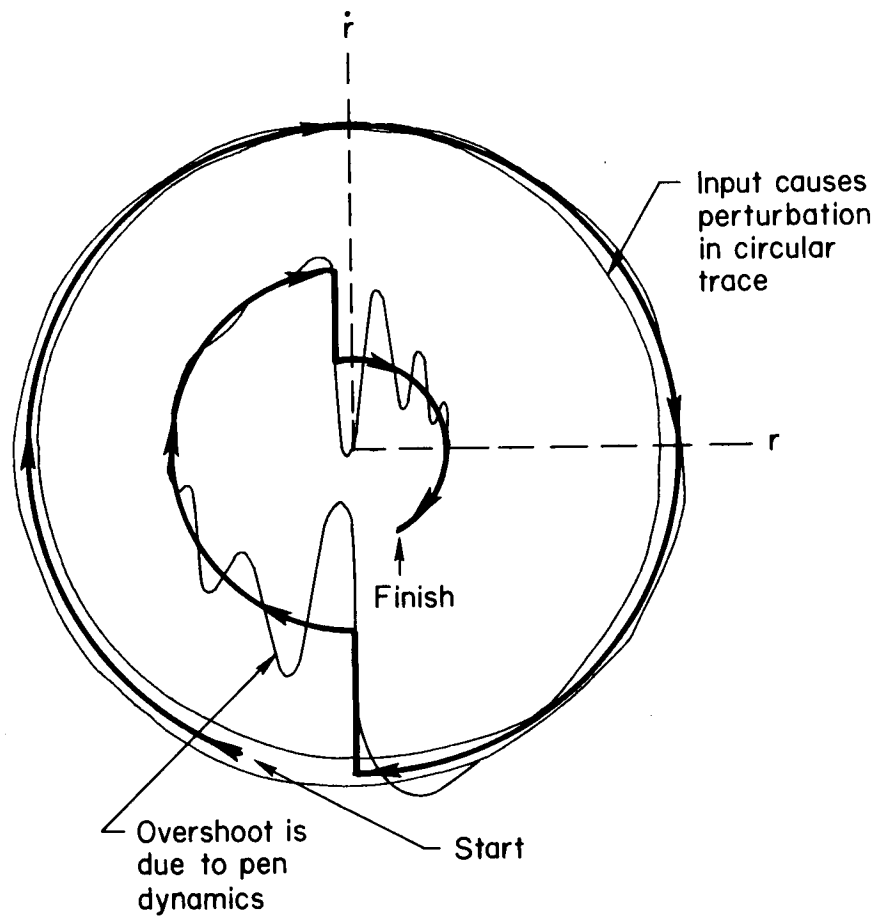
Figure 45. Phase Plane Trajectory
for Time Optimal Control of Yaw Rate
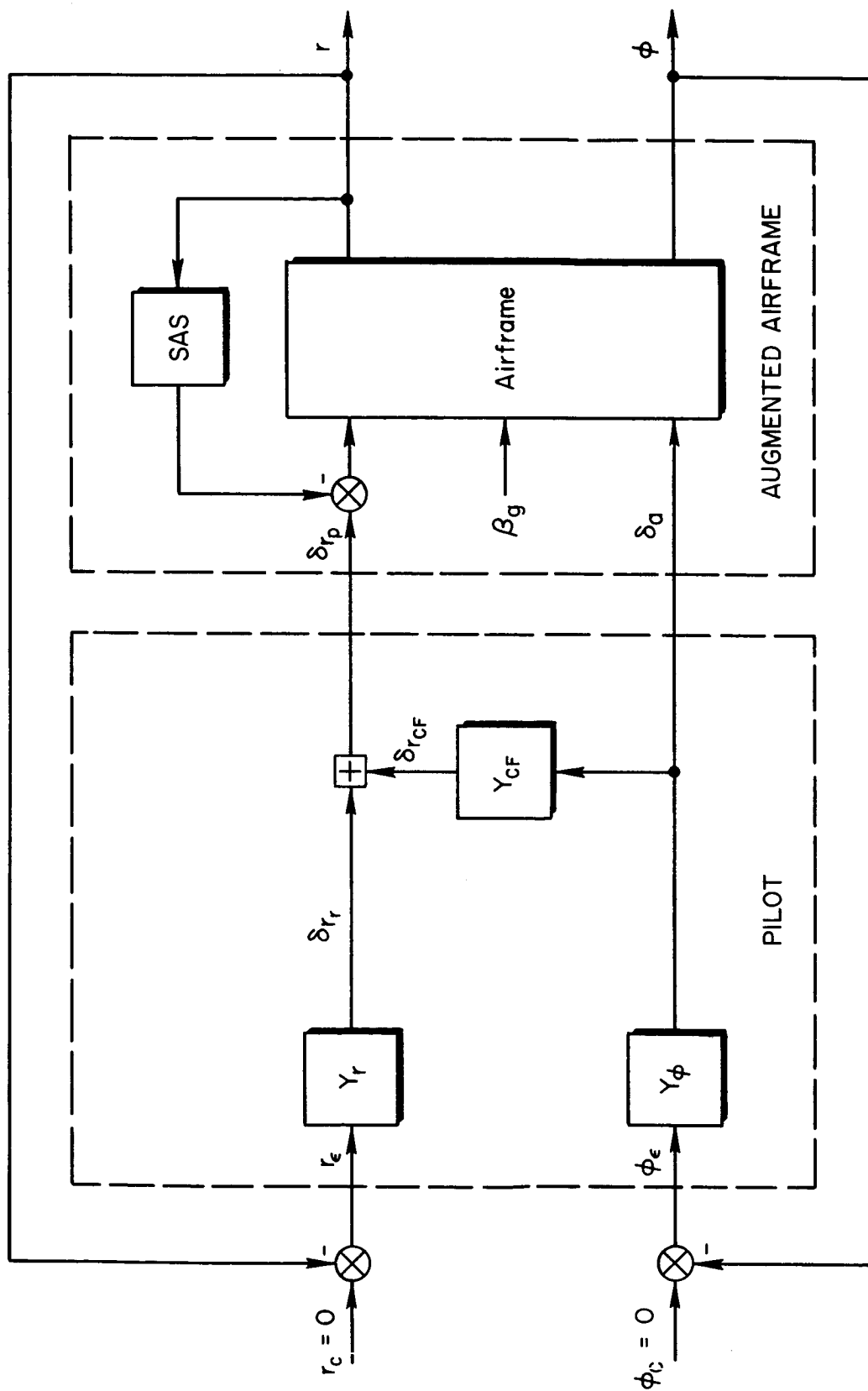
Figure 46. Pilot/Airframe/Augmenter System

121
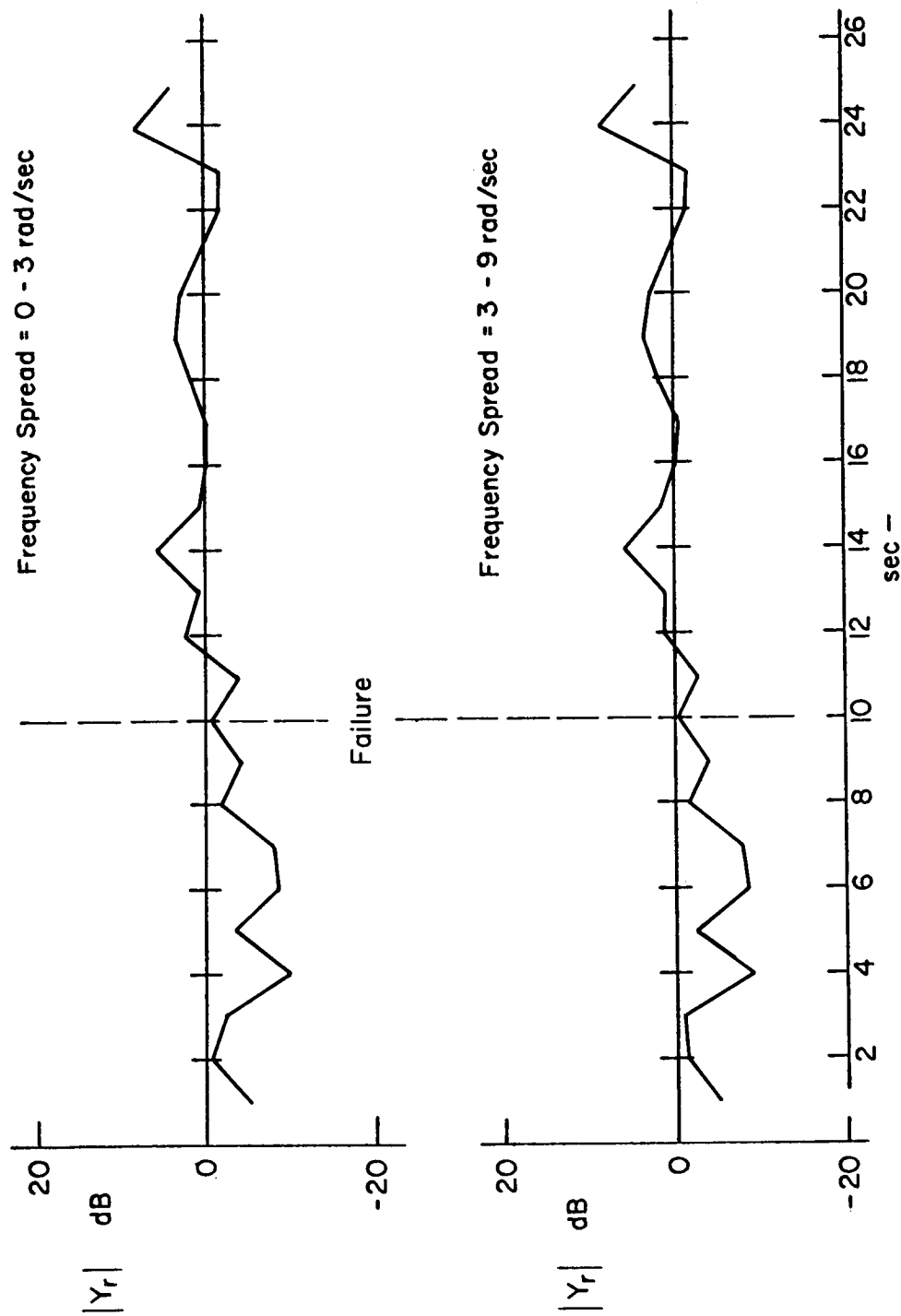
Figure 47. $|Y_r|$ for Soft-Failure from Configuration A
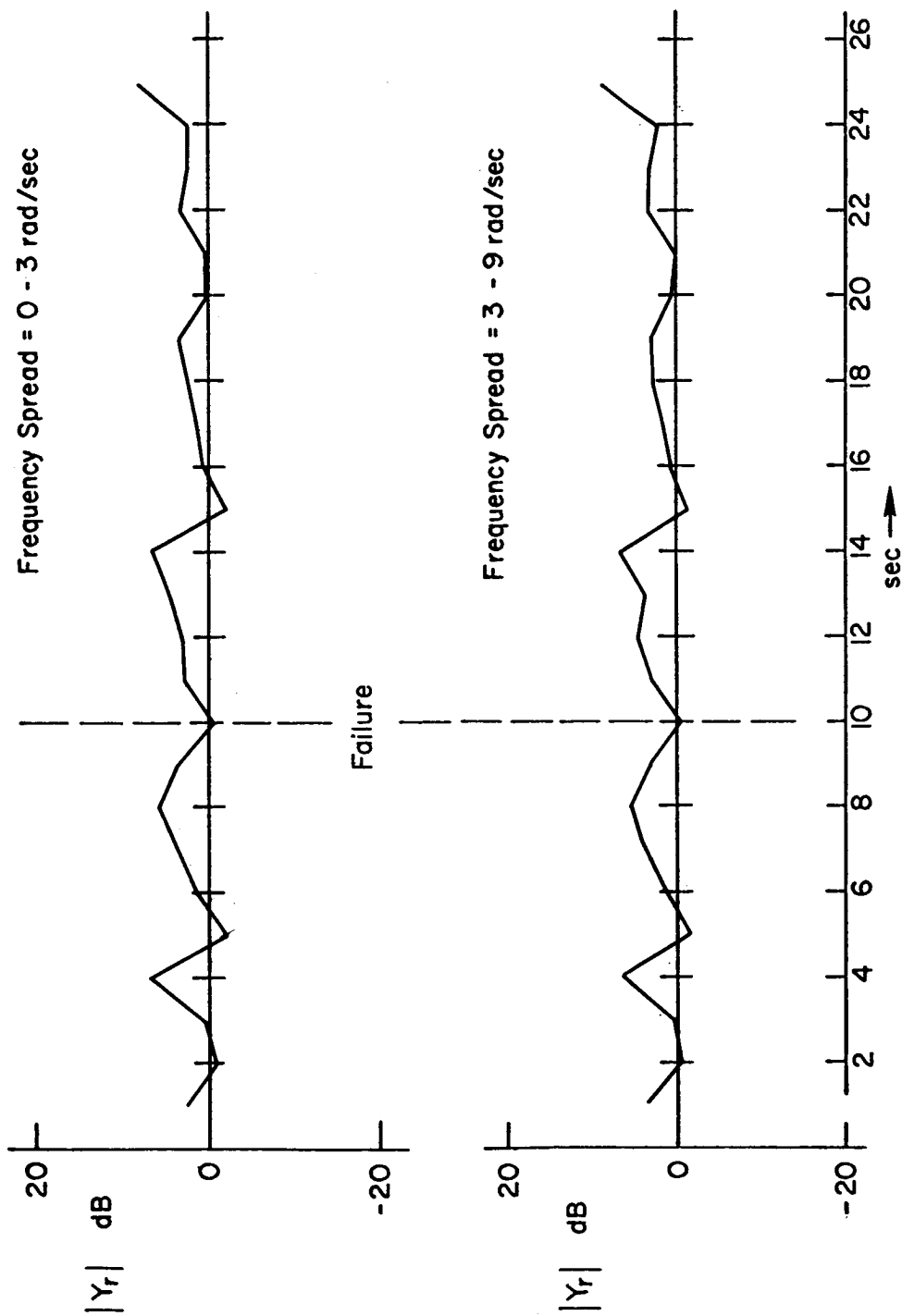
Figure 48. $|Y_r|$ for Soft-Failure from Configuration B
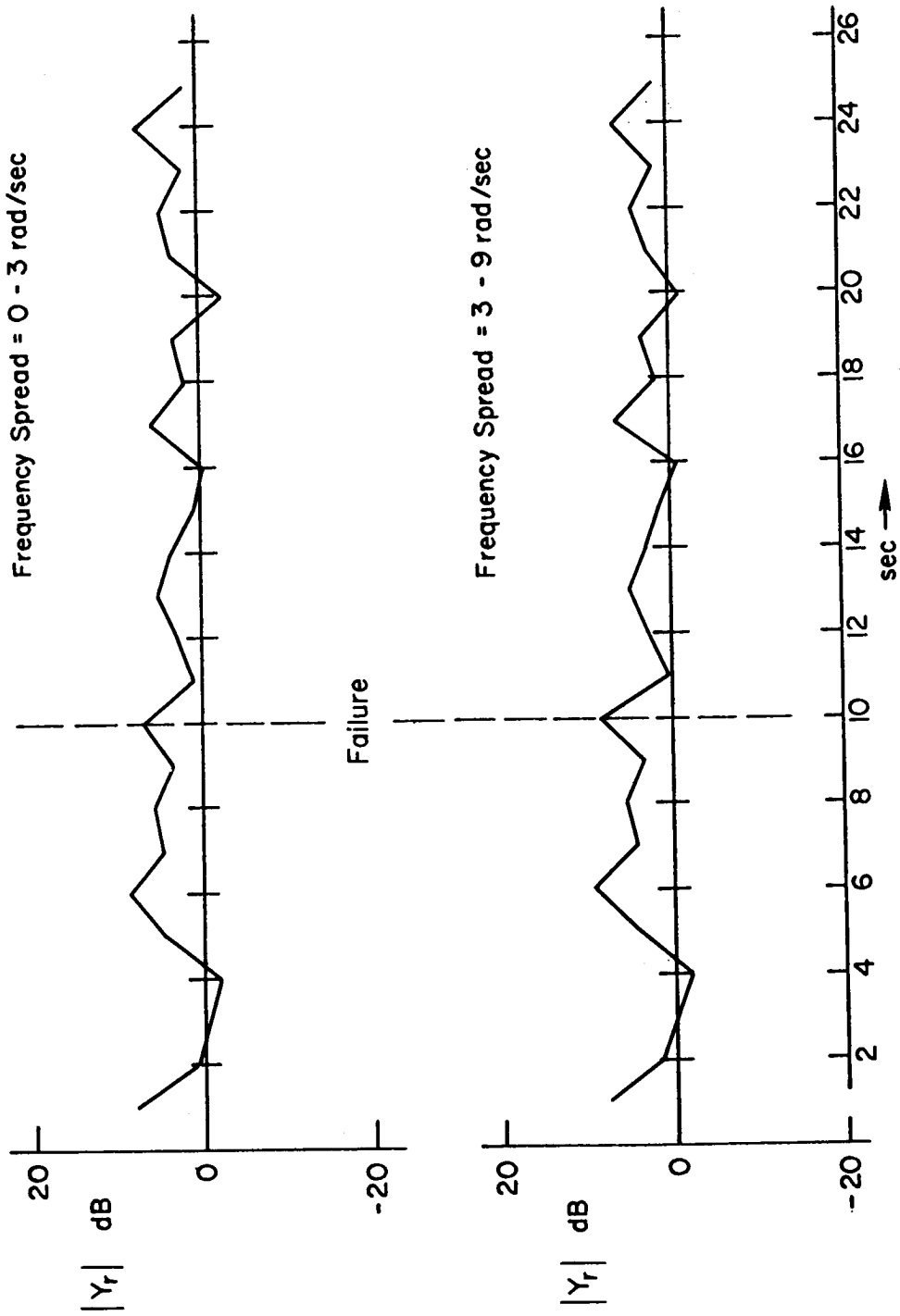
Figure 49. $|Y_r|$ for Soft-Failure from Configuration C

124
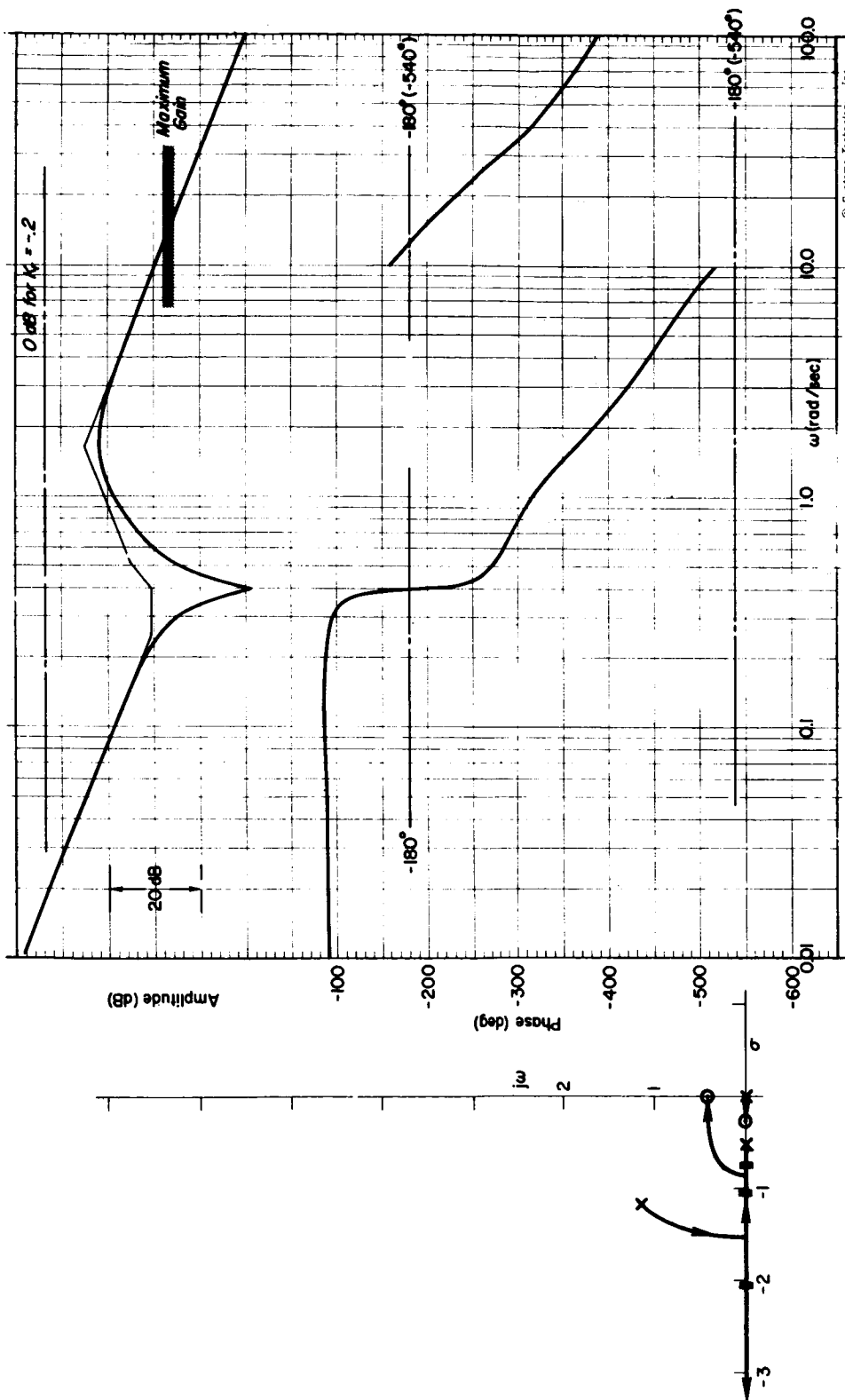
Figure 50. Estimated Pilot Closure of Yaw Rate Loop, Configuration A

125
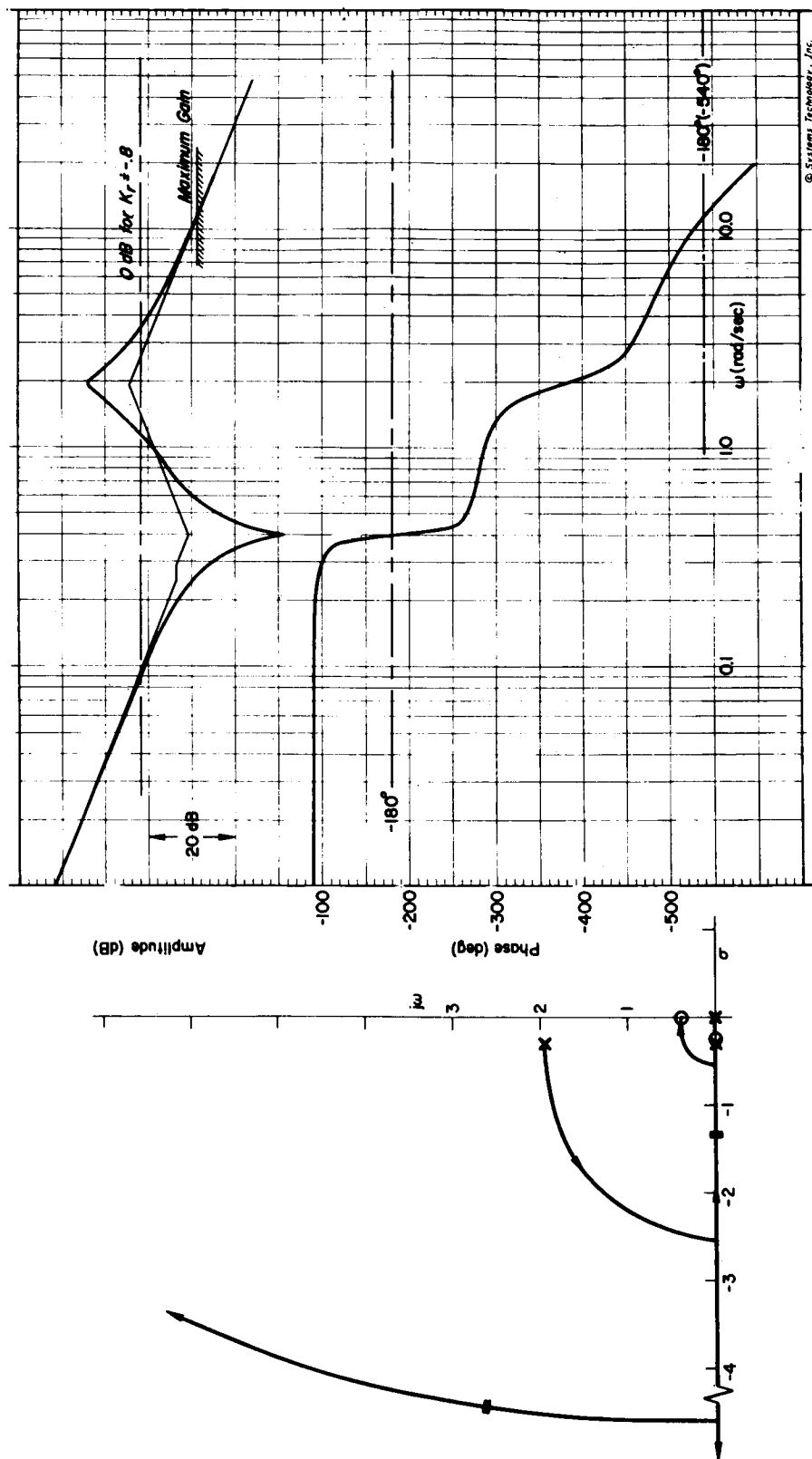
Figure 51. Estimated Pilot Closure of Yaw Rate Loop, Configurations B and C

126
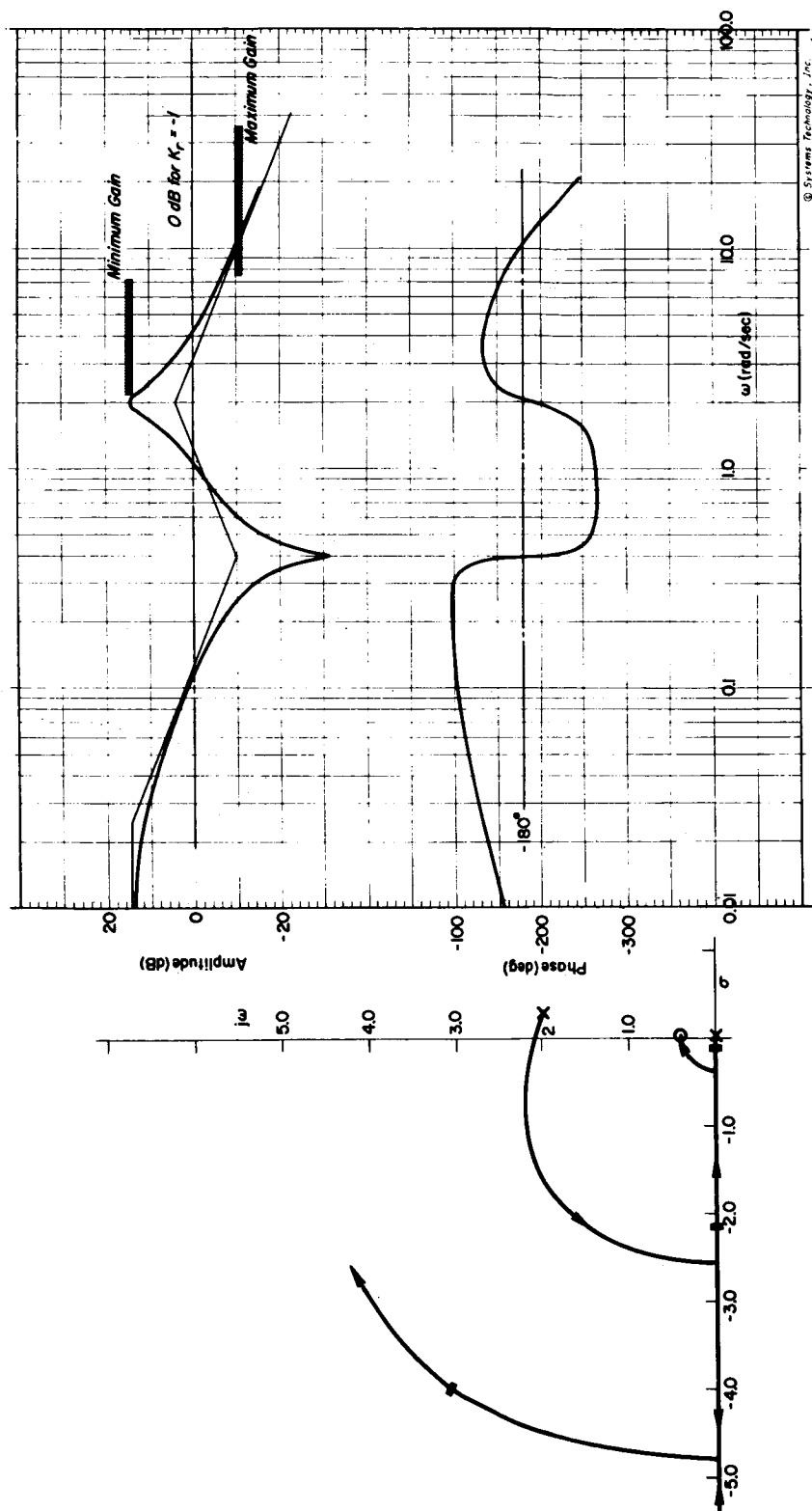
Figure 52. Estimated Pilot Closure of Yaw Rate Loop, Configuration E

127
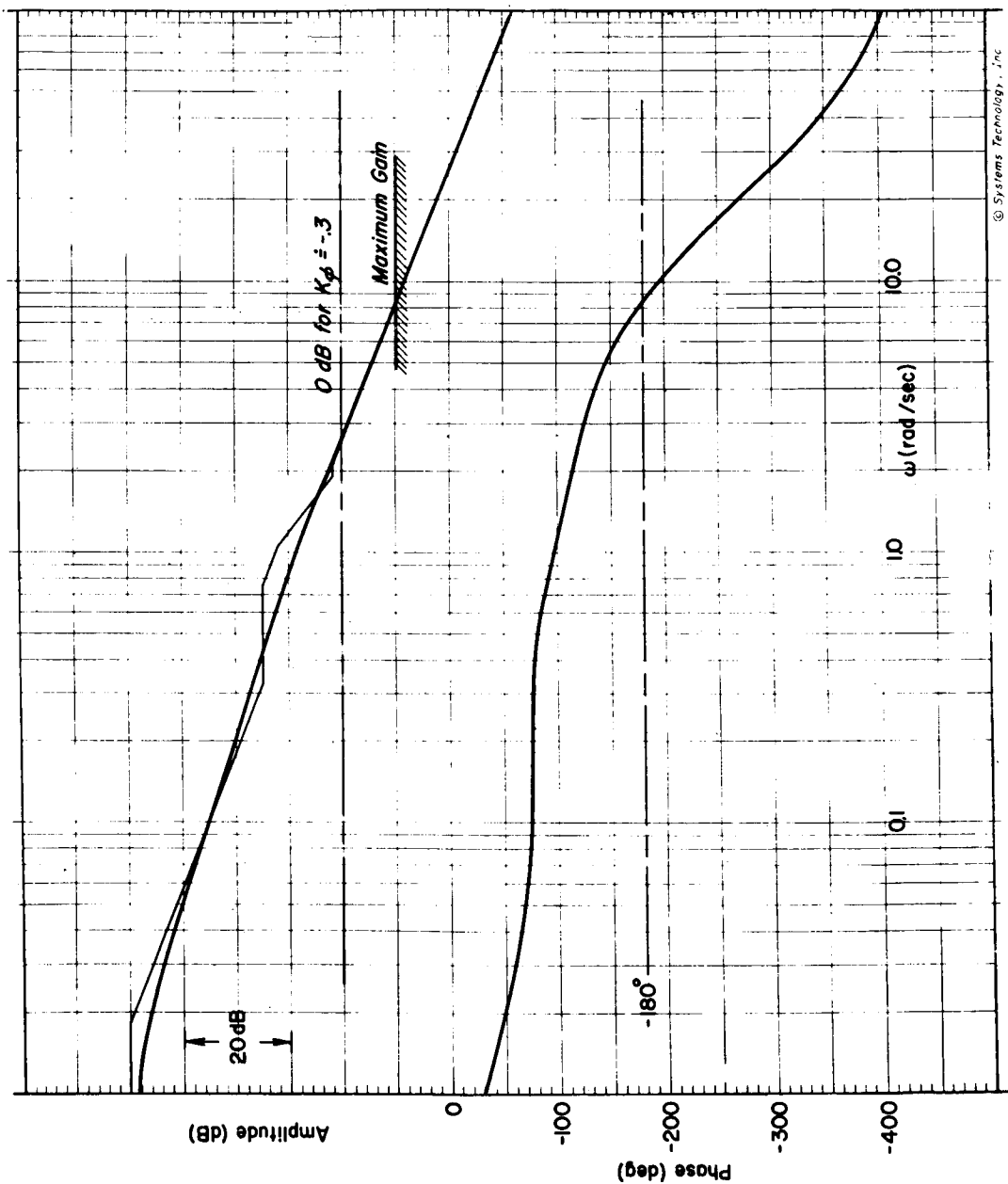
Figure 53. Estimated Pilot Closure of Roll Loop, Configuration A

128
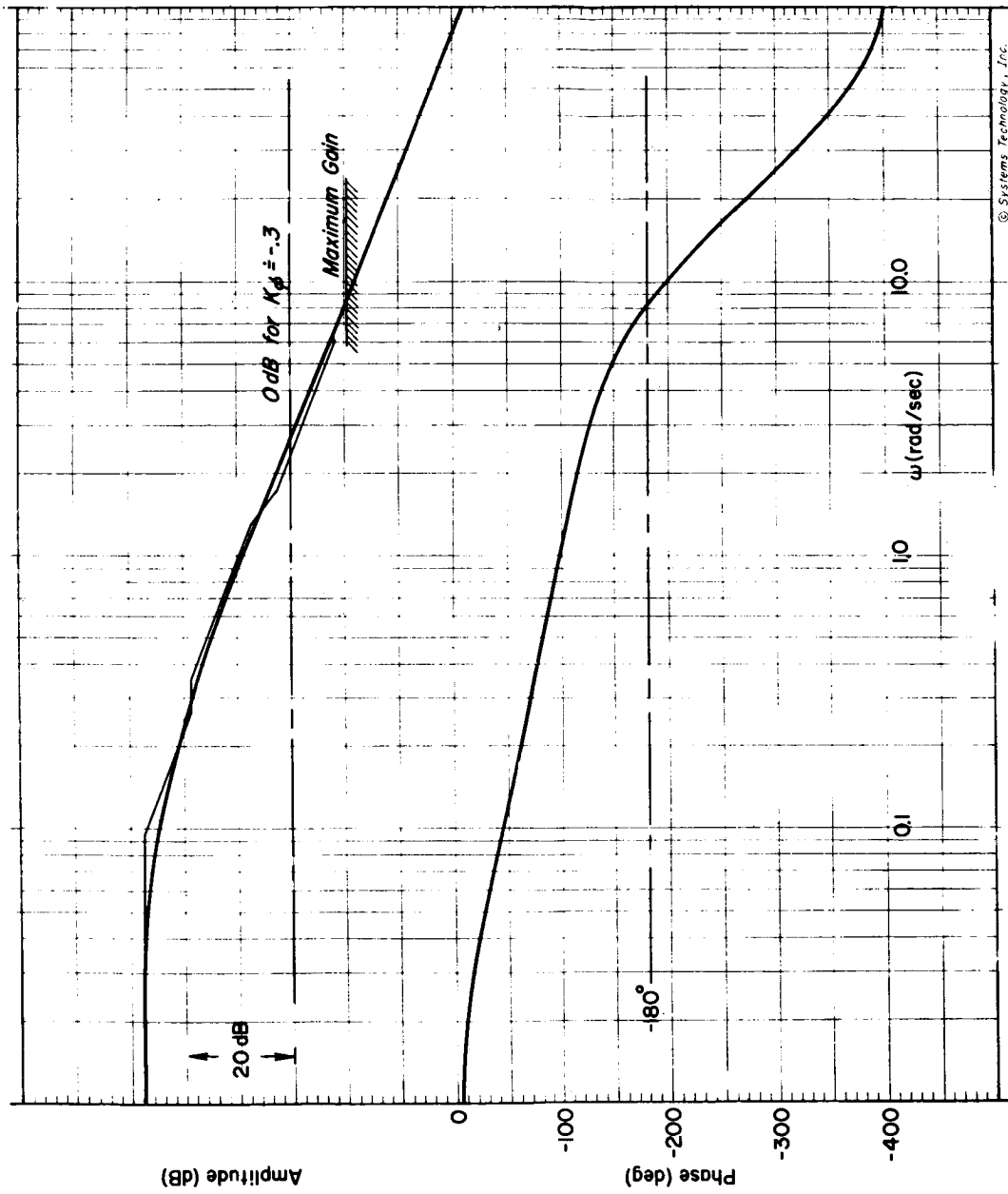
Figure 54. Estimated Pilot Closure of Roll Loop, Configurations B and C

129
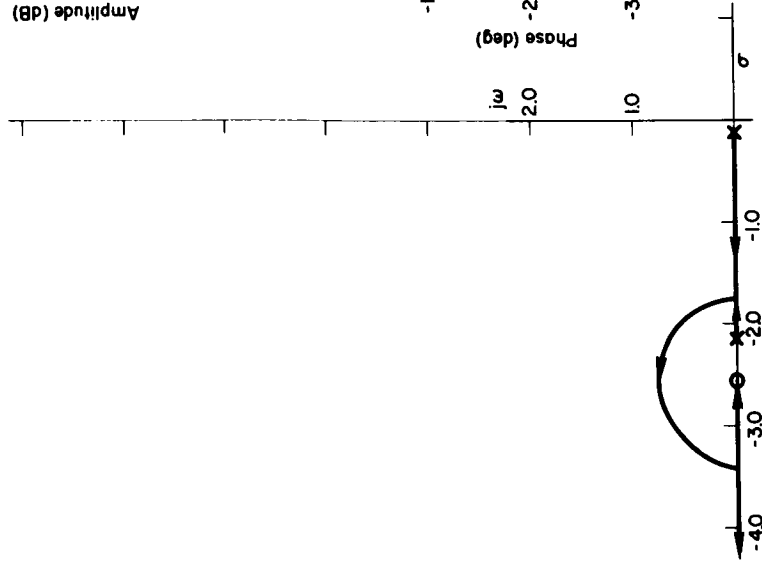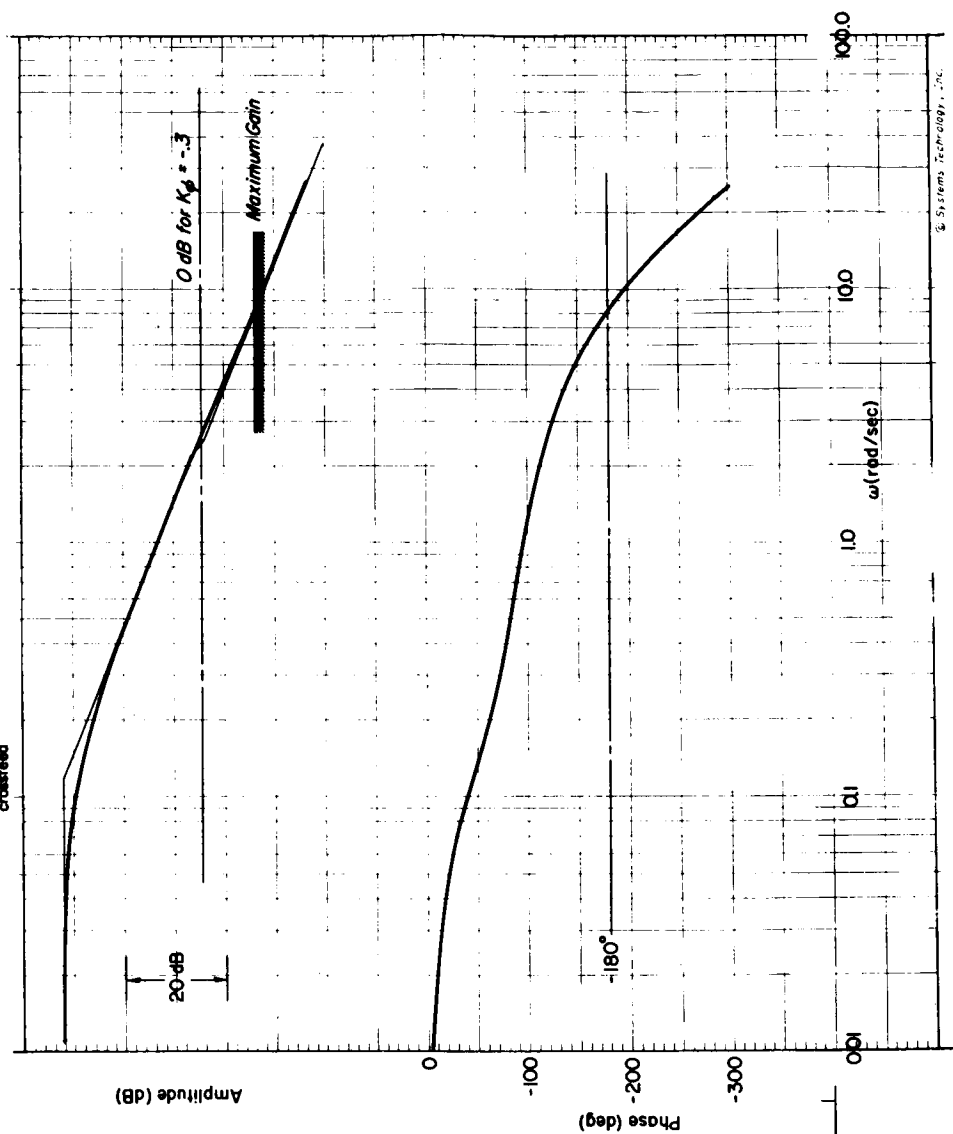
Figure 55. Estimated Pilot Closure of Roll Loop, Configuration E
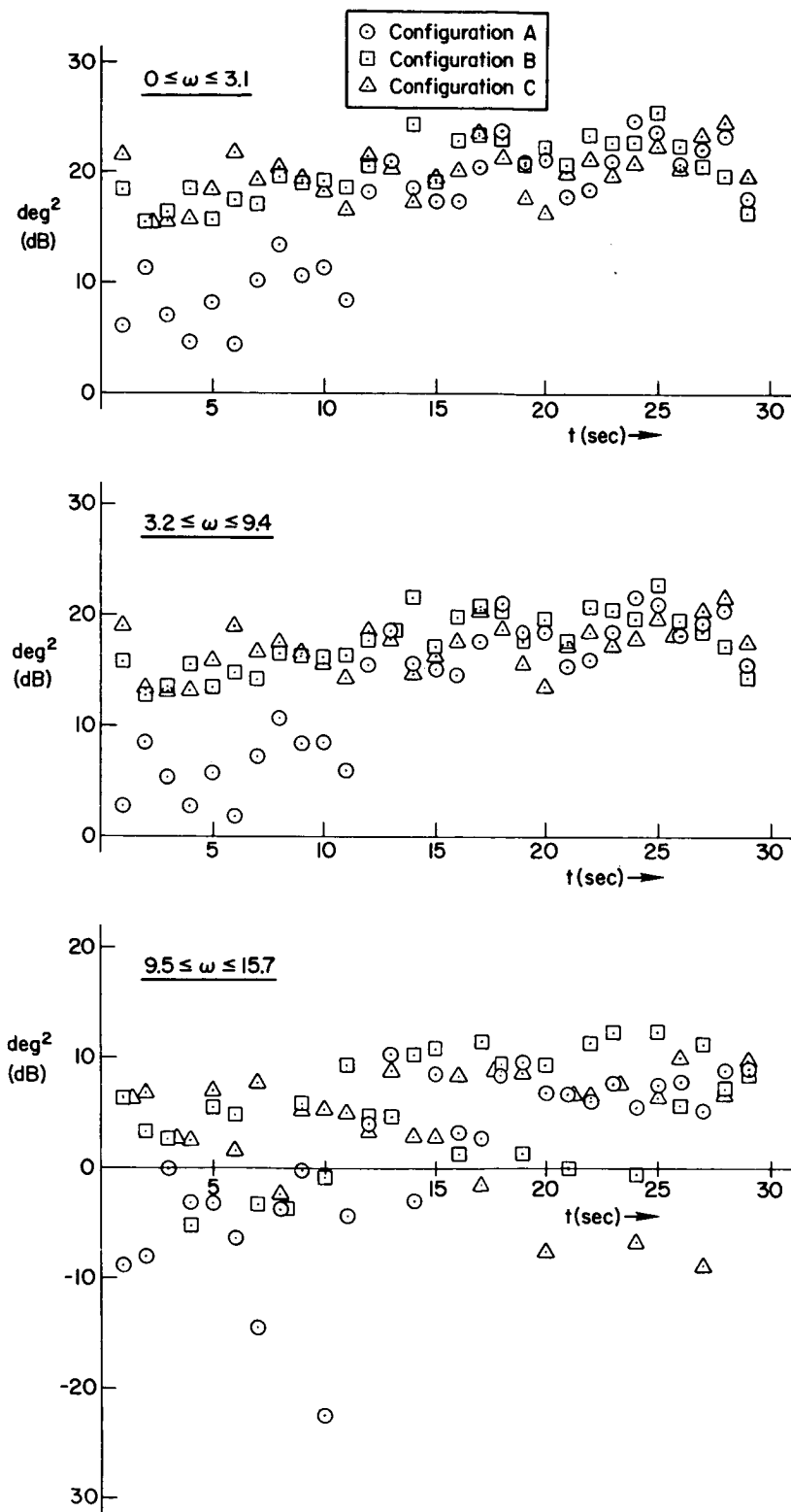
Figure 56. Pilot Rudder Deflection Spectra for Soft-Failures

131
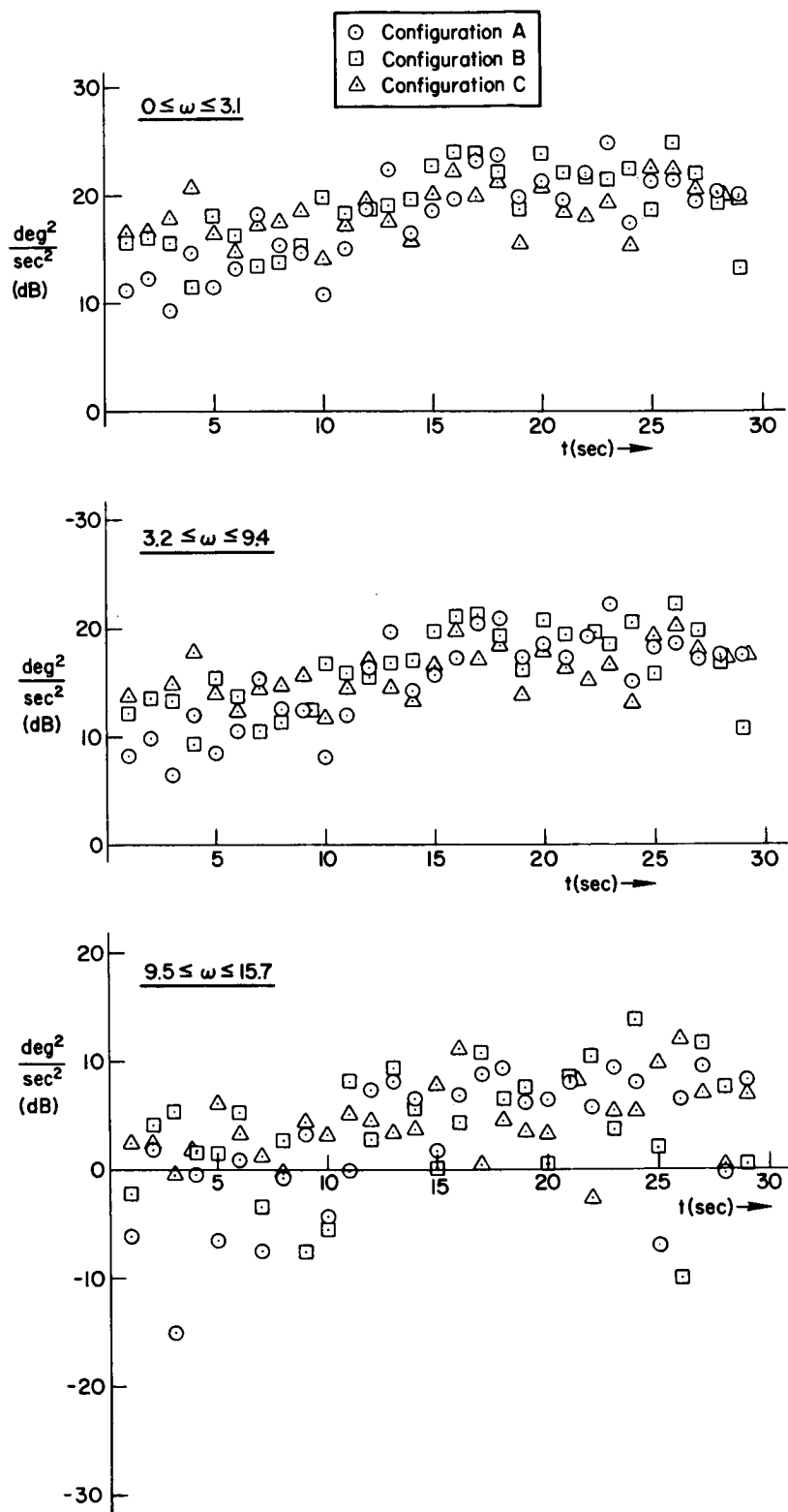
Figure 57. Yaw Rate Error Spectra for Soft-Failures

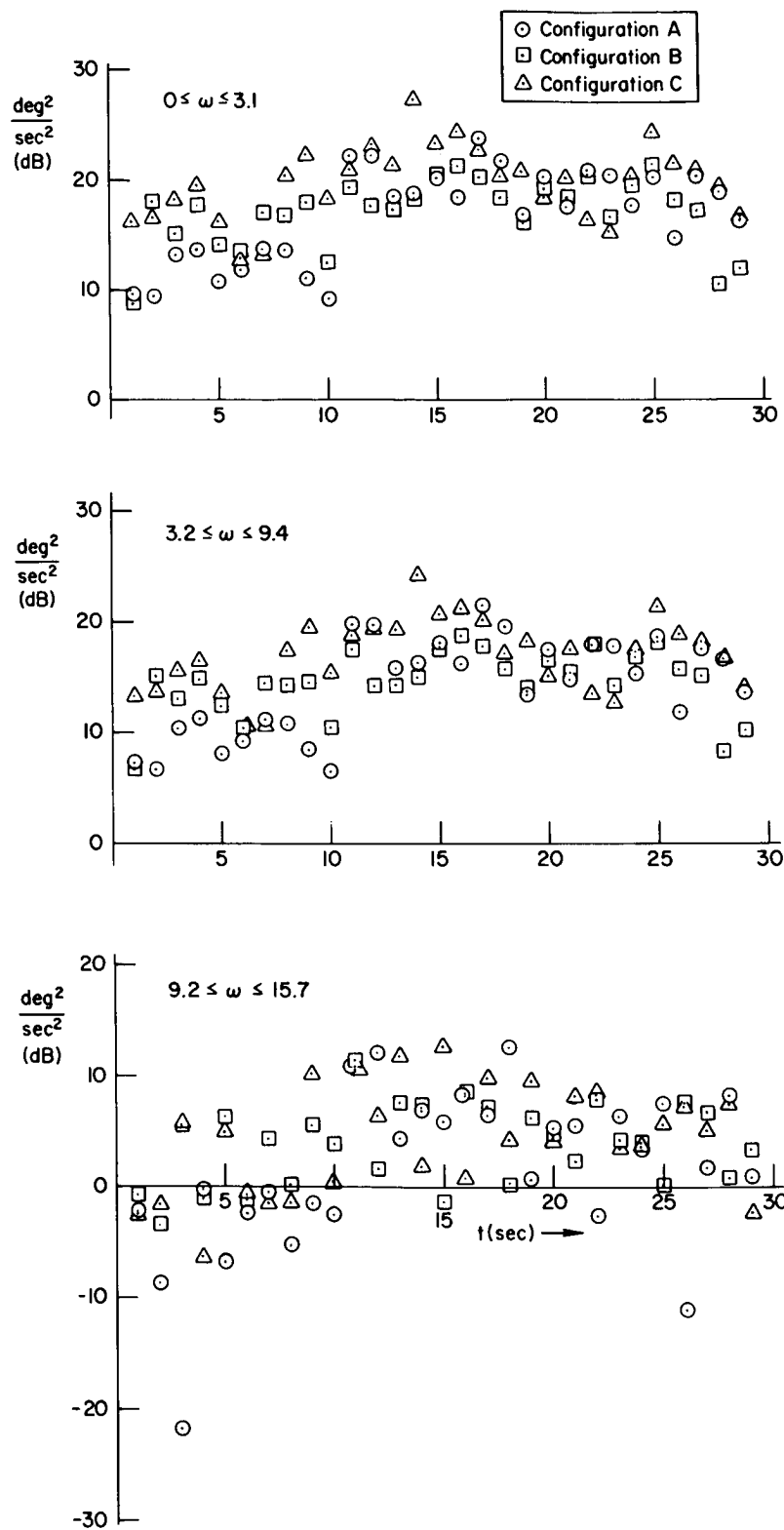132
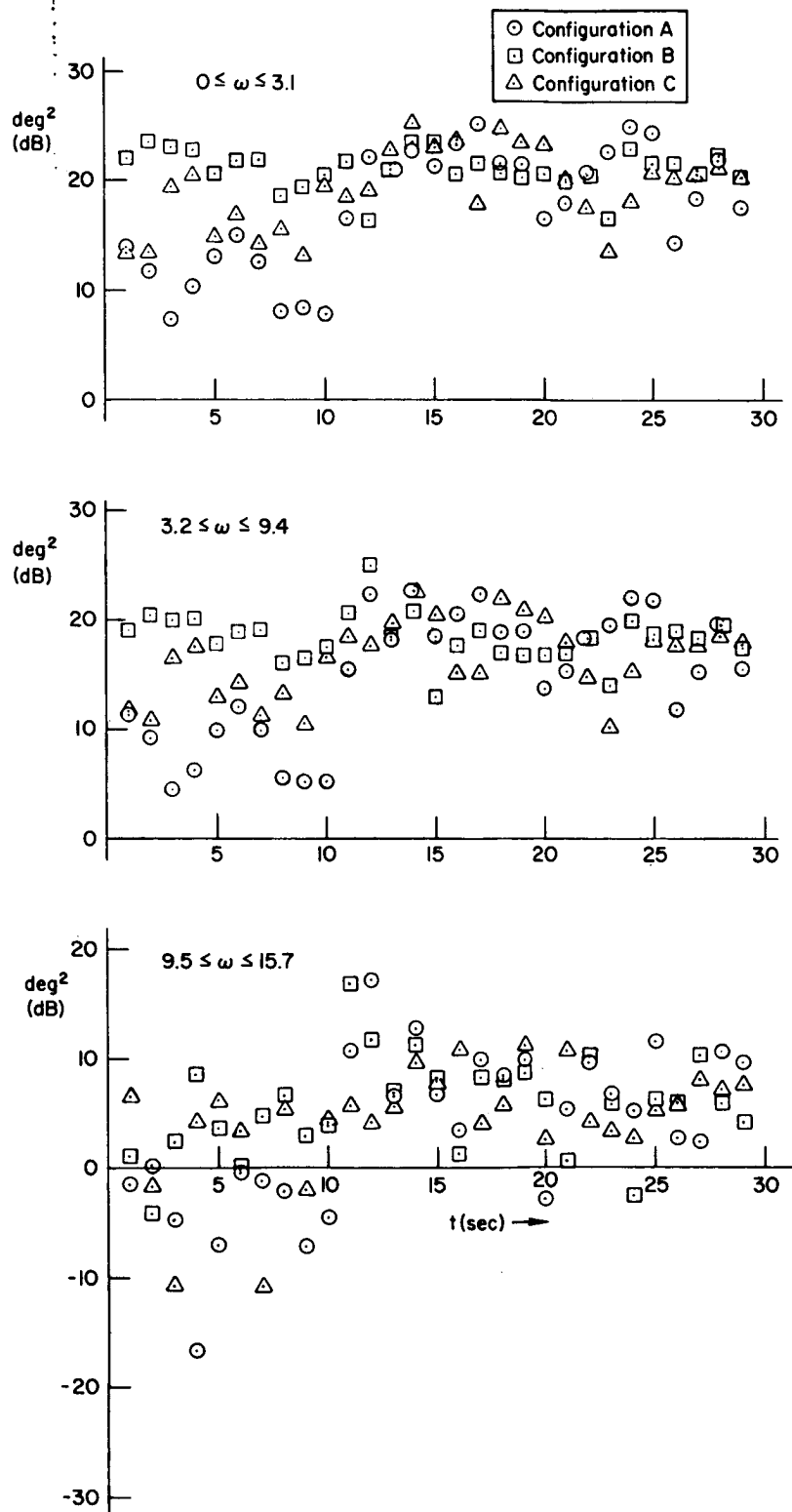
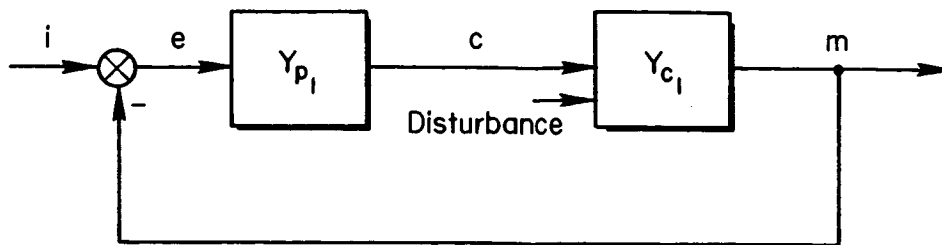Figure 58.   Pilot Rudder Deflection Spectra for Hard-Failures

133

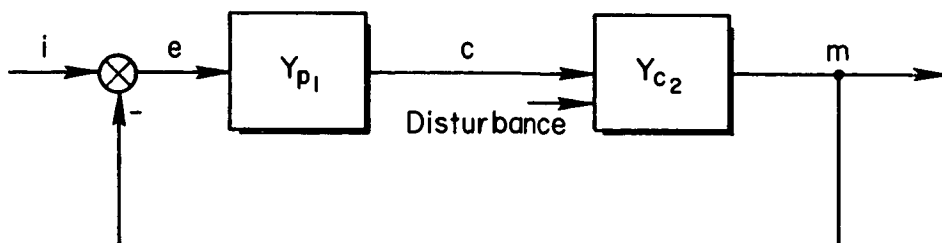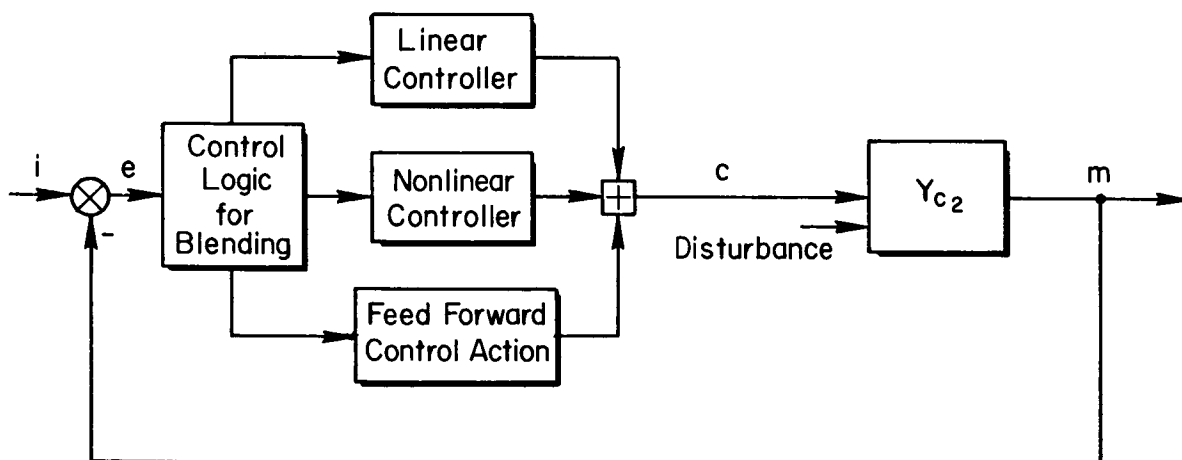Figure 59. Yaw Rate Error Spectra for Hard-Failures

134

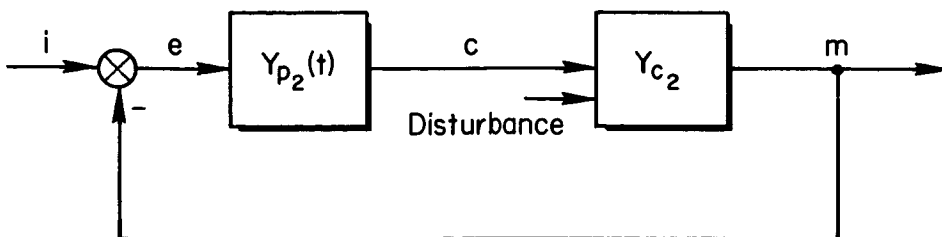Pre-Failure Steady-State Phase, $t < t_0$

Retention Phase, $t_0 < t < t_1$

Nonlinear Phase, $t_1 < t < t_2$

Adjustment and Post-Failure Steady-State Phase, $t > t_2$

Figure 60.   General Pilot Model for Step Change
in Controlled Element Dynamics

"The aeronautical and space activities of the United States shall be conducted so as to contribute . . . to the expansion of human knowledge of phenomena in the atmosphere and space. The Administration shall provide for the widest practicable and appropriate dissemination of information concerning its activities and the results thereof."

— NATIONAL AERONAUTICS AND SPACE ACT OF 1958

NASA SCIENTIFIC AND TECHNICAL PUBLICATIONS

TECHNICAL REPORTS: Scientific and technical information considered important, complete, and a lasting contribution to existing knowledge.

TECHNICAL NOTES: Information less broad in scope but nevertheless of importance as a contribution to existing knowledge.

TECHNICAL MEMORANDUMS: Information receiving limited distribution because of preliminary data, security classification, or other reasons.

CONTRACTOR REPORTS: Scientific and technical information generated under a NASA contract or grant and considered an important contribution to existing knowledge.

TECHNICAL TRANSLATIONS: Information published in a foreign language considered to merit NASA distribution in English.

SPECIAL PUBLICATIONS: Information derived from or of value to NASA activities. Publications include conference proceedings, monographs, data compilations, handbooks, sourcebooks, and special bibliographies.

TECHNOLOGY UTILIZATION PUBLICATIONS: Information on technology used by NASA that may be of particular interest in commercial and other non-aerospace applications. Publications include Tech Briefs, Technology Utilization Reports and Notes, and Technology Surveys.

Details on the availability of these publications may be obtained from:

SCIENTIFIC AND TECHNICAL INFORMATION DIVISION

NATIONAL AERONAUTICS AND SPACE ADMINISTRATION
Washington, D.C. 20546